Comparison of the Prediction Accuracy of Isothermal Compressibility and Isobaric Thermal Expansivity by Different Volume-Translated Equations of State

by

Jingyuan Guan

A thesis submitted in partial fulfillment of the requirements for the degree of

Master of Science

in

Petroleum Engineering

Department of Civil and Environmental Engineering

University of Alberta

ABSTRACT

Isothermal compressibility, κ_T, and isobaric thermal expansivity, α_P, are two important parameters that are used in the simulation and modeling of many petroleum and chemical processes. κ_T and α_P can be calculated by empirical correlations or thermodynamic models, but these predicting methods are not sufficiently accurate. Cubic equations of state (CEOSs) are widely used in the petroleum and chemical industry to describe the phase behavior of fluids. It is recognized that one of the deficiencies of CEOSs is their inaccuracy in predicting liquid-phase volumes. The volume translation (VT) strategy was then proposed by researchers to overcome this deficiency, which could significantly improve the performance of CEOSs in predicting volumetric properties. With recent developments in the volume-translated equations of state (VT-EOSs), κ_T and α_P should also be predicted more accurately by VT-EOSs. In this work, κ_T and α_P of two example fluids (i.e., methane and carbon dioxide) are predicted by seven different VT models: one constant VT model, two linear temperature-dependent VT models, two exponential temperature-dependent VT models, and two temperature-pressure-dependent VT models (i.e., models based on a distance function). The accuracy of each model is evaluated by comparing the predictions with the pseudo-experimental data for the liquid phase, the vapor phase, and the supercritical phase. The predicted results show that the distance-function-based temperature-pressure-dependent VT models exhibit relatively better performance in predicting κ_T and α_P than the temperature-dependent and the constant VT models. Overall, the VT-PR EOS model proposed by Abudour *et al*. (2012) provides the most

accurate predictions of κ_T, while the VT-SRK EOS model proposed by Chen and Li (2020) provides the most accurate predictions of α_P.

DEDICATION

This dissertation is dedicated to my dearest parents, Mr. Bing Guan and Mrs. Rong Li, and my girlfriend Minger Guo.

ACKNOWLEDGMENTS

Foremost, I would like to express my sincere gratitude to my supervisors, Dr. Xuehua Zhang and Dr. Huazhou Li, for their supervision and support during my study. None of the work described in this thesis could have been made possible without their guidance and insights. I learn critical thinking, academic rigor, and life wisdom from them. In addition, I would like to thank my thesis committee members, Dr. Japan Trivedi and Dr. Yuxiang Chen, for their constructive comments and suggestions.

I greatly acknowledge the financial support provided by two Discovery Grants from the Natural Sciences and Engineering Research Council of Canada (NSERC) to X. Zhang and H. Li, respectively.

Finally, I would also like to thank Xin Chen and other group members in Dr. Zhang's and Dr. Li's research groups for their technical suggestions on my thesis.

TABLE OF CONTENTS

LIST OF TABLES

LIST OF FIGURES

CHAPTER 1 INTRODUCTION

1.1. Research Background

Phase behavior of fluids encountered in the petroleum and chemical industry plays an important role in the efficiency of various industrial processes. The volume changes of a fluid at different temperature and pressure conditions are critical to the design and simulation of these industrial processes.[1,2] Isothermal compressibility (κ_T) and isobaric thermal expansivity (α_P) are two important properties that describe the volumetric behavior of a given fluid in response to the changes in pressure and temperature, respectively. For instance, the knowledge of κ_T is of importance in reservoir engineering since it is a useful parameter that can be used to identify the reservoir fluid type.[3] Reservoir engineers also need an accurate estimate on κ_T of reservoir fluids as κ_T is a required input parameter in the governing equations of fluid flow within reservoirs.[4-6] α_P is a very useful parameter that finds applications in many chemical and industrial processes involving heat transfer, thermal processing of materials, and the design of high-pressure injection equipment.[2,7] κ_T and α_P also play critical roles in the steady-state and transient simulations of fluid flow in pipes since they are used in empirical correlations that relate *in-situ* flow rates to those at standard conditions.[8]

κ_T can be defined as:[9]

$$\kappa_T = -\frac{1}{v}\left(\frac{\partial v}{\partial P}\right)_T \quad (1)$$

α_P, also called the coefficient of thermal expansion, can be defined as:[9]

$$\alpha_P = \frac{1}{v}\left(\frac{\partial v}{\partial T}\right)_P \quad (2)$$

where v, P, and T are molar volume, pressure, and temperature, respectively. κ_T describes the change in the molar volume of a fluid due to a change in pressure at a constant temperature, while α_P represents the change in the molar volume of a fluid caused by a temperature change at a constant pressure.

1.2. Literature Review of the Determination of κ_T and α_P and the Volume-Translated EOS

1.2.1. Determination of κ_T and α_P

There are mainly two methods to determine κ_T and α_P, namely, the experimental methods and the theoretical methods. Experimentally, robust laboratory tests are relied on to acquire pressure-volume-temperature (PVT) data, and then the acquired PVT data are used to obtain reliable and accurate results of κ_T and α_P.[6] Some correlations have been proposed to estimate κ_T and α_P. Trusler and Lemmon[10] proposed empirical correlations for κ_T and α_P based on the measurements of speed of sound.[11] Baonza *et al.*[12] proposed a method to extrapolate κ_T and α_P for mesitylene based on the measured molar densities. However, the correlations based on speed of sound and the extrapolation method are not accurate enough.[12,13] Cerdeiriña *et al.*[14] adopted a fitting equation to fit the measured density data with temperature and then analytically differentiated the equation with respect to temperature to calculate α_P. However, fitting equations obtained by different fitting strategies could result in different equations, thus leading to different temperature dependences of α_P for the same density data.[14]

1.2.2. Volume-Translated EOS

Accurate κ_T and α_P can be calculated based on accurate PVT relations.[15] Cubic equations of state (CEOSs) have been widely used to describe PVT relations. Peng-Robinson (PR) EOS[16] and Soave-Redlich-Kwong (SRK) EOS[17] are the most used CEOSs, due to their simplicity and reliability.[18,19] Although PR EOS and SRK EOS are capable of calculating the molar volumes of various substances over different temperature and pressure ranges, it is recognized that one of their deficiencies is the inaccurate liquid-phase volume prediction.[20] To overcome this shortcoming, Martin[21] first proposed the concept of volume translation (VT) for CEOSs in 1979. In this method, a volume translation is applied in the volume-pressure diagram to make the isotherms shift along the volume axis without leading to any change in the vapor-liquid equilibrium calculations.[22] Many VT models have been proposed for PR EOS and SRK EOS, leading to the so-called VT-PR EOSs and VT-SRK EOSs, respectively.

VT-EOS models can be generally divided into three categories: constant volume translations, temperature-dependent volume translations, and volume translations that are temperature-pressure-dependent.[23] In the constant volume translation models, the volume translation term is not a function of temperature, but a constant corresponding to the difference between the volume predicted by an EOS and the measured saturated liquid volume at a given reduced temperature (T_r). In 1982, Péneloux *et al*.[22] applied the constant volume translations acquired at T_r = 0.7 to SRK EOS, which significantly improved the predictions of liquid density at low reduced temperatures. Based on the CEOS models updated by Le Guennec *et al*.[24], Pina-Martinez *et al*.[25] updated the volume translation constants for more than 1000 pure substances based on the pseudo-experimental saturated

liquid molar volumes at T_r = 0.8 as reported by the DIPPR database. However, a larger volume translation is required as the temperature gets closer to the critical point, and the largest volume translation is required at the critical point.[26]

Temperature-dependent VT models can be in a linear form or an exponential form.[27–35] Ungerer and Batut[34] proposed a volume translation for PR EOS that has a linear relationship with temperature and molecular weight. Baled *et al*.[35] developed a linear temperature-dependent volume translation model for both PR EOS and SRK EOS to correct density predictions at high-temperature and high-pressure conditions, which provides better density predictions in the single-phase region than in the saturation region.[23] An exponential temperature-dependent VT model developed by Magoulas and Tassios[29] was applied to PR EOS for alkanes. However, temperature-dependent volume translations might cause the crossover of PV isotherms, implying that a lower molar volume is predicted by the VT model at a higher temperature under an isobaric condition.[36] The Ungerer and Batut model[34] and the Magoulas and Tassios model[29] were reported to induce the crossover of PV isotherms at relatively low pressures.[35–38] This crossover phenomenon is inconsistent with the basic assumptions of thermodynamics and therefore limits the application of these temperature-dependent VT models.[36] To address such an issue, Shi and Li[36] developed a criterion to determine when the crossover phenomenon of PV isotherms appears and subsequently proposed a VT-PR EOS to avoid the crossover phenomenon within a large pressure range.[32]

Since the required volume translation increases as the critical point is approached, constant volume translations and temperature-dependent volume translations have relatively poor performance.[23] Based on the fact that the required corrections for the single-phase liquid

densities are not only temperature-dependent but also volume-dependent,[26] Chou and Prausnitz[39] and Mathias *et al*.[40] introduced a volume-dependent distance function (*d*) and proposed temperature-pressure-dependent VT models. Based on this method, improved VT-PR EOS and VT-SRK EOS were proposed by Abudour *et al*.[23] and Frey *et al*.,[41,42] respectively. The Frey *et al*. model[41,42] only showed modest improvement on density predictions, while the Abudour *et al*. model[23] was reported to be the best performed VT model for saturated liquid and compressed liquid density predictions.[43] In 2020, Chen and Li[26] developed a distance-function-based VT-SRK EOS, obtaining slightly better performance than the Abudour *et al*. model[23] in predicting the molar volumes of the saturated and single-phase liquids for 56 substances.

Because of the significant improvement made towards the volume translation models in CEOSs, some authors have attempted to use CEOSs to predict thermodynamic properties that require volumetric data.[1,6,44-46] Avasthi and Kennedy[1] developed a method to predict κ_T and α_P for hydrocarbons by differentiating CEOSs. Trujillo *et al*.[45] applied PR EOS to computational fluid dynamics simulations to predict thermodynamic relationships including PVT behavior and other thermodynamic derivative properties. Adepoju *et al*.[44] proposed a mathematical method to predict κ_T for oil samples based on PR EOS. Regueira *et al*.[46] reported that the volume translation versions of PR EOS and SRK EOS yielded better performance than the original EOSs in predicting κ_T for high-pressure and high-temperature reservoir fluids. Burgess *et al*.[6] extended the VT-SRK EOS of Baled *et al*.[35] to conditions up to 533 K and 276 MPa. But they found that the predictions of κ_T could deviate from the experimental data by over 50%, and these predictions were inaccurate over the entire temperature and pressure ranges.[6]

Being designed to correct molar volume calculations, a VT-EOS can lead to a saturated molar volume different from the one by the untranslated EOS at a given temperature. As a result, some fluid properties can be affected by volume translation.[37] Jaubert *et al*. focused on the Péneloux-type VT models[22] and analytically studied the influence of the temperature-dependent and the temperature-independent VT models on several thermodynamic properties, including κ_T and α_P.[37] They found that, for a pure substance, applying a temperature-independent VT model to a given EOS affects neither the product of molar volume and isothermal compressibility $(v\kappa_T)$ nor the product of molar volume and isobaric thermal expansivity $(v\alpha_P)$, while applying a temperature-dependent VT model affects the value of $v\alpha_P$, but leaves the value of $v\kappa_T$ unchanged.[37]

1.3. Problem Statement

The experimental determination of κ_T and α_P can be reliable but expensive and time-consuming, and they are hardly conducted at *in-situ* conditions.[6] Since the existing theoretical methods for calculating κ_T and α_P are not sufficiently accurate,[12,13] there is still a need to further improve the prediction accuracy of κ_T and α_P. As the predictions of molar volume can be improved by different kinds of VT-EOS models, predicting κ_T and α_P based on the molar volumes obtained from a VT-EOS should also be improved and become more accurate over wide ranges of temperature and pressure. Due to the wide use of PR EOS and SRK EOS in the simulation of phase behavior in the petroleum and chemical industry, applying VT-PR EOS or VT-SRK EOS to predict the basic PVT properties as well as κ_T and α_P becomes a natural and consistent choice. However, the prediction accuracy of different VT-EOSs for κ_T and α_P has not been comprehensively investigated, and it is not known which VT model is the most accurate in predicting κ_T

and α_P. Therefore, the performance of different types of VT-EOSs in predicting κ_T and α_P needs to be evaluated.

1.4. Research Objectives

The main objective of this research is to determine the most accurate VT model for predicting κ_T and α_P. The detailed objectives include the following:

- To develop a numerical procedure for calculating κ_T and α_P using the temperature-pressure-dependent VT-EOS models that adopt the temperature-pressure-dependent distance function;
- To more accurately predict κ_T and α_P for pure fluids by using different VT-EOS models, including one constant VT model, two linear temperature-dependent VT models, two exponential temperature-dependent VT models, and two temperature-pressure-dependent VT models; and
- To evaluate the prediction accuracy of κ_T and α_P by different VT-EOS models and select the most accurate model for predicting κ_T and α_P thereof.

1.5. Thesis Structure

The thesis contains four chapters:

- **Chapter 1** introduces the research background, literature review, problem statement, research objectives, and thesis structure.
- **Chapter 2** presents the methodology employed in this thesis, including the untranslated EOSs and the VT models used for predicting κ_T and α_P, and the

numerical procedure for calculating κ_T and α_P by using the distance-function-based VT models.

- **Chapter 3** shows the sensitivity analysis on the numerical calculations of κ_T and α_P, and evaluates the performance of seven representative VT-EOSs in predicting κ_T and α_P for two example pure fluids, carbon dioxide (CO_2) and methane (CH_4), in different phase regions by comparing the predicted results with the pseudo-experimental data.

- **Chapter 4** summarizes the conclusions of this study and gives recommendations for future work.

References

[1] Avasthi, S. M.; Kennedy, H. T. The prediction of volumes, compressibilities and thermal expansion coefficients of hydrocarbon mixtures. *SPE J.* **1968**, *8* (02), 95–106.

[2] Chorążewski, M.; Postnikov, E. B. Thermal properties of compressed liquids: Experimental determination via an indirect acoustic technique and modeling using the volume fluctuations approach. *Int. J. Therm. Sci.* **2015**, *90*, 62–69.

[3] Ahmed, T.; Meehan, D. N. *Advanced reservoir management and engineering*; Gulf Professional Publishing, 2011.

[4] Peters, E. J. *Advanced Petrophysics: Volume 1: Geology, Porosity, Absolute Permeability, Heterogeneity and Geostatistics*; Live Oak Book Co, 2012.

[5] Beggs, H. D. *Production optimization using NODAL analysis*; 1991.

[6] Burgess, W. A.; Bamgbade, B. A.; Gamwo, I. K. Experimental and predictive PC-SAFT modeling results for density and isothermal compressibility for two crude oil samples at elevated temperatures and pressures. *Fuel* **2018,** *218*, 385–395.

[7] Navia, P.; Troncoso, J.; Romaní, L. New calibration methodology for calorimetric determination of isobaric thermal expansivity of liquids as a function of temperature and pressure. *J. Chem. Phys.* **2011**, *134* (9), No. 094502.

[8] Christie, B. On the correlation between isothermal compressibility and isobaric expansivity. *Pipeline Simulation Interest Group Annual Meeting*; Baltimore, Maryland, May 2014; PSIG 1426.

[9] Gaskell, D.R. *Introduction to the thermodynamics of materials*; CRC Press, 2012.

[10] Trusler, J. P. M.; Lemmon, E.W. Determination of the thermodynamic properties of water from the speed of sound. *J. Chem. Thermodyn.* **2017**, *109*, 61–70.

[11] Lin, C. W.; Trusler, J. P. M. The speed of sound and derived thermodynamic properties of pure water at temperatures between (253 and 473) K and at pressures up to 400 MPa. *J. Chem. Phys.* **2012**, *136* (9), No. 094511.

[12] Baonza, V. G.; Alonso, M. C.; Delgado, J. N. Application of simple expressions for the high-pressure volumetric behaviour of liquid mesitylene. *J. Chem. Soc., Faraday Trans.* **1994**, *90* (4), 553–557.

[13] Daridon, J. L.; Bazile, J. P. Computation of liquid isothermal compressibility from density measurements: An application to toluene. *J. Chem. Eng. Data* **2018**, *63* (6), 2162–2178.

[14] Cerdeiriña, C. A.; Tovar, C. A.; González-Salgado, D.; Carballo, E.; Romaní, L. Isobaric thermal expansivity and thermophysical characterization of liquids and liquid mixtures. *Phys. Chem. Chem. Phys.* **2001**, *3* (23), 5230–5236.

[15] Macias, L. C.; Ramey Jr., H. J. Multiphase, multicomponent compressibility in petroleum reservoir engineering; *SPE Annual Technical Conference and Exhibition*; New Orleans, Louisiana, October 1986; SPE-15538-MS.

[16] Peng, D. Y.; Robinson, D. B. A new two-constant equation of state. *Ind. Eng. Chem. Fundam.* **1976**, *15* (1), 59–64.

[17] Soave, G. Equilibrium constants from a modified Redlich-Kwong equation of state. *Chem. Eng. Sci.* **1972**, *27* (6), 1197–1203.

[18] Privat, R.; Jaubert, J. N. Thermodynamic models for the prediction of petroleum-fluid phase behaviour. *Crude Oil Emulsions-Composition Stability and Characterization*; InTechOpen, 2012.

[19] Valderrama, J. O. The state of the cubic equations of state. *Ind. Eng. Chem. Res.* **2003**, *43* (8), 1603–1618.

[20] Valderrama,J. O.; Alfaro, M. Liquid volumes from generalized cubic equations of state: Take it with care. *Oil Gas Sci. Technol.* **2000**, *55* (5), 523–531.

[21] Martin, J. J. Cubic equations of state-which? *Ind. Eng. Chem. Fundam.* **1979**, *18* (2), 81–97.

[22] Péneloux, A.; Rauzy, E.; Fréze, R. A consistent correction for Redlich-Kwong-Soave volumes. *Fluid Phase Equilib*. **1982**, *8* (1), 7–23.

[23] Abudour, A. M.; Mohammad, S. A.; Robinson, R. L.; Gasem, K. A. M. Volume-translated Peng–Robinson equation of state for saturated and single-phase liquid densities. *Fluid Phase Equilib*. **2012**, *335*, 74–87.

[24] Le Guennec, Y.; Lasala, S.; Privat, R.; Jaubert, J. N. A consistency test for α-functions of cubic equations of state. *Fluid Phase Equilib*. **2016**, *427*, 513–538.

[25] Pina-Martinez, A.; Le Guennec, Y.; Privat, R.; Jaubert, J. N.; Mathias, P. M. Analysis of the combinations of property data that are suitable for a safe estimation of consistent Twu α-function parameters: Updated parameter values for the translated-consistent tc-PR and tc-RK cubic equations of state. *J. Chem. Eng. Data* **2018,** *63* (10), 3980–3988.

[26] Chen, X.; Li, H. An improved volume-translated SRK EOS dedicated to more accurate determination of saturated and single-phase liquid densities. *Fluid Phase Equilib.* **2020**, *521*, No. 112724.

[27] Lin, H.; Duan, Y. Y. Empirical correction to the Peng-Robinson equation of state for the saturated region. *Fluid Phase Equilib.* **2005**, *233* (2), 194–203.

[28] Lin, H.; Duan, Y. Y.; Zhang, T.; Huang, Z. M. Volumetric property improvement for the Soave-Redlich-Kwong equation of state. *Ind. Eng. Chem. Res.* **2006**, *45* (5), 1829–1839.

[29] Magoulas, K.; Tassios, D. Thermophysical properties of n-alkanes from C1 to C20 and their prediction for higher ones. *Fluid Phase Equilib*. **1990**, *56*, 119–140.

[30] Monnery, W. D.; Svrcek, W. Y.; Satyro, M. A. Gaussian-like volume shifts for the Peng-Robinson equation of state. *Ind. Eng. Chem. Res*. **1998,** *37* (5), 1663–1672.

[31] Nazarzadeh, M.; Moshfeghian, M. New volume translated PR equation of state for pure compounds and gas condensate systems. *Fluid Phase Equilib*. **2013**, *337*, 214–223.

[32] Shi, J.; Li, H.; Pang, W. An improved volume translation strategy for PR EOS without crossover issue. *Fluid Phase Equilib*. **2018**, *470*, 164–175.

[33] Watson, P.; Cascella, M.; May, D.; Salerno, S.; Tassios, D. Prediction of vapor pressures and saturated molar volumes with a simple cubic equation of state: Part II: The Van der Waals - 711 EOS. *Fluid Phase Equilib*. **1986**, *27*, 35–52.

[34] Ungerer, P.; Batut, C.; Prédiction des propriétés volumétriques des hydrocarbures par une translation de volume améliorée. *Rev. Inst. Fr. Pét.* **1997**, *52* (6), 609–623.

[35] Baled, H.; Enick, R. M.; Wu, Y.; McHugh, M. A.; Burgess, W.; Tapriyal, D.; Morreale, B. D. Prediction of hydrocarbon densities at extreme conditions using volume-translated SRK and PR equations of state fit to high temperature, high pressure PVT data. *Fluid Phase Equilib*. **2012**, *317*, 65–76.

[36] Shi, J.; Li, H. Criterion for determining crossover phenomenon in volume-translated equation of states. *Fluid Phase Equilib*. **2016**, *430*, 1–12.

[37] Jaubert, J. N.; Privat, R.; Le Guennec, Y.; Coniglio, L. Note on the properties altered by application of a Péneloux-type volume translation to an equation of state. *Fluid Phase Equilib*. **2016**, *419*, 88–95.

[38] Kalikhman, V.; Kost, D.; Polishuk, I. About the physical validity of attaching the repulsive terms of analytical EOS models by temperature dependencies. *Fluid Phase Equilib*. **2010**, *293* (2), 164–167.

[39] Chou, G. F.; Prausnitz, J. M. A phenomenological correction to an equation of state for the critical region. *AIChE J.* **1989**, *35* (9), 1487–1496.

[40] Mathias, P. M.; Naheiri, T.; Oh, E. M. A density correction for the Peng-Robinson equation of state. *Fluid Phase Equilib.* **1989**, *47*, 77–87.

[41] Frey, K.; Modell, M.; Tester, J. Density-and-temperature-dependent volume translation for the SRK EOS: 1. Pure fluids. *Fluid Phase Equilib.* **2009**, *279* (1), 56–63.

[42] Frey, K.; Modell, M.; Tester, J. Density-and-temperature-dependent volume translation for the SRK EOS: 2. Mixtures. *Fluid Phase Equilib.* **2013**, *343*, 13–23.

[43] Young, A. F.; Pessoa, F. L. P.; Ahón, V. R. R. Comparison of volume translation and co-volume functions applied in the Peng-Robinson EoS for volumetric corrections. *Fluid Phase Equilib.* **2017**, *435*, 73–87.

[44] Adepoju, O. O. Coefficient of isothermal oil compressibility for reservoir fluids by cubic equation-of-state. M.Sc. thesis, Texas Tech University, 2006.

[45] Trujillo, M. F.; Torres, D. J.; O'Rourke, P. J. High-pressure multicomponent liquid sprays: Departure from ideal behaviour. *Int. J. Engine Res.* **2004**, *5* (3), 229–246.

[46] Regueira, T.; Glykioti, M. L.; Kottaki, N.; Stenby, E. H.; Yan, W. Density, compressibility and phase equilibrium of high pressure-high temperature reservoir fluids up to 473 K and 140 MPa. *J. Supercrit. Fluids* **2020**, *159*, No. 104781.

CHAPTER 2 METHODOLOGY

The prediction accuracy of κ_T and α_P by seven representative VT-EOS models is examined. These VT models include one constant VT for the SRK EOS updated by Pina-Martinez *et al*.,[1] two linear temperature-dependent VT-PR EOSs including the Ungerer and Batut model[2] and the Baled *et al*. model,[3] two exponential temperature-dependent VT-PR EOSs including the Magoulas and Tassios model[4] and the Shi *et al*. model,[5] and two temperature-pressure-dependent models including the VT-PR EOS proposed by Abudour *et al*.[6] and the VT-SRK EOS proposed by Chen and Li.[7]

2.1. PR EOS

PR EOS[8] is given as:

$$P^{PR} = \frac{RT}{v^{PR}-b^{PR}} - \frac{a^{PR}(T)}{v^{PR}(v^{PR}+b^{PR})+b^{PR}(v^{PR}-b^{PR})} \quad (3)$$

$$a^{PR}(T) = \frac{0.457535R^2T_c^2}{P_c}\alpha^{PR}(T) \quad (4)$$

$$b^{PR} = \frac{0.077796RT_c}{P_c} \quad (5)$$

where P^{PR} and v^{PR} are pressure and molar volume in PR EOS, respectively, T is temperature, R is the gas constant, a^{PR} and b^{PR} are EOS parameters in PR EOS, which can be expressed in terms of critical temperature (T_c) and critical pressure (P_c). The $\alpha^{PR}(T)$ term in Equation (4) is the dimensionless α-function for PR EOS, which has been developed into various modifications to improve the property predictions for pure substances. The α-function used in the original PR EOS can be written as:[9]

$$\alpha^{PR}(T) = \left[1 + m(1 - \sqrt{T_r})\right]^2 \quad (6)$$

$$m = 0.37464 + 1.54226\omega - 0.26992\omega^2 \quad (7)$$

where ω is acentric factor and T_r is the reduced temperature ($T_r = \frac{T}{T_c}$). Different versions of α-function in the PR EOS are available in the literature.

2.2. SRK EOS

SRK EOS[9] is given as:

$$P^{SRK} = \frac{RT}{v^{SRK} - b^{SRK}} - \frac{a^{SRK}}{v^{SRK}\left(v^{SRK} + b^{SRK}\right)} \quad (8)$$

$$a^{SRK}(T) = \frac{1}{9(\sqrt[3]{2} - 1)} \frac{R^2 T_c^2}{P_c} \alpha^{SRK}(T) \quad (9)$$

$$b^{SRK} = \frac{\sqrt[3]{2} - 1}{3} \frac{RT_c}{P_c} \quad (10)$$

where P^{SRK} and v^{SRK} are pressure and molar volume in SRK EOS, respectively, a^{SRK} and b^{SRK} are EOS parameters in SRK EOS, and $\alpha^{SRK}(T)$ is the α-function for SRK EOS. The $\alpha^{SRK}(T)$ term used in the SRK EOS and the VT-SRK EOS models studied in this work is the α-function proposed by Twu *et al.*[10], which can be expressed as:

$$\alpha^{SRK}(T) = T_r^{N^{SRK}(M^{SRK} - 1)} \exp\left[L^{SRK}\left(1 - T_r^{M^{SRK} N^{SRK}}\right)\right] \quad (11)$$

where L^{SRK}, M^{SRK}, and N^{SRK} are substance-dependent parameters. The values of L^{SRK}, M^{SRK}, and N^{SRK} updated by Pina-Martinez[11] are used in this work.

2.3. Volume Translation Methods

A general form of the volume translation term in an EOS can be expressed as:[12]

$$v^{VT-EOS} = v^{EOS} - c \quad (12)$$

where v^{VT-EOS} and v^{EOS} are the corrected molar volume after volume translation and the untranslated molar volume calculated by an EOS, respectively, and c is the volume translation term.

2.3.1. Constant Volume Translation Updated by Pina-Martinez *et al.*[11]

Pina-Martinez *et al.*[11] updated the value of the volume translation term based on the pseudo-experimental saturated liquid volume at $T_r = 0.8$ and optimized the Twu α-function for SRK EOS with three parameters, L^{SRK}, M^{SRK}, and N^{SRK}, as shown in Equation (11). The volume translation in this model is a constant for a given substance, which is given by:

$$c = v_L^{SRK} - v_L^{exp} \quad (13)$$

where v_L^{SRK} is the molar volume calculated from the untranslated SRK EOS and v_L^{exp} is the pseudo-experimental saturated liquid volume obtained from the DIPPR database.[11]

2.3.2. VT-PR EOS Proposed by Ungerer and Batut[2]

Ungerer and Batut[2] proposed a VT model for PR EOS for paraffin, naphthenic, and aromatic hydrocarbons at temperatures under 200ºC and pressures below 120 MPa. The volume translation term is linearly dependent on temperature, as given by:[2]

$$c = -34.5 + 0.46666MW + (0.023 - 0.00056MW)T \quad (14)$$

where MW is molecular weight. The α-function used in this model is calculated by Equations (6) and (7).

2.3.3. VT-PR EOS Proposed by Baled *et al.*[3]

Baled *et al*.[3] proposed a VT model for PR EOS to predict the properties of reservoir fluids under high-temperature and high-pressure conditions. The volume translation term in this model is linearly temperature-dependent and is given by:[3]

$$c = -(A_b + B_b \frac{T}{T_c}) \quad (15)$$

$$A_b, B_b = f(MW, \omega) = k_{b0} + k_{b1} \exp\left(\frac{-1}{k_{b2} MW \omega}\right) + k_{b3} \exp\left(\frac{-1}{k_{b4} MW \omega}\right) + k_{b5} \exp\left(\frac{-1}{k_{b6} MW \omega}\right) \quad (16)$$

where A_b and B_b are model parameters that depend on molecular weight and acentric factor; k_{b0} through k_{b6} are model parameters used to determine A_b and B_b. For determining A_b, k_{b0} to k_{b6} should have the values of -4.1034, 31.723, 0.0531, 188.68, 0.0057, 20.196, and 0.0003, respectively; for determining B_b, k_{b0} to k_{b6} should have the values of -0.3489, -28.547, 0.0687, -817.73, 0.0007, -65.067, and 0.0076, respectively.[3] The α-function calculated by Equations (6) and (7) is also used in this model.

2.3.4. VT-PR EOS Proposed by Magoulas and Tassios[4]

Magoulas and Tassios[4] developed an exponential temperature-dependent volume translation for PR EOS for n-alkanes with carbon numbers between 1 and 20:

$$c = -\left[c_{m0} + (\delta_c - c_{m0}) \exp\left(\beta \left|1 - \frac{T}{T_c}\right|\right)\right] \quad (17)$$

$$c_{m0} = \frac{RT_c}{P_c}(k_{m0} + k_{m1}\omega + k_{m2}\omega^2 + k_{m3}\omega^3 + k_{m4}\omega^4) \quad (18)$$

$$\beta = l_{m0} + l_{m1}\omega^2 \quad (19)$$

$$\delta_c{}^{PR} = \frac{RT_c}{P_c}(Z_c^{PR} - Z_c^{exp}) \quad (20)$$

$$Z_c^{exp} = 0.289 - 0.0701\omega - 0.0207\omega^2 \quad (21)$$

where k_{m0} to k_{m4}, l_{m0} and l_{m1} are model parameters. The values of k_{m0} to k_{m4} are -0.014471, 0.067498, -0.084852, 0.067298, and -0.017366, respectively. The values of l_{m0} and l_{m1} are -10.2447 and -28.6312, respectively. $\delta_c{}^{PR}$ is the volume correction at the critical temperature in PR EOS, Z_c^{PR} is the critical compressibility factor in PR EOS with a universal value of 0.3074, and Z_c^{exp} is the experimental critical compressibility factor that can be estimated by Equation (21). Magoulas and Tassios[4] suggested using Equation (6) to calculate the α-function with the m term calculated by Equation (22) instead of Equation (7):

$$m = d_{m0} + d_{m1}\omega + d_{m2}\omega^2 + d_{m3}\omega^3 + d_{m4}\omega^4 \quad (22)$$

where d_{m0} to d_{m4} are model parameters with the values of 0.384401, 1.52276, -0.213808, 0.034616, and -0.001976, respectively.[4]

2.3.5. VT-PR EOS Proposed by Shi *et al.*[5]

Shi *et al.*[5] developed an exponential temperature-dependent VT model for PR EOS with the constraint proposed by Shi and Li.[13] The constraint was applied to avoid the PV

isotherm crossover phenomenon at temperatures up to 1000 K and pressures up to 100 MPa. The expression is given as:[5]

$$c = \frac{Z_c^{exp} RT_c}{P_c}\left\{A_s \exp\left[-\frac{(\frac{T}{T_c}-1)^2}{2{B_s}^2}\right] + C_s\right\} \quad (23)$$

where A_s, B_s, and C_s are substance-dependent model parameters. The α-function revised by Le Guennec *et al*.[14] is applied together with this VT model:

$$\alpha^{PR}(T) = (\frac{T}{T_c})^{2(M_s-1)} \exp\left\{L_s\left[1-(\frac{T}{T_c})^{2M_s}\right]\right\} \quad (24)$$

$$M_s = 0.1760\omega^2 - 0.2600\omega + 0.8884 \quad (25)$$

$$L_s = 0.1290\omega^2 + 0.6039\omega + 0.0877 \quad (26)$$

2.3.6. VT-PR EOS Proposed by Abudour *et al*.[6]

The VT model proposed by Abudour *et al*.[6] is presented as below:

$$c = -\left[c_{a0} - {\delta_c}^{PR}\left(\frac{0.35}{0.35+d^{PR}}\right)\right] \quad (27)$$

$$c_{a0} = \frac{RT_c}{P_c}\left[c_{a1} - (0.004 + c_{a1})\exp(-2d^{PR})\right] \quad (28)$$

$$d^{PR} = \frac{1}{RT_c}\left(\frac{\partial P^{PR}}{\partial \rho}\right)_T = -\frac{{v^{PR}}^2}{RT_c}\left(\frac{\partial P^{PR}}{\partial v^{PR}}\right)_T = \frac{{v^{PR}}^2}{RT_c}\left[\frac{RT}{(v^{PR}-b^{PR})^2} - \frac{2a^{PR}(v^{PR}+b^{PR})}{\left({v^{PR}}^2+2v^{PR}b^{PR}-{b^{PR}}^2\right)^2}\right] \quad (29)$$

where c_{a1} is a substance-dependent parameter, d^{PR} is the dimensionless distance function in PR EOS, 0.35 is a universal constant for all substances, and ρ is molar density. To avoid iterative solutions, d^{PR} is calculated from the untranslated PR EOS. The

distance function represents the distance between the critical point and the point of interest on the PV isotherm. [6] In this model, the α-function developed by Gasem *et al.*[15] is used:

$$\alpha^{PR}(T) = \exp\left\{(A_a + B_a\frac{T}{T_c})\left[1 - \left(\frac{T}{T_c}\right)^{c_a + D_a\omega + E_a\omega^2}\right]\right\} \quad (30)$$

where A_a to E_a are model parameters with the values of 2.0, 0.836, 0.134, 0.508, and −0.0467, respectively.[6]

2.3.7. VT-SRK EOS Proposed by Chen and Li[7]

Chen and Li[7] developed a VT model with three substance-dependent parameters for SRK EOS by modifying the distance function:

$$c = c_{c1}\left(\frac{RT_c}{P_c}\right) + {\delta_c}^{SRK}\left(\frac{1}{c_{c2} + c_{c3}d^{SRK}}\right) \quad (31)$$

$${\delta_c}^{SRK} = \frac{RT_c}{P_c}(Z_c^{SRK} - Z_c^{exp}) \quad (32)$$

where c_{c1}, c_{c2}, and c_{c3} are substance-dependent parameters, ${\delta_c}^{SRK}$ is the volume correction at the critical temperature in SRK EOS, Z_c^{SRK} is the critical compressibility factor in SRK EOS with a universal value of $\frac{1}{3}$, and d^{SRK} is the distance function calculated by the untranslated SRK EOS:

$$d^{SRK} = \frac{1}{RT_c}\left(\frac{\partial P^{SRK}}{\partial \rho}\right)_T = -\frac{{v^{SRK}}^2}{RT_c}\left(\frac{\partial P^{SRK}}{\partial v^{SRK}}\right)_T = \frac{{v^{SRK}}^2 T}{T_c\left(v^{SRK} - b^{SRK}\right)^2} - \frac{a^{SRK}(2v^{SRK} + b^{SRK})}{RT_c\left(v^{SRK} + b^{SRK}\right)^2} \quad (33)$$

2.4. Numerical Procedure for Calculating κ_T and α_P Using the Distance-Function-Based VT Models

Because the molar volume calculated with the distance-function-based VT models is a function of both temperature and pressure, analytical expressions of κ_T and α_P cannot be obtained using the distance-function-based VT-EOS models proposed by Abudour *et al*.[6] and Chen and Li.[7] Therefore, a numerical method should be used for calculating κ_T and α_P based on the distance-function-based VT models. The central finite difference method is the simplest way to numerically calculate the derivatives by approximating the partial derivative as the slope of the secant line of two adjacent points at the point of interest (i.e., (T_i, P_i) in this case).[16] With temperature and pressure condition, (T_i, P_i), at the point of interest as input information, the secant line slope used to calculate κ_T at this input point, $\frac{\Delta v}{2\Delta P}$, can be obtained from the molar volumes calculated at two adjacent points (i.e., $(T_i, P_i + \Delta P)$ and $(T_i, P_i - \Delta P)$):

$$\frac{\Delta v}{2\Delta P} = \frac{v(T_i, P_i + \Delta P) - v(T_i, P_i - \Delta P)}{2\Delta P} \quad (34)$$

where Δv is the molar volume change and ΔP is the pressure difference. Similarly, the secant line slope for calculating α_P at (T_i, P_i), $\frac{\Delta v}{2\Delta T}$, can be obtained from the molar volumes at the adjacent points (i.e., $(T_i + \Delta T, P_i)$ and $(T_i - \Delta T, P_i)$):

$$\frac{\Delta v}{2\Delta T} = \frac{v(T_i + \Delta T, P_i) - v(T_i - \Delta T, P_i)}{2\Delta T} \quad (35)$$

where ΔT is the temperature difference. The slope of the secant line converges to the slope of the tangent line at the point of interest (i.e., (T_i, P_i)) only when ΔT or ΔP approaches zero. Therefore, the following relations can be obtained:

$$\left(\frac{\partial v}{\partial P_i}\right)_{T_i} = \lim_{\Delta P \to 0} \frac{v(T_i, P_i+\Delta P) - v(T_i, P_i-\Delta P)}{2\Delta P} \quad (36)$$

$$\left(\frac{\partial v}{\partial T_i}\right)_{P_i} = \lim_{\Delta T \to 0} \frac{v(T_i+\Delta T, P_i) - v(T_i-\Delta T, P_i)}{2\Delta T} \quad (37)$$

The sensitivity of Δv to the values of ΔT and ΔP should be evaluated to determine the appropriate values of ΔT and ΔP to ensure that the calculations by Equations (36) and (37) are sufficiently accurate. To calculate $\left(\frac{\partial v}{\partial P_i}\right)_{T_i}$ at a given temperature and pressure point, (T_i, P_i), the molar volumes at $(T_i, P_i + \Delta P)$, (T_i, P_i), and $(T_i, P_i - \Delta P)$ are obtained from a VT-EOS model with an initial value of ΔP. The secant line slope at (T_i, P_i) is calculated by Equation (34). By gradually reducing ΔP, the value of the secant line slope at each ΔP can be evaluated. When ΔP is reduced to a sufficiently small value and the slope of the secant line does not change significantly even if ΔP is further reduced, the convergence of the secant line slope is considered to be reached. Consequently, this converged value of the secant line slope can be considered as the value of $\left(\frac{\partial v}{\partial P_i}\right)_{T_i}$ at (T_i, P_i). As such, the value of κ_T at (T_i, P_i) can be evaluated by using Equation (1). A similar approach should be implemented to determine $\left(\frac{\partial v}{\partial T_i}\right)_{P_i}$ and α_P. A sensitivity analysis is needed to determine appropriate ΔT and ΔP that can be used as the maximum allowable temperature and pressure differences to approximate the partial derivatives of molar volume.

CO_2 and CH_4 are not only greenhouse gases but also two fluids frequently encountered in petroleum engineering. CO_2 injection has been widely used in hydrocarbon reservoirs for enhancing oil recovery.[17] CH_4 is the main component of natural gas, and it can be used as an injection gas in enhanced oil recovery methods as well.[18,19] CO_2 can also be used to replace CH_4 in natural gas hydrates without causing damage to the gas hydrate reservoirs.[20,21] Therefore, CO_2 and CH_4 are selected as two pure example fluids to evaluate the prediction accuracy of κ_T and α_P by different VT models.

References

[1] Pina-Martinez, A.; Le Guennec, Y.; Privat, R.; Jaubert, J. N.; Mathias, P. M. Analysis of the combinations of property data that are suitable for a safe estimation of consistent Twu α-function parameters: Updated parameter values for the translated-consistent tc-PR and tc-RK cubic equations of state. *J. Chem. Eng. Data* **2018,** *63* (10), 3980–3988.

[2] Ungerer, P.; Batut, C.; Prédiction des propriétés volumétriques des hydrocarbures par une translation de volume améliorée. *Rev. Inst. Fr. Pét.* **1997**, *52* (6), 609–623.

[3] Baled, H.; Enick, R. M.; Wu, Y.; McHugh, M. A.; Burgess, W.; Tapriyal, D.; Morreale, B. D. Prediction of hydrocarbon densities at extreme conditions using volume-translated SRK and PR equations of state fit to high temperature, high pressure PVT data. *Fluid Phase Equilib*. **2012**, *317*, 65–76.

[4] Magoulas, K.; Tassios, D. Thermophysical properties of n-alkanes from C1 to C20 and their prediction for higher ones. *Fluid Phase Equilib*. **1990**, *56*, 119–140.

[5] Shi, J.; Li, H.; Pang, W. An improved volume translation strategy for PR EOS without crossover issue. *Fluid Phase Equilib*. **2018**, *470*, 164–175.

[6] Abudour, A. M.; Mohammad, S. A.; Robinson, R. L.; Gasem, K. A. M. Volume-translated Peng–Robinson equation of state for saturated and single-phase liquid densities. *Fluid Phase Equilib*. **2012**, *335*, 74–87.

[7] Chen, X.; Li, H. An improved volume-translated SRK EOS dedicated to more accurate determination of saturated and single-phase liquid densities. *Fluid Phase Equilib.* **2020**, *521*, No. 112724.

[8] Peng, D. Y.; Robinson, D. B. A new two-constant equation of state. *Ind. Eng. Chem. Fundam.* **1976**, *15* (1), 59–64.

[9] Soave, G. Equilibrium constants from a modified Redlich-Kwong equation of state. *Chem. Eng. Sci.* **1972**, *27* (6), 1197–1203.

[10] Twu, C. H.; Bluck, D.; Cunningham, J. R.; Coon, J. E. A cubic equation of state with a new alpha function and a new mixing rule. *Fluid Phase Equilib*. **1991**, *69*, 33–50.

[11] Pina-Martinez, A.; Le Guennec, Y.; Privat, R.; Jaubert, J. N.; Mathias, P. M. Analysis of the combinations of property data that are suitable for a safe estimation of consistent Twu α-function parameters: Updated parameter values for the translated-consistent tc-PR and tc-RK cubic equations of state. *J. Chem. Eng. Data* **2018,** *63* (10), 3980–3988.

[12] Péneloux, A.; Rauzy, E.; Fréze, R. A consistent correction for Redlich-Kwong-Soave volumes. *Fluid Phase Equilib*. **1982**, *8* (1), 7–23.

[13] Shi, J.; Li, H. Criterion for determining crossover phenomenon in volume-translated equation of states. *Fluid Phase Equilib*. **2016**, *430*, 1–12.

[14] Le Guennec, Y.; Lasala, S.; Privat, R.; Jaubert, J. N. A consistency test for α-functions of cubic equations of state. *Fluid Phase Equilib*. **2016**, *427*, 513–538.

[15] Gasem, K. A. M.; Gao, W.; Pan, Z.; Robinson Jr., R. L. A modified temperature dependence for the Peng-Robinson equation of state. *Fluid Phase Equilib*. **2001**, *181* (1–2), 113–125.

[16] Daridon, J. L.; Bazile, J. P. Computation of liquid isothermal compressibility from density measurements: An application to toluene. *J. Chem. Eng. Data* **2018**, *63* (6), 2162–2178.

[17] Izgec, O.; Demiral, B.; Bertin, H. J.; Akin, S. CO_2 injection in carbonates; *SPE Western Regional Meeting*, Irvine, California, March 2005; SPE-93773-MS.

[18] Cho, J.; Park, G.; Kwon, S.; Lee, K. S.; Lee, H. S.; Min, B. Compositional modeling to analyze the effect of CH_4 on coupled carbon storage and enhanced oil recovery process. *Appl. Sci.* **2020**, *10* (12), 4272.

[19] Zanganeh, P.; Dashti, H.; Ayatollahi, S. Comparing the effects of CH_4, CO_2, and N_2 injection on asphaltene precipitation and deposition at reservoir condition: A visual and modeling study. *Fuel* **2018**, *217*, 633–641.

[20] Zhu, T.; McGrail, P.; Kulkarni, A.; White, M. D.; Phale, H. A. Development of a thermodynamic model and reservoir simulator for the CH_4, CO_2, and CH_4-CO_2 gas

hydrate system; *SPE Western Regional Meeting*, Irvine, California, March 2005; SPE-93976-MS.

[21] Choi, W.; Lee, Y.; Seo, Y. Experimental verification of CH_4-CO_2 replacement in various gas hydrate structures for CH_4 production and CO_2 sequestration; *The Twenty-eighth International Ocean and Polar Engineering Conference*, Sapporo, Japan, June 2018; ISOPE-I-18-735.

CHAPTER 3 RESULTS AND DISCUSSION

The predictions of κ_T and α_P are conducted by the VT models studied in this work for pure CO_2 and CH_4. Figure 1 shows the temperature and pressure ranges examined in this study. Since κ_T and α_P can vary in different phase states,[1,2] three phase regions are considered, which are the liquid-phase region, the vapor-phase region, and the supercritical-phase region. The predictions are made between the triple point temperature (T_{triple}) and $T_r = 3$ for each substance. The pressure range starts from the reduced pressure ($P_r = \frac{P}{P_c}$) of 0.1 to $P_r = 3$. Table 1 lists the properties of CO_2 and CH_4 (including critical temperature, critical pressure, critical compressibility factor, acentric factor, and molecular weight), the temperature and pressure ranges examined in this study as well as the number of the predicted data. Table 2 lists the substance-dependent parameters in the studied VT models that are retrieved from the literature.[3-6]

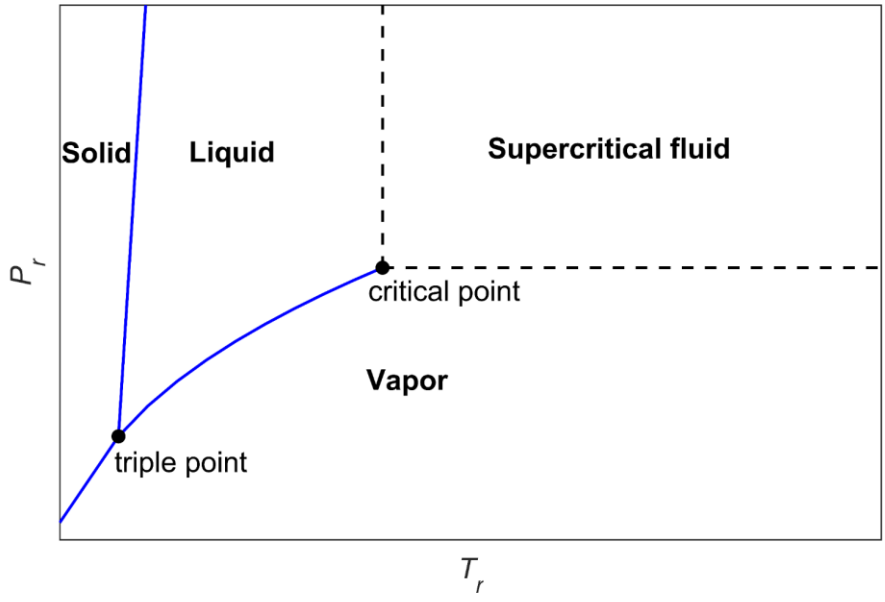

Figure 1 Different regions in the phase diagram of a pure substance.

Table 1 Physical properties of CO_2 and CH_4.[7]

Substance	T_c (K)	P_c (MPa)	ω	Z_c	MW (g/mol)	Temperature range (K)	Pressure range (MPa)	Number of data points
CO_2	304.128	7.3770	0.22394	0.27493	44.0095	217-912	0.7377-22.1310	20810
CH_4	190.564	4.5992	0.01140	0.28640	16.0425	91-571	0.45992-13.7976	14371

Table 2 Model parameters in the various VT-EOS models for CO_2 and CH_4.

Substance	Parameters of the Shi *et al*. VT-PR EOS[6]			Parameters of the Abudour *et al*. VT-PR EOS[3]	Parameters of the Chen and Li VT-SRK EOS[5]			Constant VT updated by Pina-Martinez *et al*.[4]	Parameters of the α-function in the SRK EOS[4]		
	A_s	B_s	C_s	c_{a1}	c_{c1}	c_{c2}	c_{c3}	c (cm^3/mol)	L^{SRK}	M^{SRK}	N^{SRK}
CO_2	0.0320	0.1053	-0.0173	0.00652	0.00608	0.92912	2.65917	4.1585	0.2806	0.8684	2.2782
CH_4	0.0228	0.1288	-0.0429	0.01313	-0.00195	0.79540	2.13497	2.0509	0.2170	0.9082	1.8172

To evaluate the performance of different VT models, the predicted κ_T and α_P are compared with the pseudo-experimental data provided by the National Institute of Standards and Technology (NIST) Web Thermo Tables (WTT) Standard Reference Database Version 2-2012-1-Pro.[7] The absolute average percentage deviation (*%AAD*) is used as a performance indicator:

$$\%AAD = \frac{100}{N}\sum_{i=1}^{N}\left|\frac{Y^{EOS}-Y^{exp}}{Y^{exp}}\right|_i \quad (38)$$

where N is the number of data points, Y^{EOS} is the property calculated by the EOS model, and Y^{exp} is the pseudo-experimental value obtained from NIST.[7] In addition, the relative deviation (*%RD*) is used to demonstrate the model performance for the predicted κ_T along an isotherm and the predicted α_P along an isobar:

$$\%RD = 100 \times \left(\frac{Y^{EOS} - Y^{exp}}{Y^{exp}}\right) \quad (39)$$

3.1. Sensitivity Analysis on the Numerical Calculations of κ_T and α_P

To determine appropriate ΔT and ΔP that can be used as the maximum allowable temperature and pressure differences to approximate the partial derivatives of molar volume, the sensitivity analysis on the numerical calculations of κ_T and α_P is conducted based on the calculations for liquid CH_4 by the untranslated SRK EOS[8]. Figure 2 shows the difference between $\frac{\Delta v_i}{2\Delta T_i}$ and $\frac{\Delta v_{i-1}}{2\Delta T_{i-1}}$ (i.e., $\varepsilon = \left|\frac{\Delta v_i}{2\Delta T_i} - \frac{\Delta v_{i-1}}{2\Delta T_{i-1}}\right|$ $cm^3\ mol^{-1}\ K^{-1}$) calculated at $P_r = 1$ and different temperatures with a decreasing ΔT. It is obvious that the value of $\frac{\Delta v}{2\Delta T}$ can converge to a constant when ΔT is reduced to 1×10^{-3} K and below.

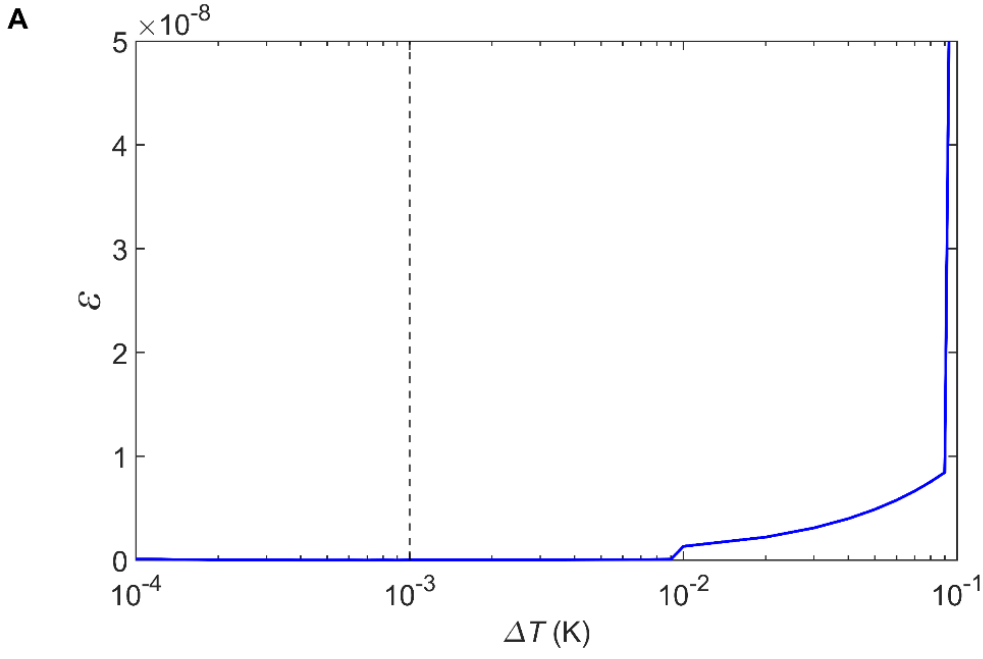

B

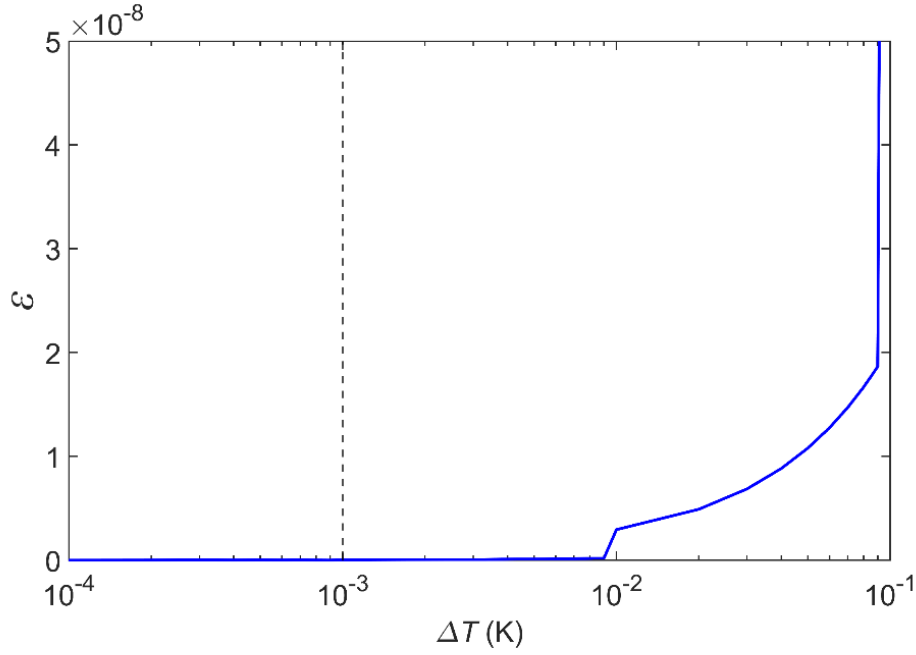
×10^-8
5
4
3
2
1
0
ε
10^-4
10^-3
10^-2
10^-1
ΔT (K)

C

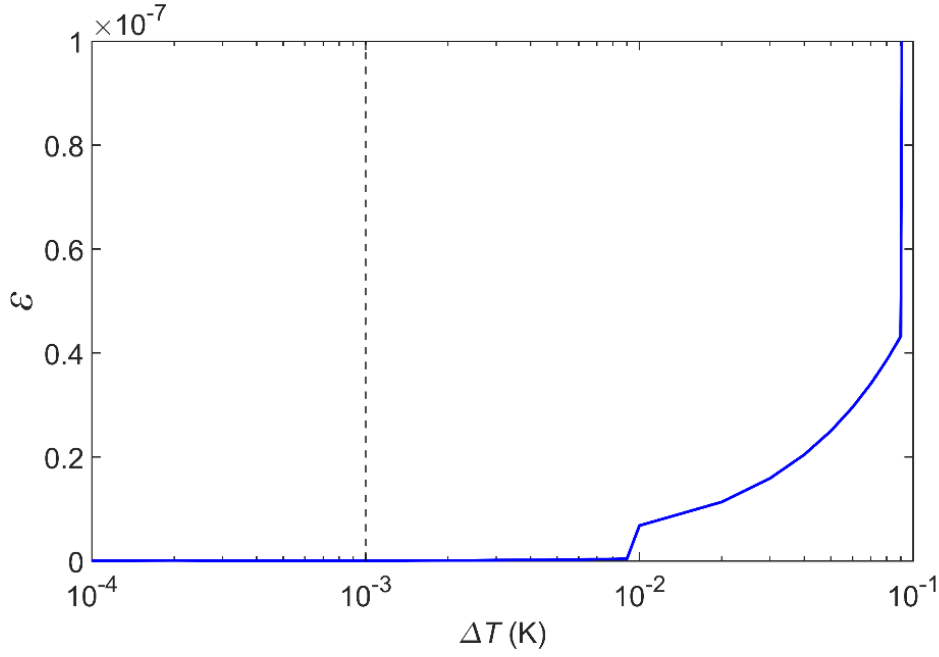
×10^-7
1
0.8
0.6
0.4
0.2
0
ε
10^-4
10^-3
10^-2
10^-1
ΔT (K)

D

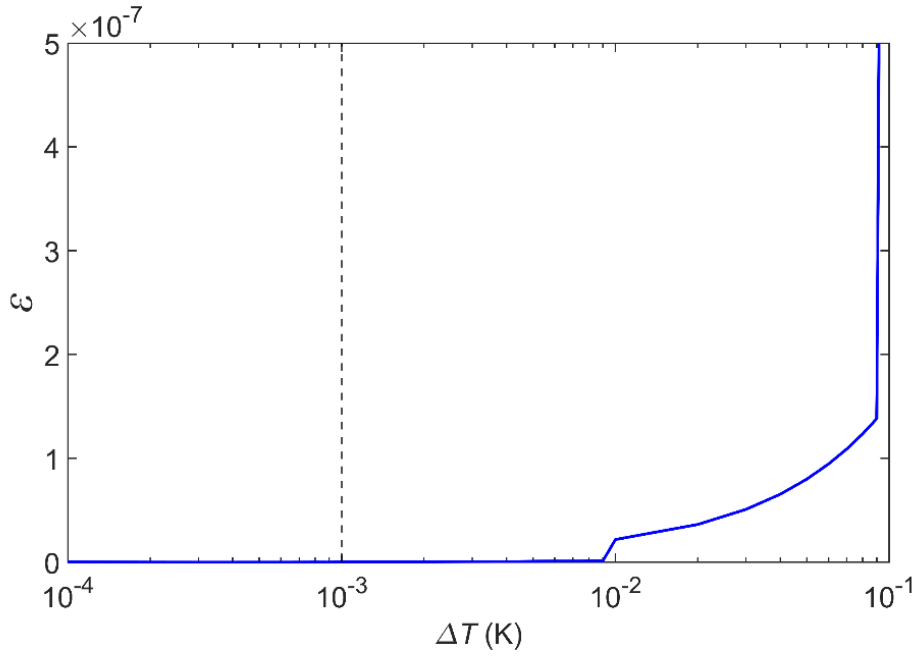
×10^-7
5
4
3
2
1
0
ε
10^-4
10^-3
10^-2
10^-1
ΔT (K)

E

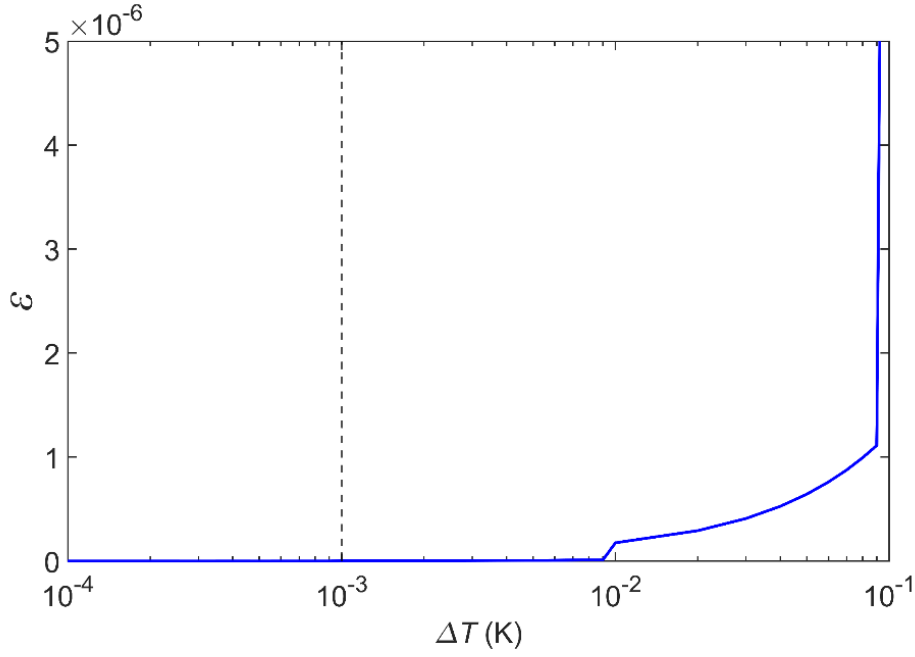
×10^-6
5
4
3
2
1
0
ε
10^-4
10^-3
10^-2
10^-1
ΔT (K)

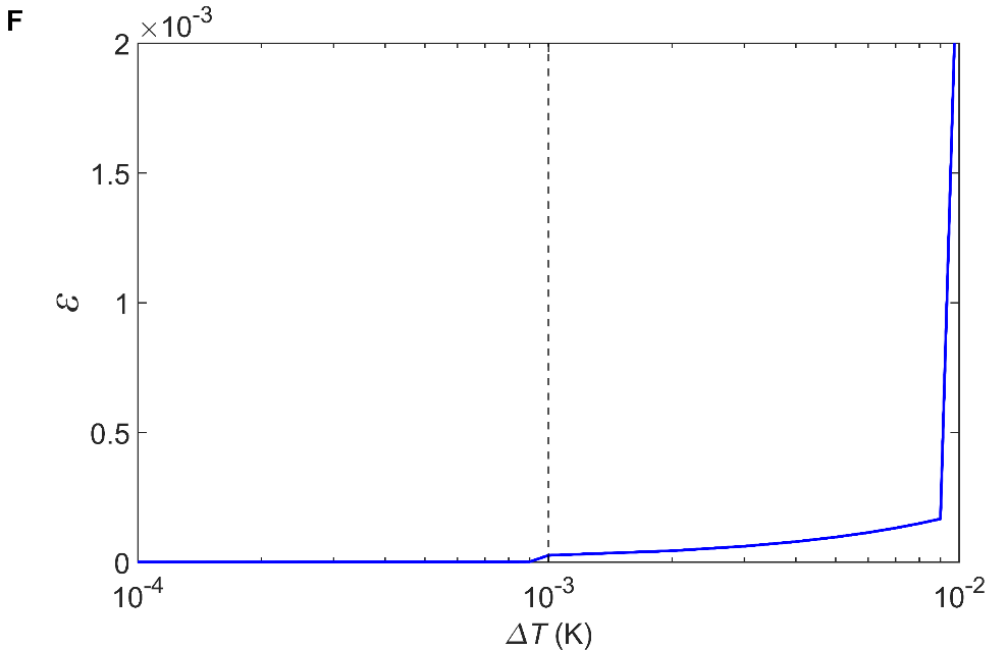

Figure 2 The difference between $\frac{\Delta v_i}{2\Delta T_i}$ and $\frac{\Delta v_{i-1}}{2\Delta T_{i-1}}$ ($\varepsilon = \left|\frac{\Delta v_i}{2\Delta T_i} - \frac{\Delta v_{i-1}}{2\Delta T_{i-1}}\right|$ cm^3 mol^{-1} K^{-1}) calculated by using the untranslated SRK EOS[8] for the liquid-phase CH_4 when the temperature difference (ΔT) is reduced. The calculations are done at P_r = 1 and different temperatures: the triple point temperature (A), T_r = 0.6 (B), T_r = 0.7 (C), T_r = 0.8 (D), T_r = 0.9 (E), and T_r = 1 (F).

Figure 3 shows the difference between $\frac{\Delta v_i}{2\Delta P_i}$ and $\frac{\Delta v_{i-1}}{2\Delta P_{i-1}}$ (i.e., $\varepsilon = \left|\frac{\Delta v_i}{2\Delta P_i} - \frac{\Delta v_{i-1}}{2\Delta P_{i-1}}\right|$ cm^3 mol^{-1} MPa^{-1}) at $T_r = 1$ and different pressures when ΔP is reduced. It can be seen from Figure 3 that the convergence of $\frac{\Delta v}{2\Delta P}$ can be reached as ΔP is reduced to $1 \times 10^{-6} \times P_c$ MPa and below. Therefore, $\Delta P = 1 \times 10^{-6} \times P_c$ MPa and $\Delta T = 1 \times 10^{-3}$ K are adopted to approximate the partial derivatives appearing in Equations (36) and (37), respectively.

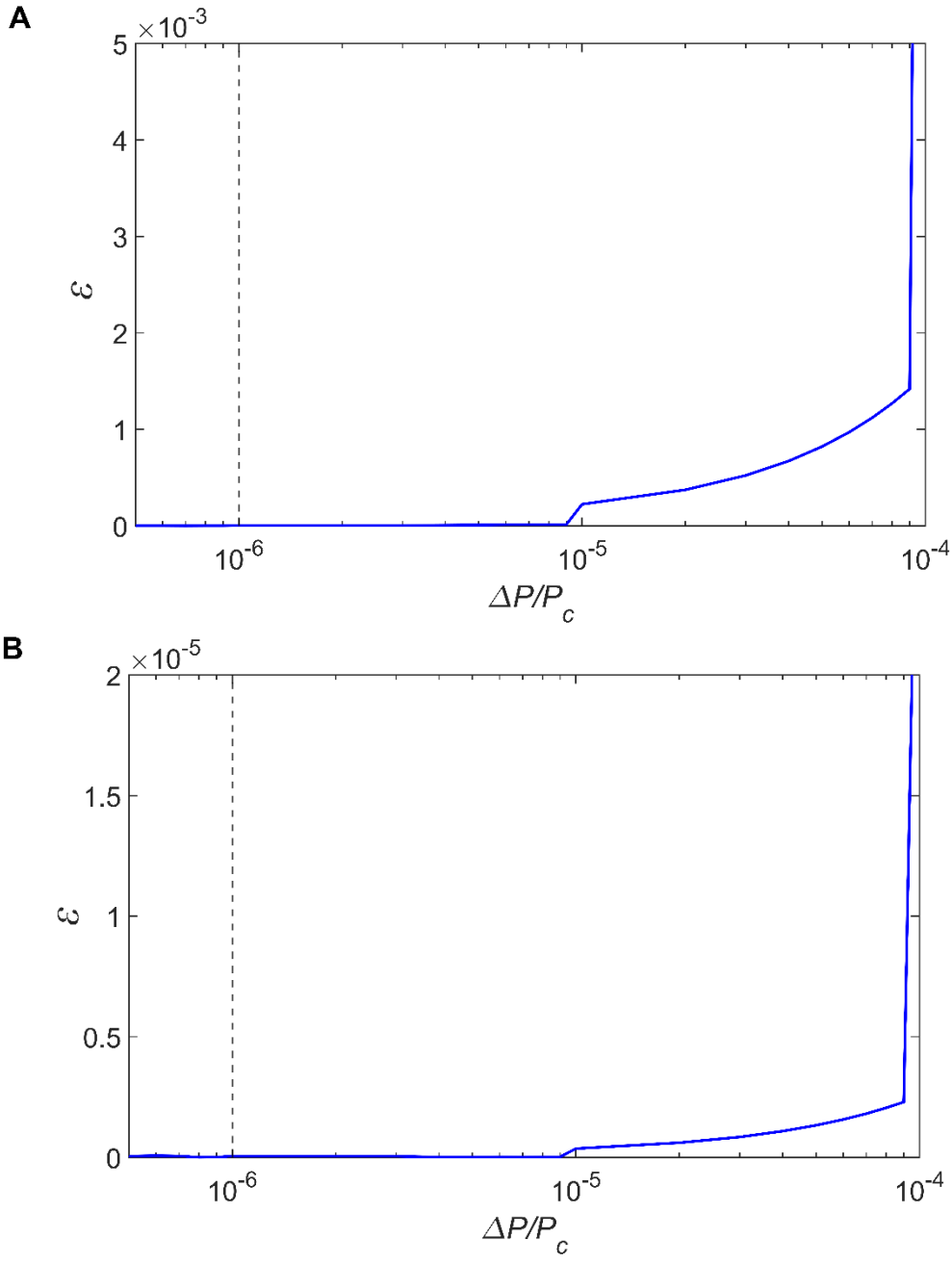
A
×10^-3
5
4
3
2
1
0
ε
10^-6
10^-5
10^-4
ΔP/P_c
B
×10^-5
2
1.5
1
0.5
0
ε
10^-6
10^-5
10^-4
ΔP/P_c

C

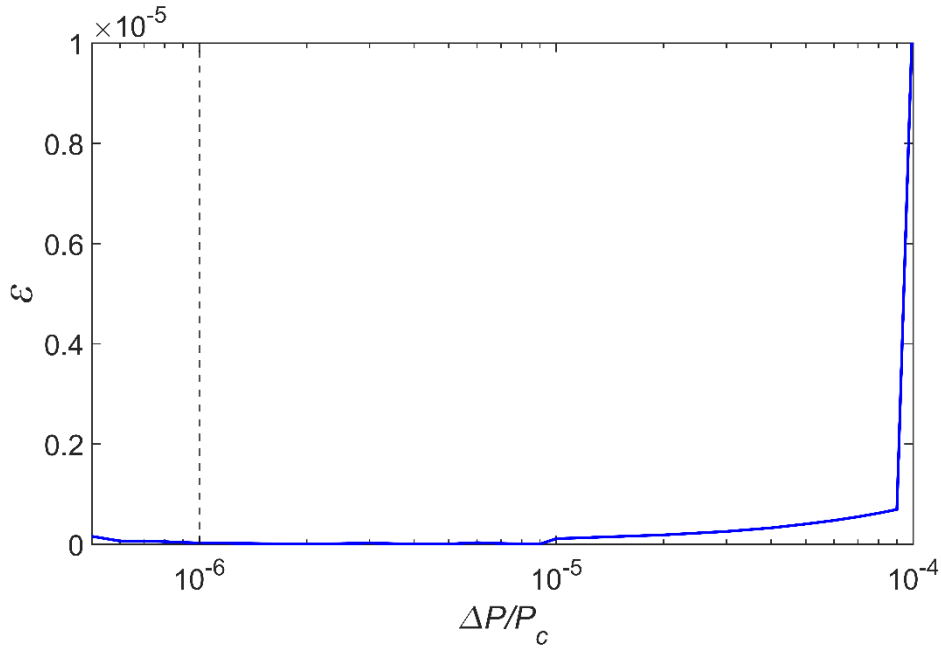

D

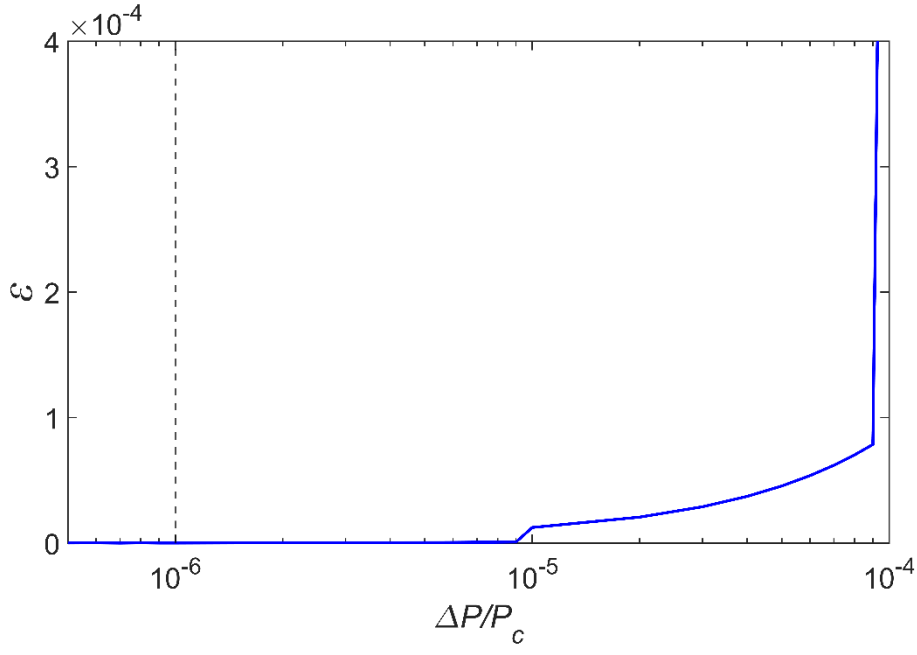

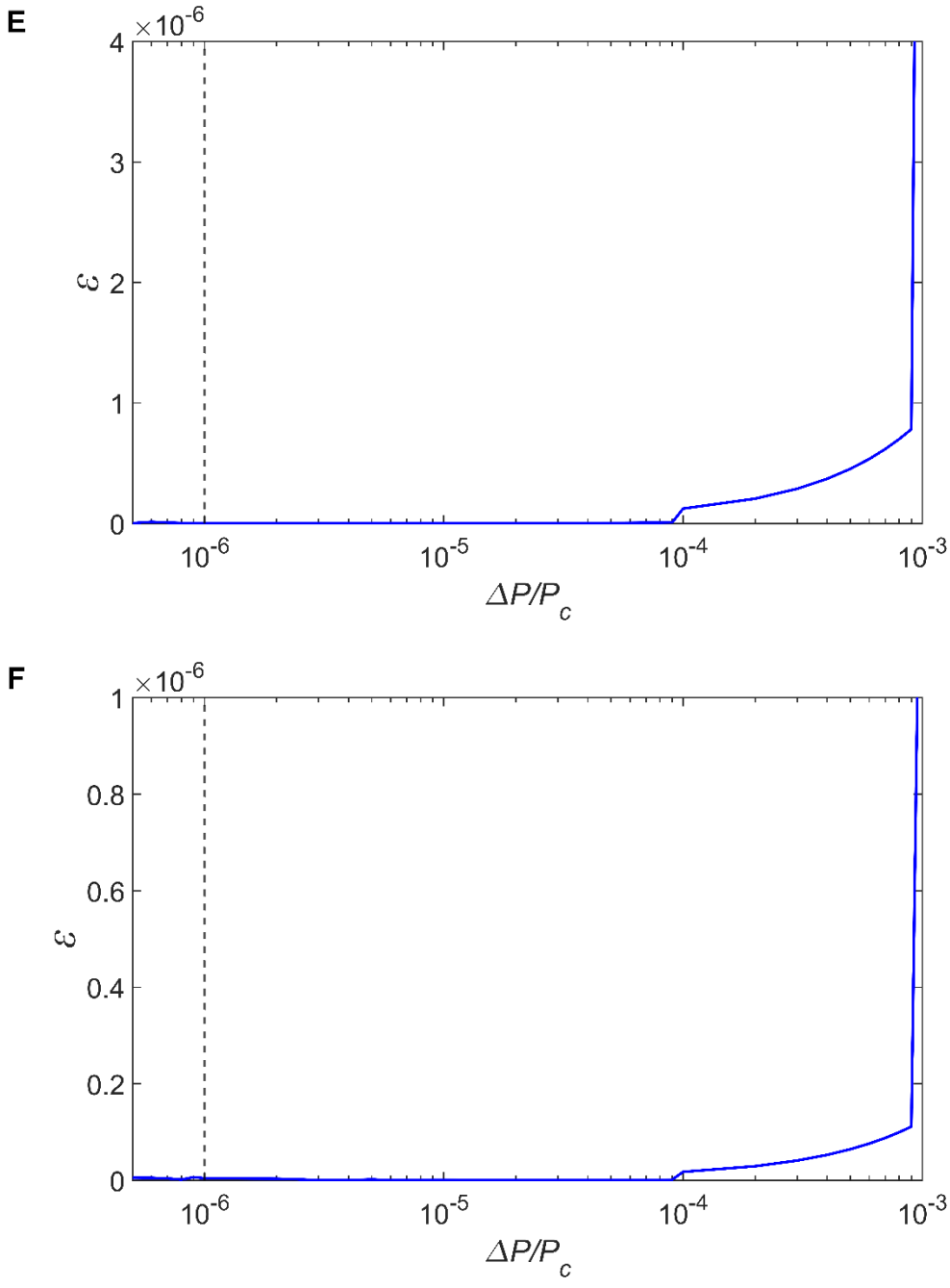

Figure 3 The difference between $\frac{\Delta v_i}{2\Delta P_i}$ and $\frac{\Delta v_{i-1}}{2\Delta P_{i-1}}$ ($\varepsilon = \left|\frac{\Delta v_i}{2\Delta P_i} - \frac{\Delta v_{i-1}}{2\Delta P_{i-1}}\right|$ cm^3 mol^{-1} MPa^{-1}) calculated by using the untranslated SRK EOS[8] for the liquid-phase CH_4 when the pressure difference (ΔP) is reduced. The calculations are done at T_r = 1 and different reduced pressures: P_r = 0.1 (A), P_r = 0.5 (B), P_r = 0.7, (C), P_r = 1 (D), P_r = 1.5 (E), and P_r = 2 (F).

3.2. Predictions of κ_T and α_P

Table 3 lists the *%AADs* of the κ_T predictions yielded by each EOS model for the liquid-phase regions, the vapor-phase regions, and the supercritical-phase regions of CO_2 and CH_4. The calculation results of α_P are presented in Table 4. Tables 3 and 4 show that the VT-PR EOS proposed by Abudour *et al*.[3] yields the best overall results for κ_T predictions with a *%AAD* of 5.11%, while the VT-SRK EOS proposed by Chen and Li[5] yields the best overall results for α_P predictions with a *%AAD* of 2.77%.

Table 3 Comparison of the prediction accuracy of κ_T yielded by different VT-EOS models.

Substance	Phase region	*%AADs* yielded by PR EOS models						*%AADs* yielded by SRK EOS models		
		PR EOS[9]	Ungerer and Batut model[10]	Baled *et al*. model[11]	Magoulas and Tassios model[12]	Shi *et al*. model[6]	Abudour *et al*. model[3]	SRK EOS[8]	Chen and Li model[5]	Constant VT updated by Pina-Martinez *et al*.[4]
			Linear temperature-dependent		Exponential temperature-dependent		Temperature-pressure-dependent		Temperature-pressure-dependent	Constant VT
CO_2	Liquid	52.27	**14.20**	74.00	50.57	50.86	15.93	52.16	18.22	39.73
	Vapor	0.49	1.01	1.29	0.59	**0.35**	0.62	1.12	0.70	1.51
	Supercritical	2.21	5.64	4.90	2.04	2.66	**1.11**	5.31	2.67	6.21
CH_4	Liquid	26.86	25.38	27.11	34.37	21.76	11.05	36.59	**6.81**	30.49
	Vapor	0.72	1.47	0.77	1.02	**0.32**	0.55	0.63	0.56	0.82
	Supercritical	2.84	7.30	2.97	3.52	3.09	**1.41**	4.42	2.26	4.85
Overall		14.23	9.17	18.51	15.35	13.17	**5.11**	16.71	5.20	13.94

Table 4 Comparison of the prediction accuracy of α_P yielded by different VT-EOS models.

Substance	Phase region	*%AADs* yielded by PR EOS models						*%AADs* yielded by SRK EOS models		
		PR EOS[9]	Ungerer and Batut model[10]	Baled *et al.* model[11]	Magoulas and Tassios model[12]	Shi *et al.* model[6]	Abudour *et al.* model[3]	SRK EOS[8]	Chen and Li model[5]	Constant VT updated by Pina-Martinez *et al.*[4]
			Linear temperature-dependent		Exponential temperature-dependent		Temperature-pressure-dependent		Temperature-pressure-dependent	Constant VT
CO_2	Liquid	18.48	12.60	26.75	67.16	13.21	**3.34**	16.72	4.21	9.27
	Vapor	1.39	**0.86**	1.64	1.75	1.48	1.67	1.28	1.59	1.37
	Supercritical	**2.29**	4.70	3.36	4.59	2.35	2.42	5.09	2.88	6.12
CH_4	Liquid	18.09	34.23	17.51	64.44	9.88	7.49	16.60	**5.10**	12.64
	Vapor	1.44	1.35	1.43	1.84	1.33	1.55	0.73	1.19	**0.70**
	Supercritical	3.06	8.10	3.04	4.97	2.58	2.03	2.99	**1.65**	3.44
Overall		7.46	10.30	8.96	24.12	5.14	3.08	7.23	**2.77**	5.59

3.2.1. Predicted Results for the Liquid-phase κ_T and α_P

For the predictions of the liquid-phase κ_T, the Ungerer and Batut VT-PR EOS[10] gives the lowest *%AAD* of 14.20% for CO_2. The Abudour *et al.* VT-PR EOS[3] and the Chen and Li VT-SRK EOS[5] also present good results for CO_2, yielding *%AADs* of 15.93% and 18.22%, respectively. As for the liquid-phase κ_T of CH_4, the Ungerer and Batut model[10] performs poorly with a *%AAD* of 25.38%, while the Abudour *et al.* model[3] and the Chen and Li model[5] maintain their decent accuracy. The VT-PR EOS of Baled *et al.*[11] yields higher *%AADs* of the liquid-phase κ_T predictions than the PR EOS for both CO_2 and CH_4. The Shi *et al.* VT-PR EOS[6] and the constant VT-SRK EOS updated by Pina-Martinez *et al.*[4] only have slight improvement to their corresponding untranslated EOS models. Figure

4 compares the κ_T predicted by each model against the NIST data[7] at different isotherms for the liquid-phase CH_4. Figure 5 shows the same comparison for liquid CO_2. The distribution of *%RDs* as a function of pressure is also illustrated. It is clear that all models give a similar trend of κ_T versus pressure at different temperatures that κ_T decreases with pressure. As temperature approaches the critical temperature, the change of κ_T with pressure becomes more significant. The prediction errors of the liquid-phase κ_T by most VT models tend to be larger at lower pressures for a given temperature.

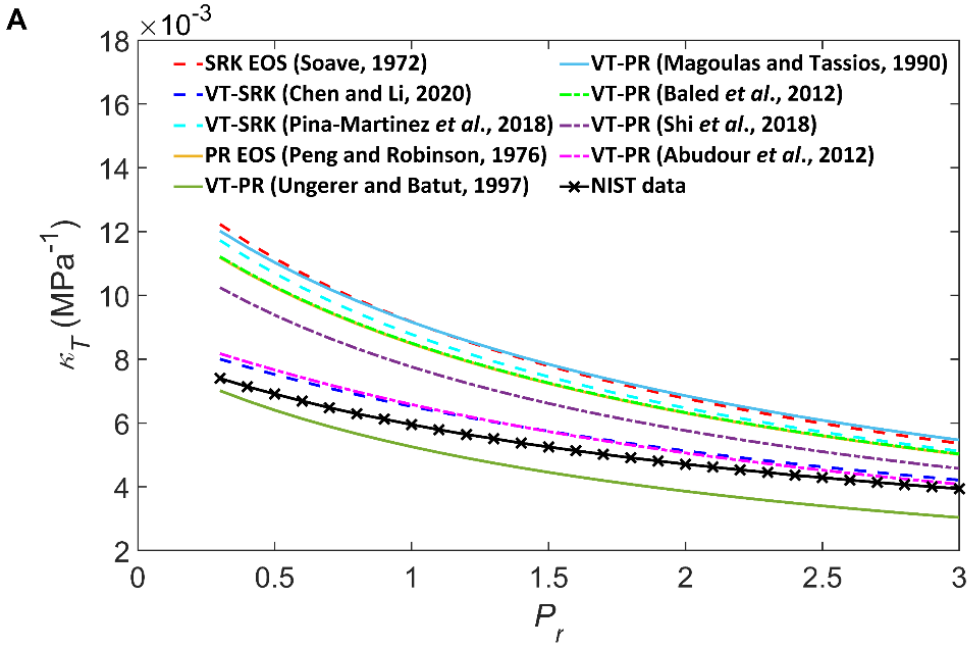

B

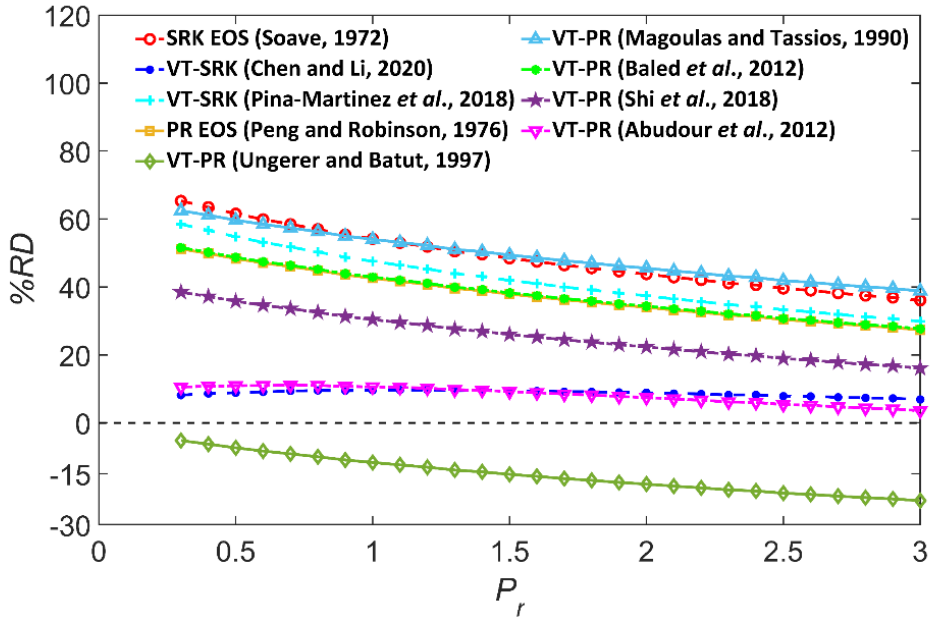
SRK EOS (Soave, 1972)
VT-SRK (Chen and Li, 2020)
VT-SRK (Pina-Martinez et al., 2018)
PR EOS (Peng and Robinson, 1976)
VT-PR (Ungerer and Batut, 1997)
VT-PR (Magoulas and Tassios, 1990)
VT-PR (Baled et al., 2012)
VT-PR (Shi et al., 2018)
VT-PR (Abudour et al., 2012)
%RD
P_r

C

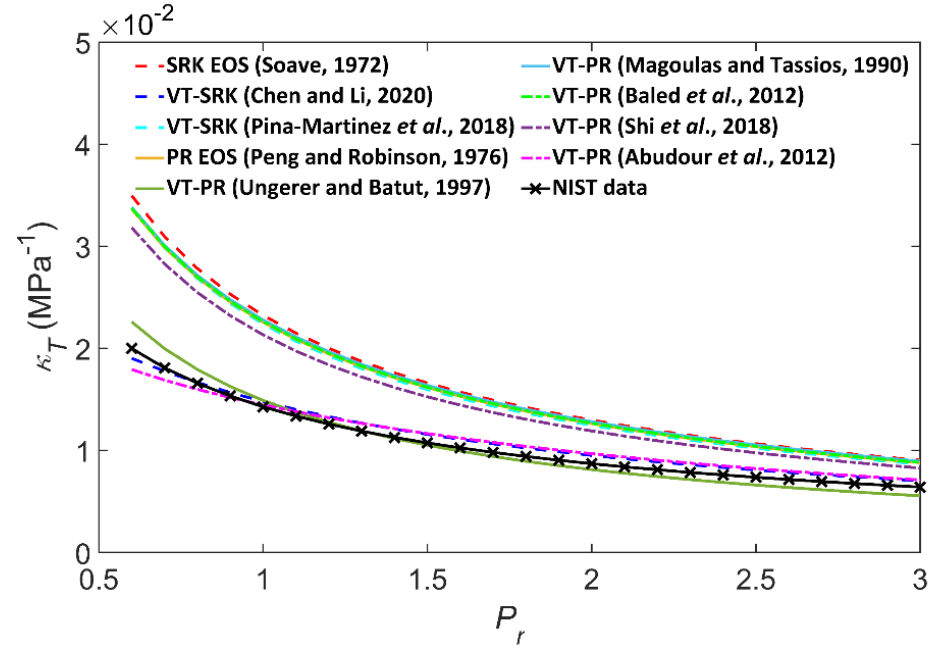
×10^-2
SRK EOS (Soave, 1972)
VT-SRK (Chen and Li, 2020)
VT-SRK (Pina-Martinez et al., 2018)
PR EOS (Peng and Robinson, 1976)
VT-PR (Ungerer and Batut, 1997)
VT-PR (Magoulas and Tassios, 1990)
VT-PR (Baled et al., 2012)
VT-PR (Shi et al., 2018)
VT-PR (Abudour et al., 2012)
NIST data
κ_T (MPa^{-1})
P_r

D

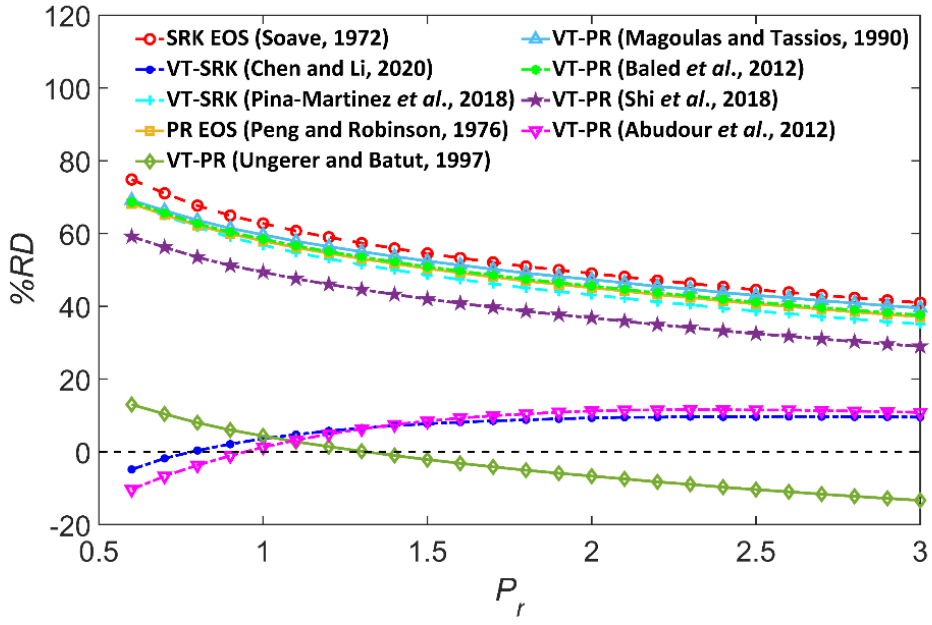
SRK EOS (Soave, 1972)
VT-SRK (Chen and Li, 2020)
VT-SRK (Pina-Martinez et al., 2018)
PR EOS (Peng and Robinson, 1976)
VT-PR (Ungerer and Batut, 1997)
VT-PR (Magoulas and Tassios, 1990)
VT-PR (Baled et al., 2012)
VT-PR (Shi et al., 2018)
VT-PR (Abudour et al., 2012)
%RD
P_r

E

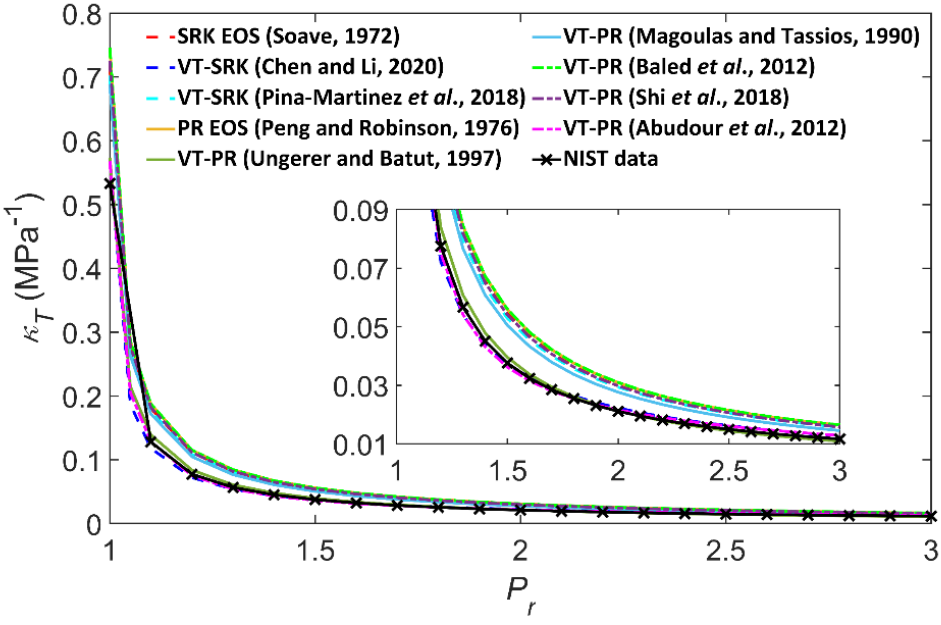
SRK EOS (Soave, 1972)
VT-SRK (Chen and Li, 2020)
VT-SRK (Pina-Martinez et al., 2018)
PR EOS (Peng and Robinson, 1976)
VT-PR (Ungerer and Batut, 1997)
VT-PR (Magoulas and Tassios, 1990)
VT-PR (Baled et al., 2012)
VT-PR (Shi et al., 2018)
VT-PR (Abudour et al., 2012)
NIST data
κ_T (MPa^{-1})
P_r

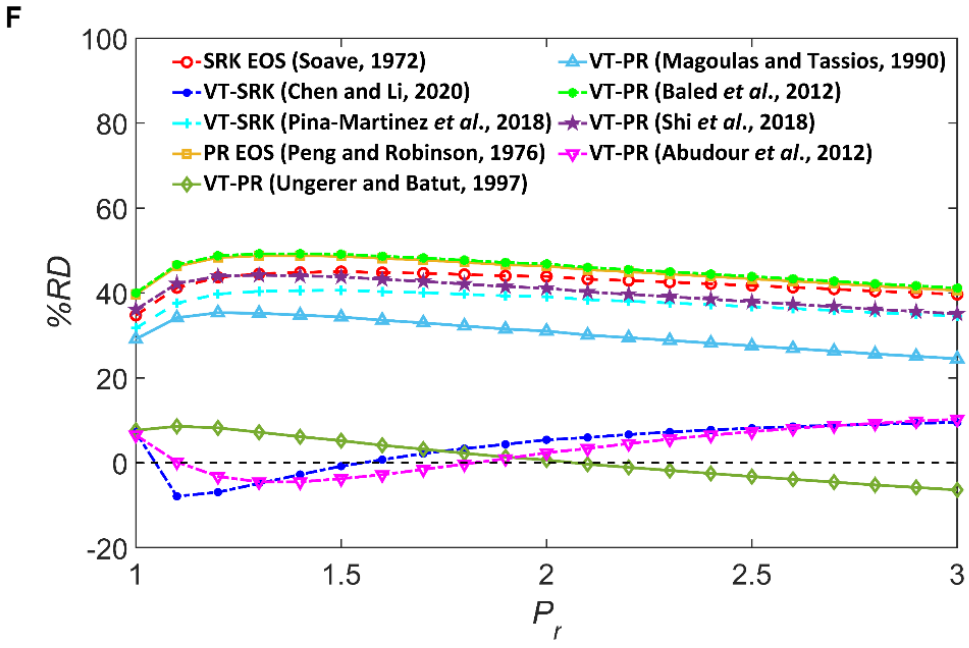

Figure 4 Comparison of the calculated κ_T for the liquid-phase CH_4 against the NIST data (A, C, and E) and *%RDs* yielded by the models studied in this work (B, D, and F) at pressures from the saturated vapor pressures to $P_r = 3$ and different temperatures: $T_r = 0.8$ (A and B), $T_r = 0.9$ (C and D), and $T_r = 1$ (E and F).

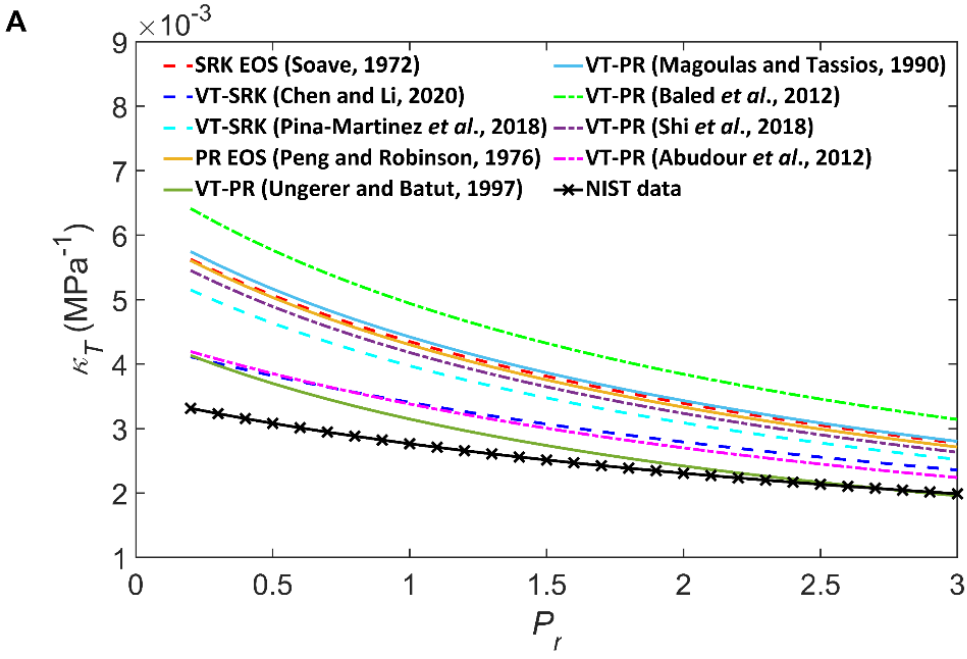

B

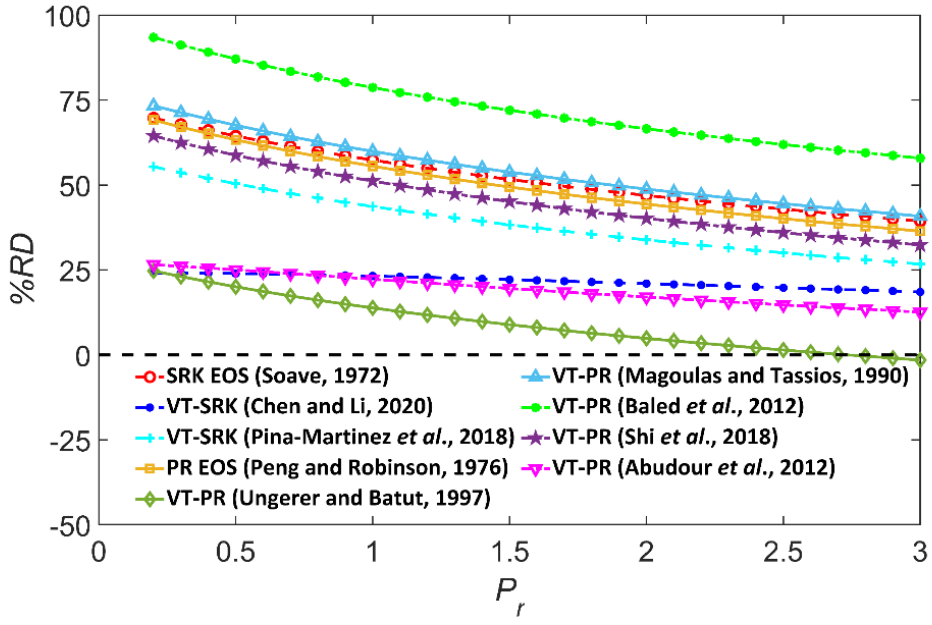
100
75
50
25
0
-25
-50
%RD
0
0.5
1
1.5
2
2.5
3
P_r
SRK EOS (Soave, 1972)
VT-SRK (Chen and Li, 2020)
VT-SRK (Pina-Martinez et al., 2018)
PR EOS (Peng and Robinson, 1976)
VT-PR (Ungerer and Batut, 1997)
VT-PR (Magoulas and Tassios, 1990)
VT-PR (Baled et al., 2012)
VT-PR (Shi et al., 2018)
VT-PR (Abudour et al., 2012)

C

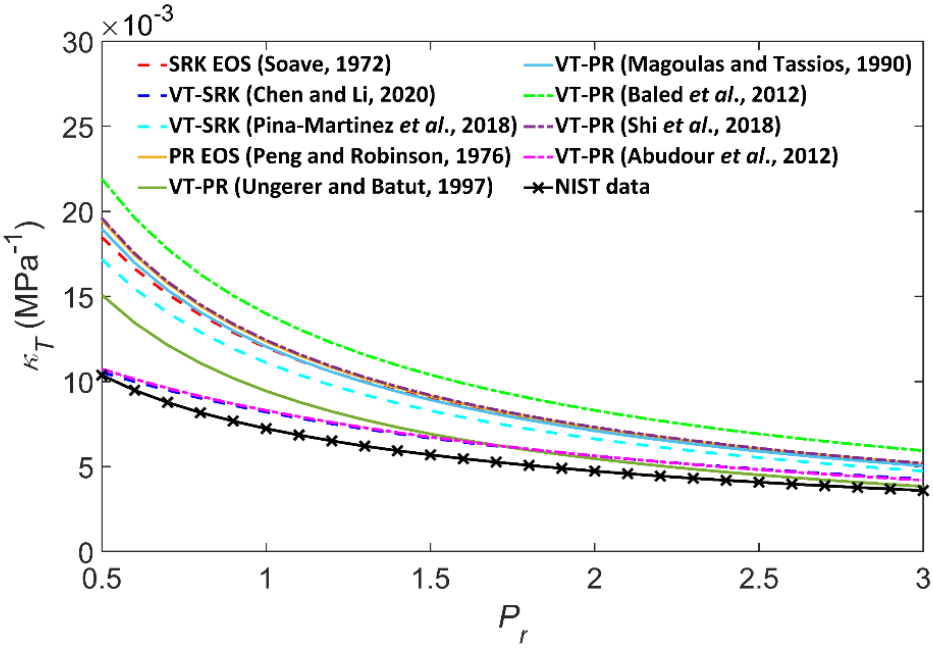
$\times 10^{-3}$
30
25
20
15
10
5
0
κ_T (MPa^{-1})
0.5
1
1.5
2
2.5
3
P_r
SRK EOS (Soave, 1972)
VT-SRK (Chen and Li, 2020)
VT-SRK (Pina-Martinez et al., 2018)
PR EOS (Peng and Robinson, 1976)
VT-PR (Ungerer and Batut, 1997)
VT-PR (Magoulas and Tassios, 1990)
VT-PR (Baled et al., 2012)
VT-PR (Shi et al., 2018)
VT-PR (Abudour et al., 2012)
NIST data

D

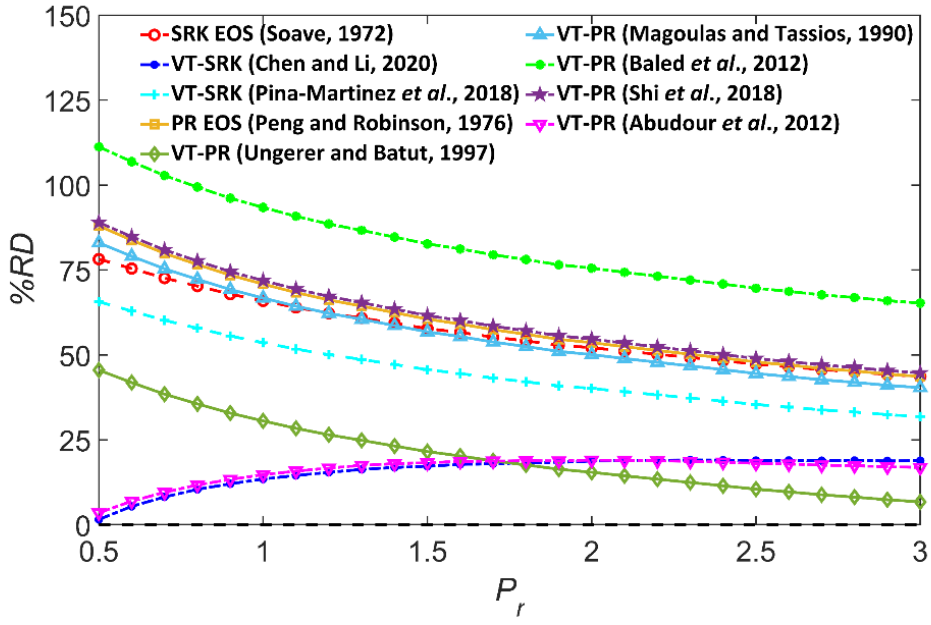
SRK EOS (Soave, 1972)
VT-SRK (Chen and Li, 2020)
VT-SRK (Pina-Martinez et al., 2018)
PR EOS (Peng and Robinson, 1976)
VT-PR (Ungerer and Batut, 1997)
VT-PR (Magoulas and Tassios, 1990)
VT-PR (Baled et al., 2012)
VT-PR (Shi et al., 2018)
VT-PR (Abudour et al., 2012)
%RD
P_r

E

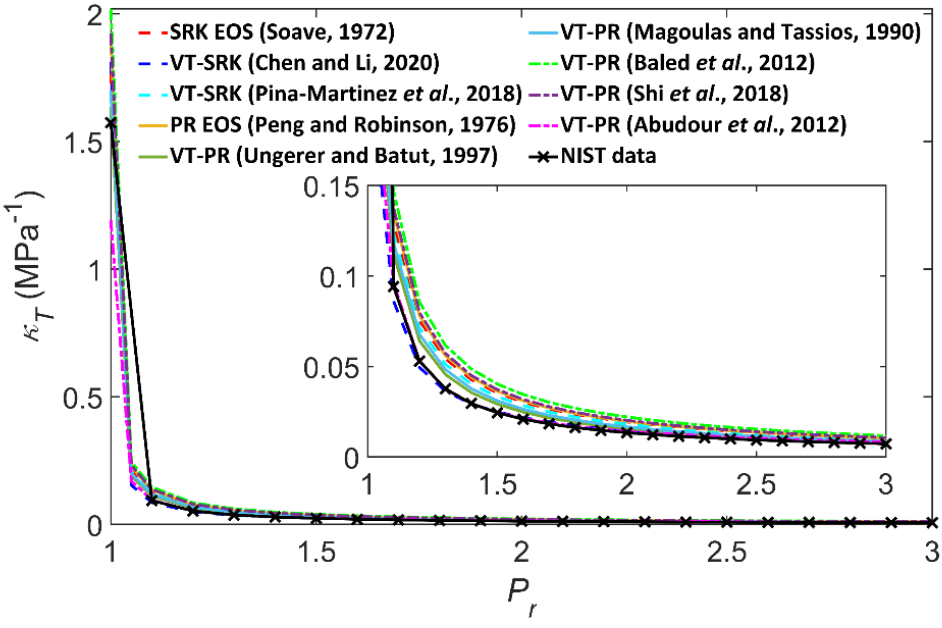
SRK EOS (Soave, 1972)
VT-SRK (Chen and Li, 2020)
VT-SRK (Pina-Martinez et al., 2018)
PR EOS (Peng and Robinson, 1976)
VT-PR (Ungerer and Batut, 1997)
VT-PR (Magoulas and Tassios, 1990)
VT-PR (Baled et al., 2012)
VT-PR (Shi et al., 2018)
VT-PR (Abudour et al., 2012)
NIST data
κ_T (MPa^{-1})
P_r

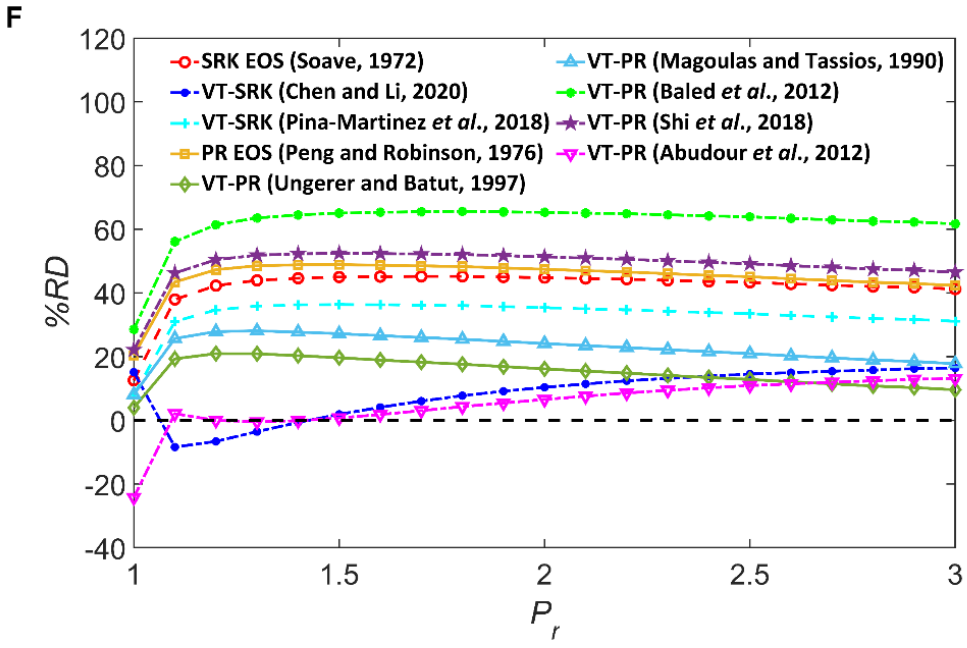

Figure 5 Comparison of the calculated κ_T for the liquid-phase CO_2 against the NIST data (A, C, and E) and *%RDs* yielded by the models studied in this work (B, D, and F) at pressures from the saturated vapor pressures to $P_r = 3$ and different temperatures: $T_r = 0.8$ (A and B), $T_r = 0.9$ (C and D), and $T_r = 1$ (E and F).

As for the liquid-phase CH_4 and CO_2, the prediction accuracy of α_P by different VT models is relatively better than those of κ_T. The Abudour *et al.* model[3] yields the lowest *%AAD* of 3.34% for CO_2, while the Chen and Li model[5] yields the lowest *%AAD* of 5.10% for CH_4. Similar to the liquid-phase κ_T results, the Ungerer and Batut model[10] performs better for CO_2 than CH_4 in predicting the liquid-phase α_P. The VT-PR EOS of Shi *et al.*[6] and the constant VT-SRK EOS updated by Pina-Martinez *et al.*[4] also show relatively accurate results for the liquid-phase α_P. The VT-PR EOSs of Baled *et al.*[11] and Magoulas and Tassios[12] show poorer performance than the untranslated PR EOS. Figure 6 compares the predicted α_P against the NIST data[7] and shows the distribution of *%RDs* for the liquid-phase CH_4. Figure 7 shows the same results for the liquid-phase CO_2. The constant VT-SRK EOS updated by Pina-Martinez *et al.*[4] and the models of Abudour *et al.*[3] and Chen and Li[5] exhibit decent accuracy over the entire temperature and pressure ranges

in the liquid-phase region. The other models can predict a similar trend of α_P changing with temperature, but their *%RDs* tend to be larger as pressure increases. The Magoulas and Tassios VT-PR EOS[12] yields poor prediction accuracy of α_P for the liquid phases. The *%RDs* yielded by this model can be greater than 100% at pressures larger than the critical pressure.

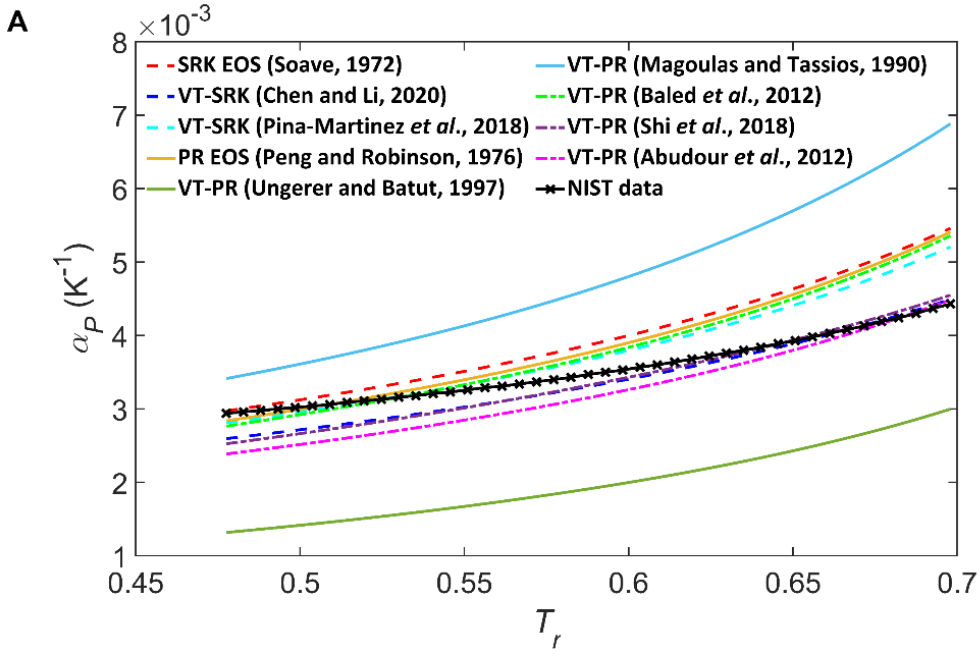

B

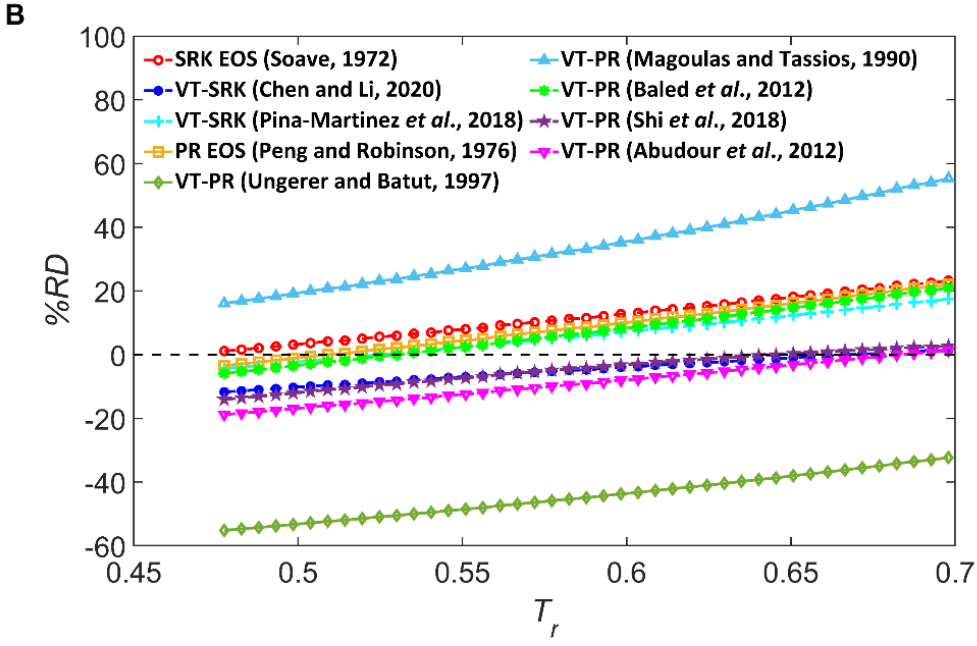
SRK EOS (Soave, 1972)
VT-SRK (Chen and Li, 2020)
VT-SRK (Pina-Martinez et al., 2018)
PR EOS (Peng and Robinson, 1976)
VT-PR (Ungerer and Batut, 1997)
VT-PR (Magoulas and Tassios, 1990)
VT-PR (Baled et al., 2012)
VT-PR (Shi et al., 2018)
VT-PR (Abudour et al., 2012)
%RD
T_r

C

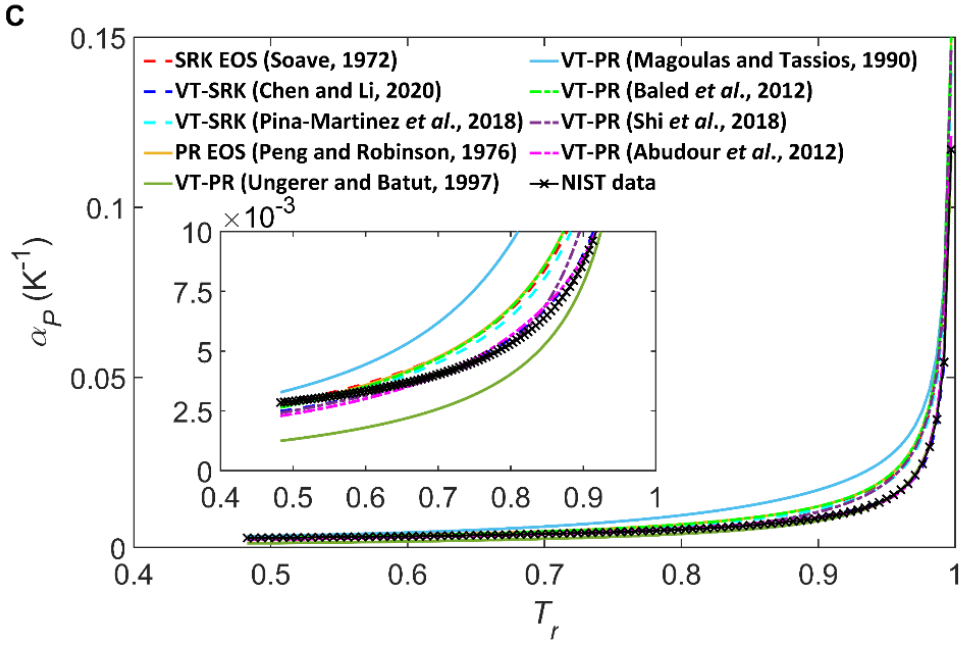
SRK EOS (Soave, 1972)
VT-SRK (Chen and Li, 2020)
VT-SRK (Pina-Martinez et al., 2018)
PR EOS (Peng and Robinson, 1976)
VT-PR (Ungerer and Batut, 1997)
VT-PR (Magoulas and Tassios, 1990)
VT-PR (Baled et al., 2012)
VT-PR (Shi et al., 2018)
VT-PR (Abudour et al., 2012)
NIST data
α_P (K^{-1})
$\times 10^{-3}$
T_r

D

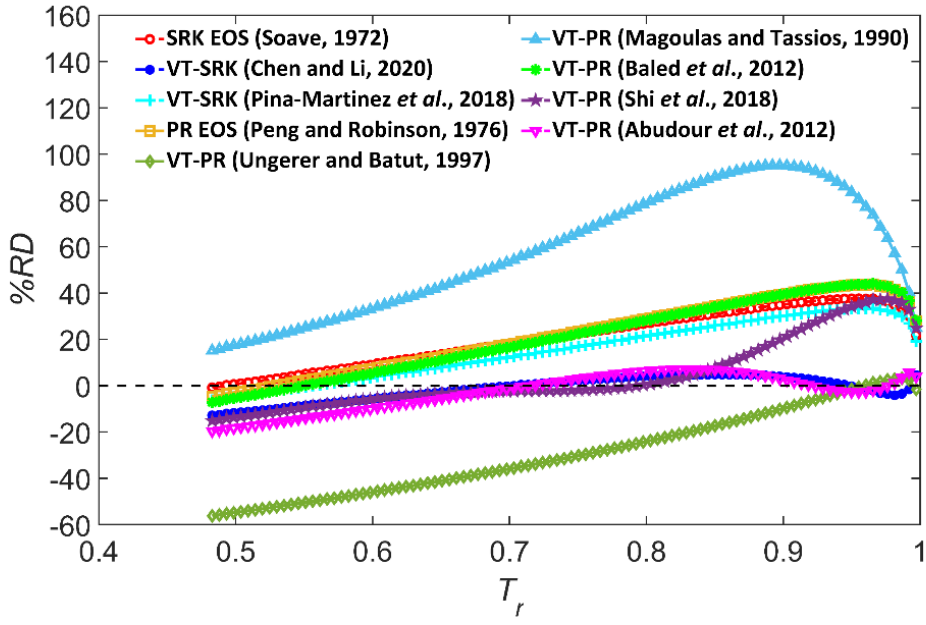
SRK EOS (Soave, 1972)
VT-SRK (Chen and Li, 2020)
VT-SRK (Pina-Martinez et al., 2018)
PR EOS (Peng and Robinson, 1976)
VT-PR (Ungerer and Batut, 1997)
VT-PR (Magoulas and Tassios, 1990)
VT-PR (Baled et al., 2012)
VT-PR (Shi et al., 2018)
VT-PR (Abudour et al., 2012)
%RD
T_r

E

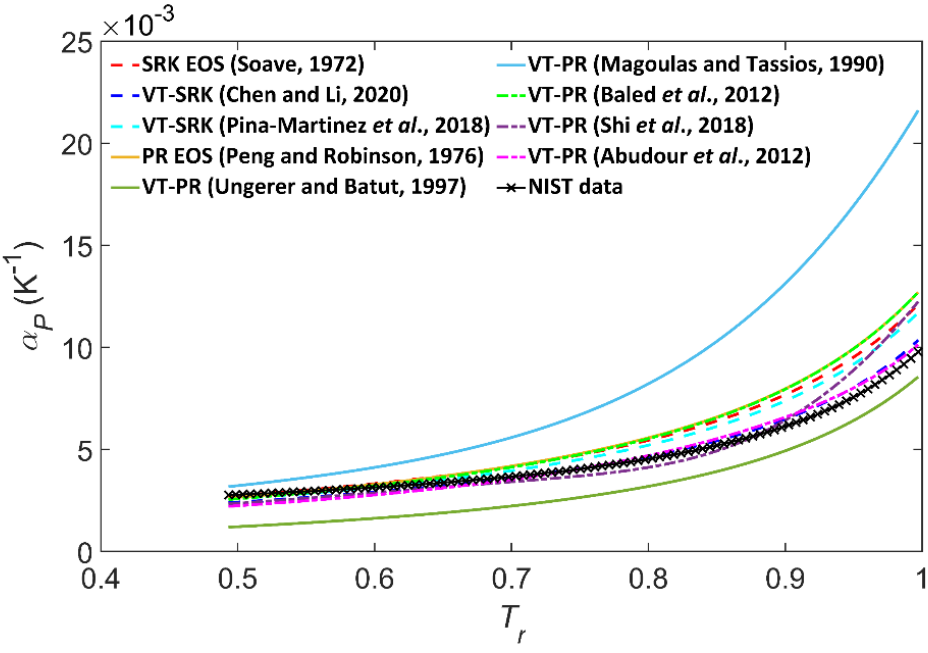
$\times 10^{-3}$
SRK EOS (Soave, 1972)
VT-SRK (Chen and Li, 2020)
VT-SRK (Pina-Martinez et al., 2018)
PR EOS (Peng and Robinson, 1976)
VT-PR (Ungerer and Batut, 1997)
VT-PR (Magoulas and Tassios, 1990)
VT-PR (Baled et al., 2012)
VT-PR (Shi et al., 2018)
VT-PR (Abudour et al., 2012)
NIST data
α_P (K^{-1})
T_r

F

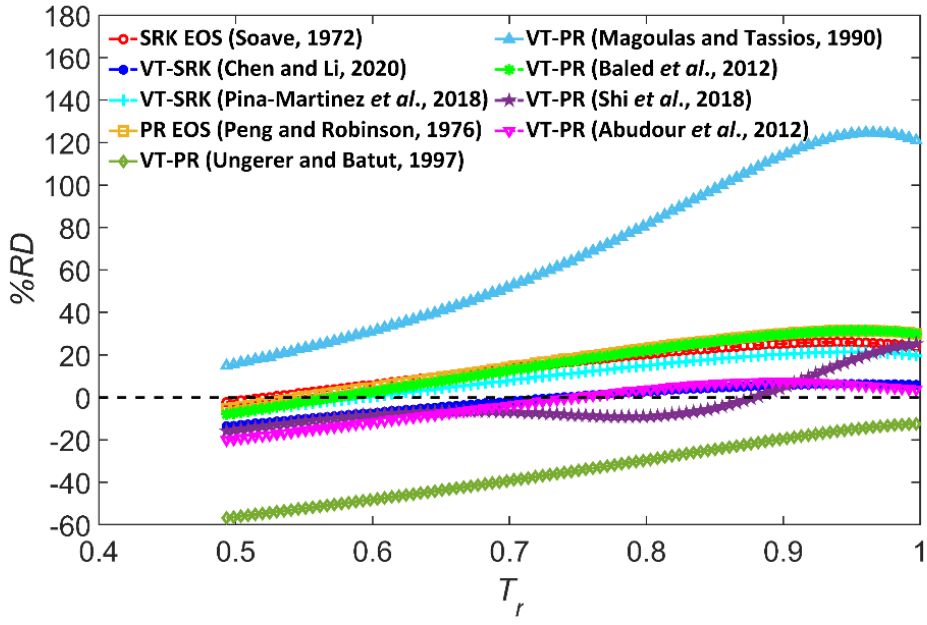
SRK EOS (Soave, 1972)
VT-SRK (Chen and Li, 2020)
VT-SRK (Pina-Martinez et al., 2018)
PR EOS (Peng and Robinson, 1976)
VT-PR (Ungerer and Batut, 1997)
VT-PR (Magoulas and Tassios, 1990)
VT-PR (Baled et al., 2012)
VT-PR (Shi et al., 2018)
VT-PR (Abudour et al., 2012)
%RD
T_r

G

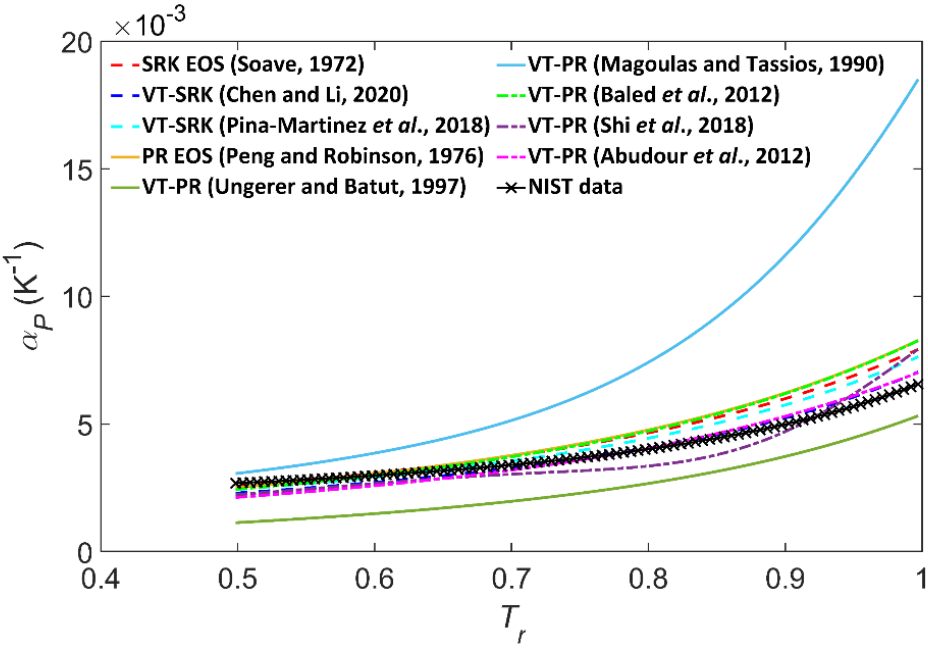
$\times 10^{-3}$
SRK EOS (Soave, 1972)
VT-SRK (Chen and Li, 2020)
VT-SRK (Pina-Martinez et al., 2018)
PR EOS (Peng and Robinson, 1976)
VT-PR (Ungerer and Batut, 1997)
VT-PR (Magoulas and Tassios, 1990)
VT-PR (Baled et al., 2012)
VT-PR (Shi et al., 2018)
VT-PR (Abudour et al., 2012)
NIST data
α_P (K^{-1})
T_r

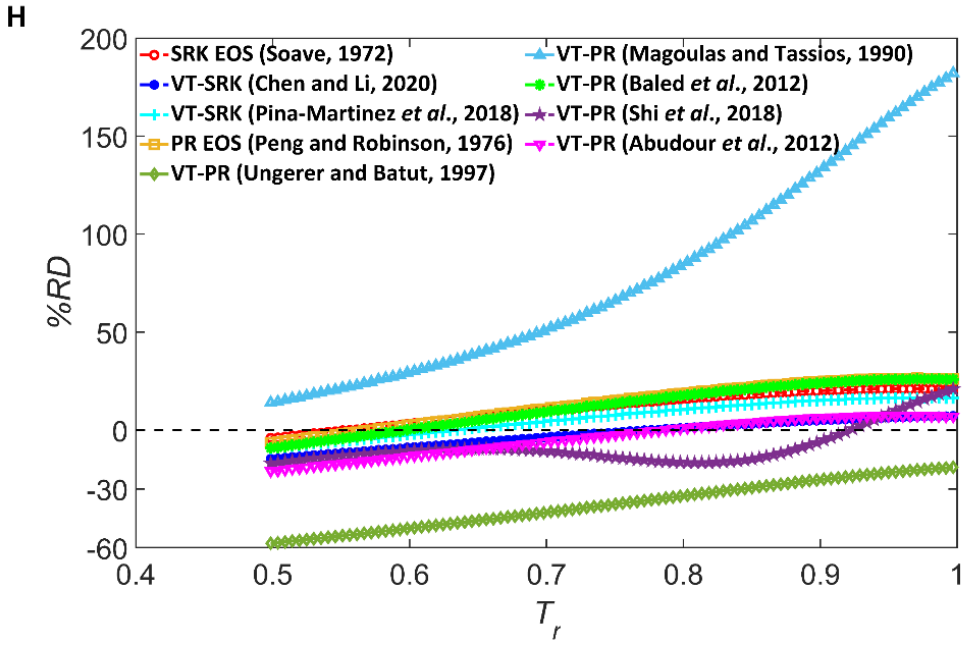

Figure 6 Comparison of the calculated α_P for the liquid-phase CH_4 against the NIST data (A, C, E, and G) and *%RDs* yielded by the models studied in this work (B, D, F, and H) at temperatures from the triple point temperature to $T_r = 1$ and different pressures: $P_r = 0.1$ (A and B), $P_r = 1$ (C and D), $P_r = 2$ (E and F), and $P_r = 3$ (G and H).

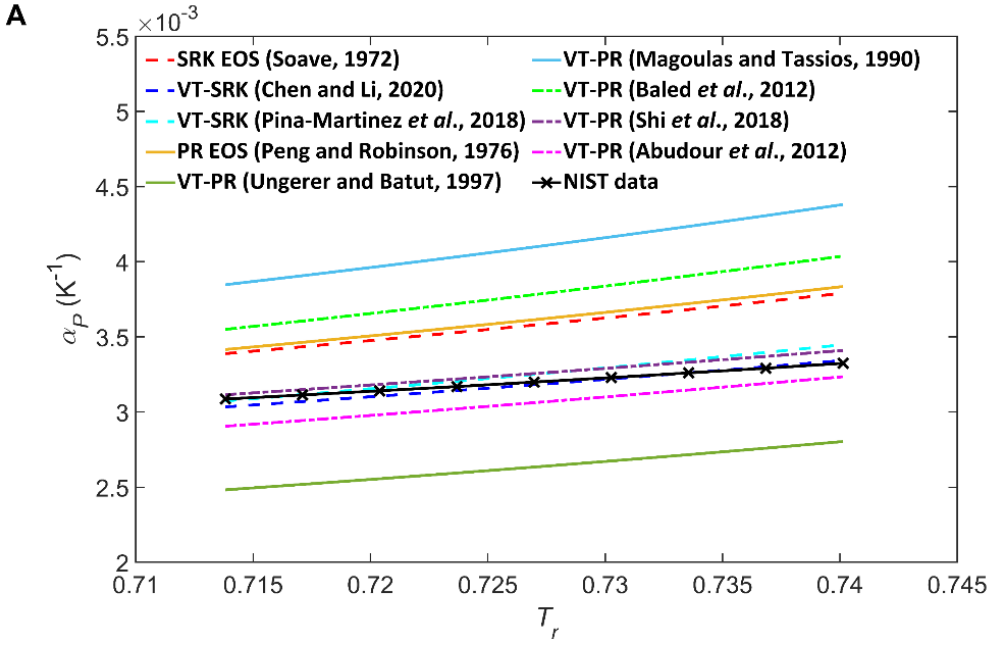

B

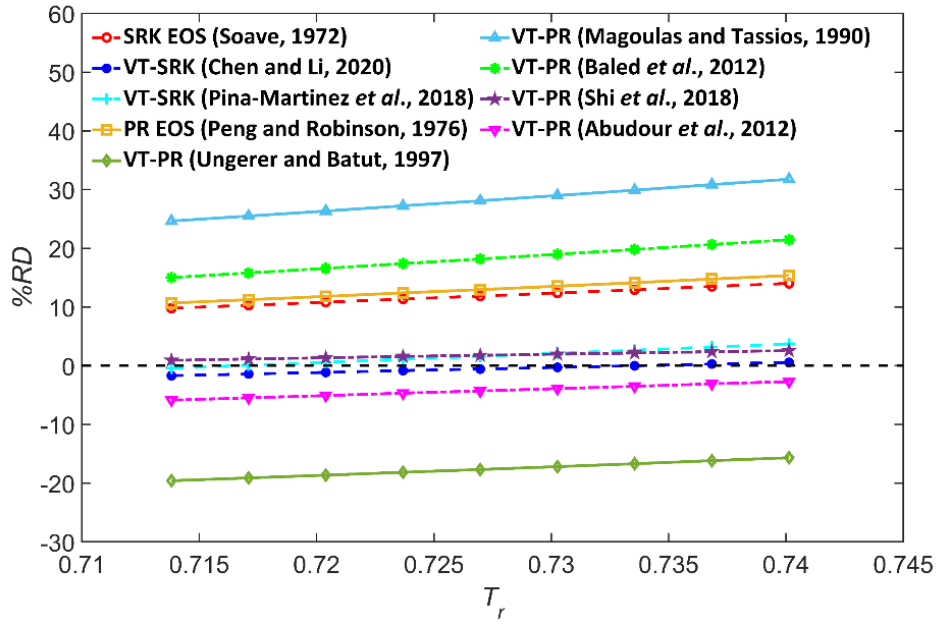
SRK EOS (Soave, 1972)
VT-SRK (Chen and Li, 2020)
VT-SRK (Pina-Martinez et al., 2018)
PR EOS (Peng and Robinson, 1976)
VT-PR (Ungerer and Batut, 1997)
VT-PR (Magoulas and Tassios, 1990)
VT-PR (Baled et al., 2012)
VT-PR (Shi et al., 2018)
VT-PR (Abudour et al., 2012)
%RD
T_r

C

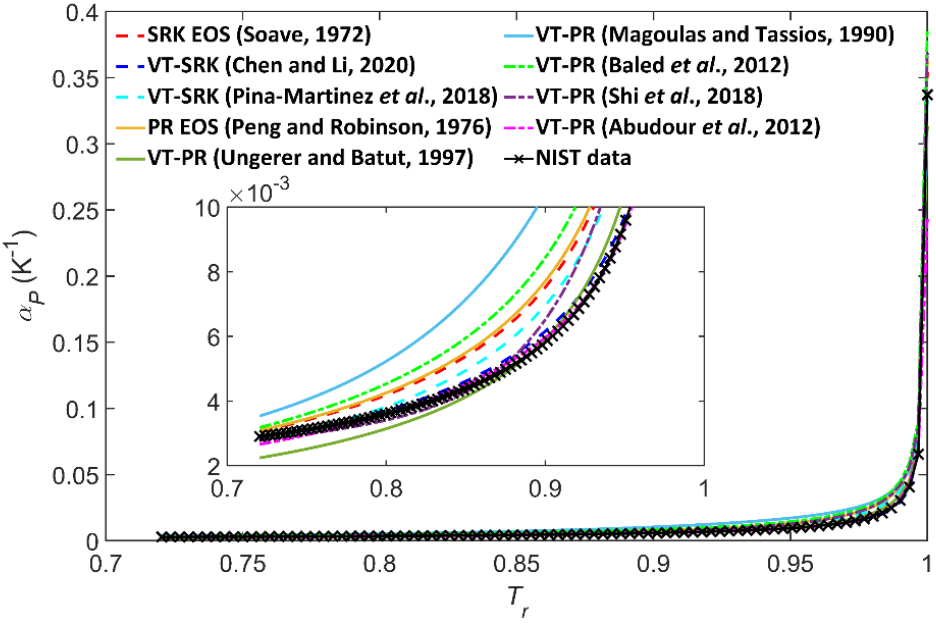
SRK EOS (Soave, 1972)
VT-SRK (Chen and Li, 2020)
VT-SRK (Pina-Martinez et al., 2018)
PR EOS (Peng and Robinson, 1976)
VT-PR (Ungerer and Batut, 1997)
VT-PR (Magoulas and Tassios, 1990)
VT-PR (Baled et al., 2012)
VT-PR (Shi et al., 2018)
VT-PR (Abudour et al., 2012)
NIST data
α_P (K^{-1})
$\times 10^{-3}$
T_r

D

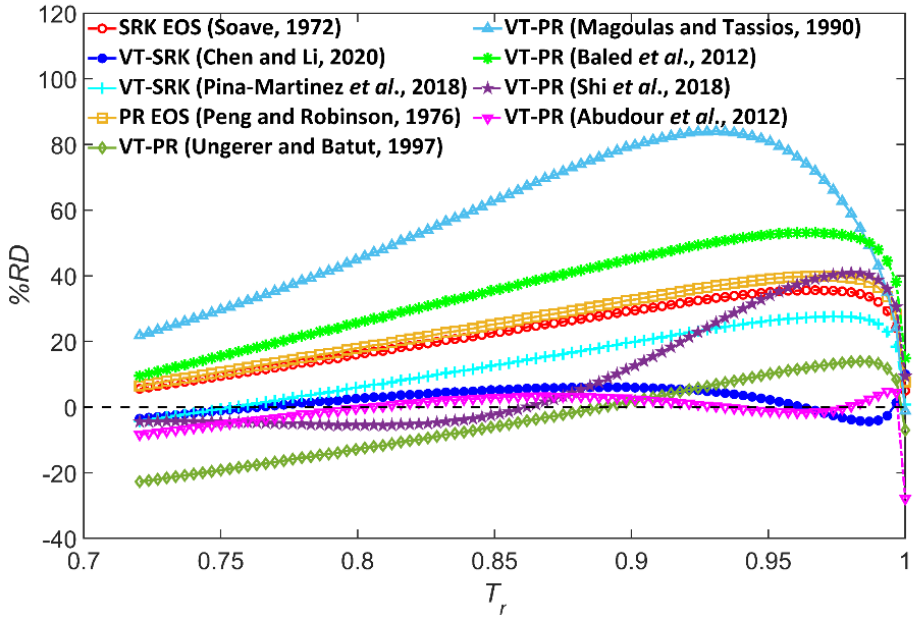
SRK EOS (Soave, 1972)
VT-SRK (Chen and Li, 2020)
VT-SRK (Pina-Martinez et al., 2018)
PR EOS (Peng and Robinson, 1976)
VT-PR (Ungerer and Batut, 1997)
VT-PR (Magoulas and Tassios, 1990)
VT-PR (Baled et al., 2012)
VT-PR (Shi et al., 2018)
VT-PR (Abudour et al., 2012)
%RD
T_r

E

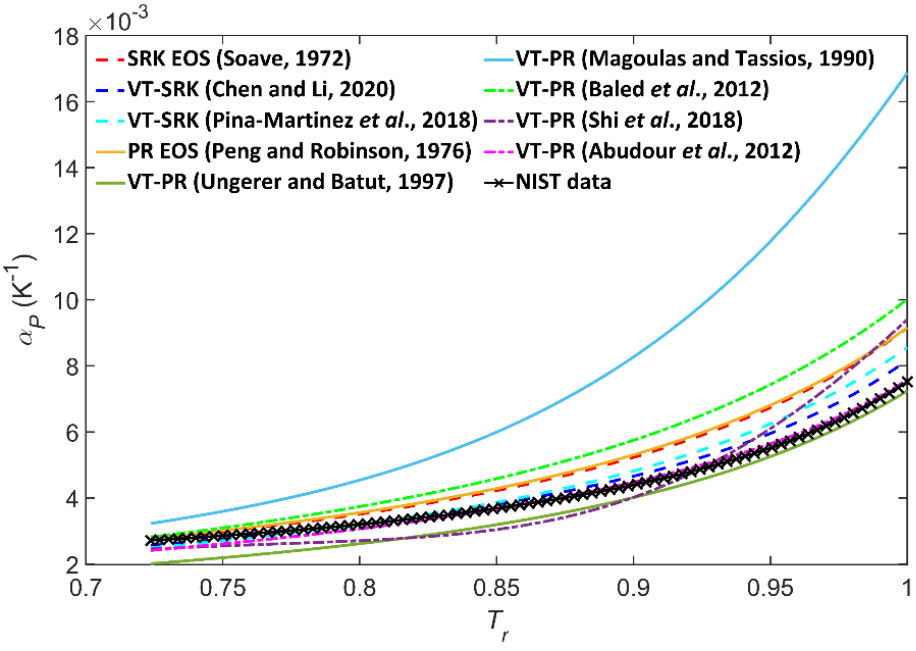
×10^-3
SRK EOS (Soave, 1972)
VT-SRK (Chen and Li, 2020)
VT-SRK (Pina-Martinez et al., 2018)
PR EOS (Peng and Robinson, 1976)
VT-PR (Ungerer and Batut, 1997)
VT-PR (Magoulas and Tassios, 1990)
VT-PR (Baled et al., 2012)
VT-PR (Shi et al., 2018)
VT-PR (Abudour et al., 2012)
NIST data
α_P (K^{-1})
T_r

F

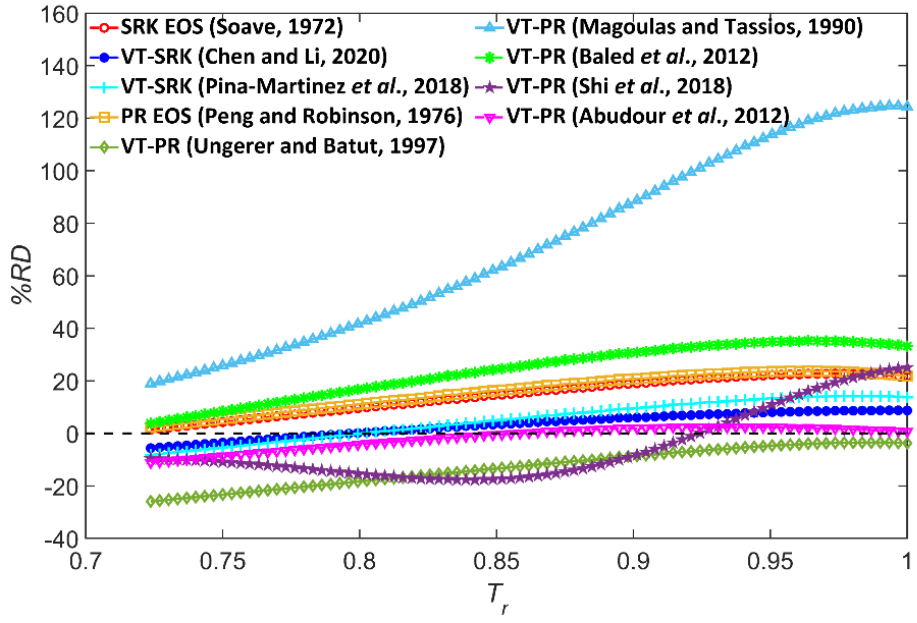
SRK EOS (Soave, 1972)
VT-SRK (Chen and Li, 2020)
VT-SRK (Pina-Martinez et al., 2018)
PR EOS (Peng and Robinson, 1976)
VT-PR (Ungerer and Batut, 1997)
VT-PR (Magoulas and Tassios, 1990)
VT-PR (Baled et al., 2012)
VT-PR (Shi et al., 2018)
VT-PR (Abudour et al., 2012)
%RD
T_r

G

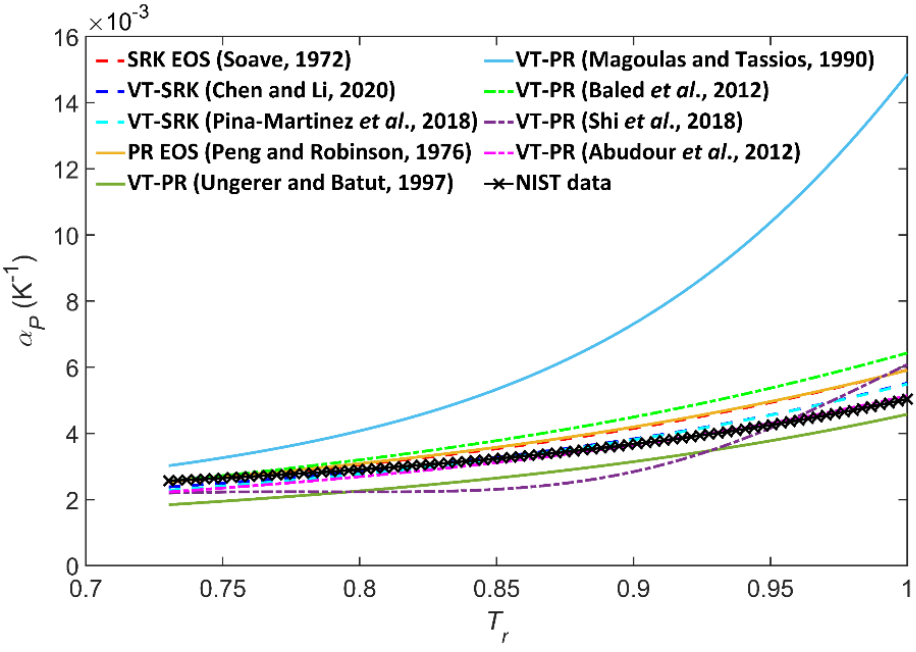
×10^-3
SRK EOS (Soave, 1972)
VT-SRK (Chen and Li, 2020)
VT-SRK (Pina-Martinez et al., 2018)
PR EOS (Peng and Robinson, 1976)
VT-PR (Ungerer and Batut, 1997)
VT-PR (Magoulas and Tassios, 1990)
VT-PR (Baled et al., 2012)
VT-PR (Shi et al., 2018)
VT-PR (Abudour et al., 2012)
NIST data
α_P (K^{-1})
T_r

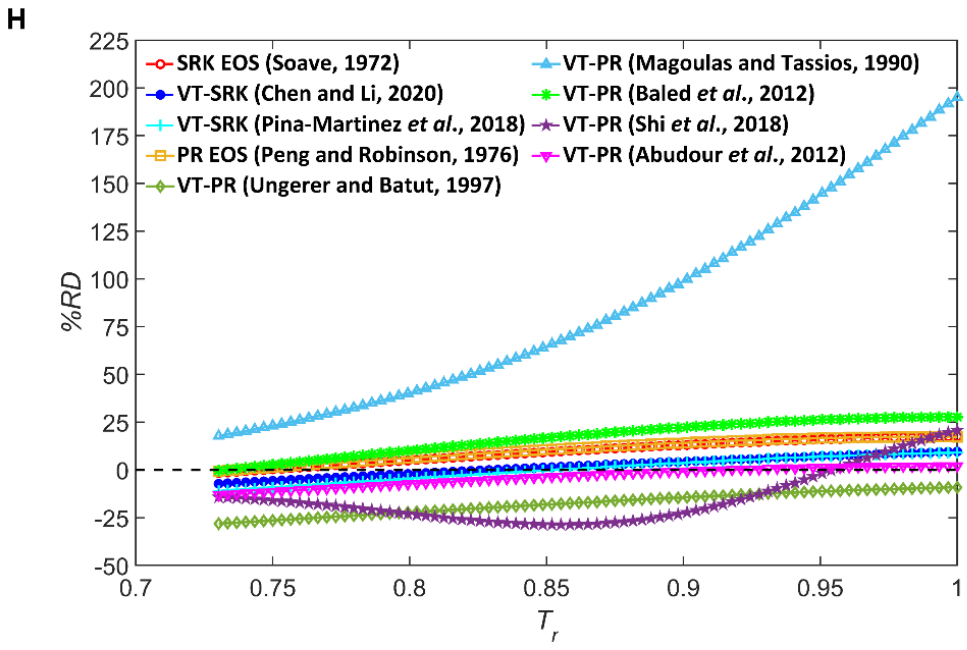

Figure 7 Comparison of the calculated α_P for the liquid-phase CO_2 against the NIST data (A, C, E, and G) and *%RDs* yielded by the models studied in this work (B, D, F, and H) at temperatures from the triple point temperature to $T_r = 1$ and different pressures: $P_r = 0.1$ (A and B), $P_r = 1$ (C and D), $P_r = 2$ (E and F), and $P_r = 3$ (G and H).

3.2.2. Predicted Results for the Vapor-phase κ_T and α_P

It is noted that the original untranslated PR EOS and SRK EOS already give pretty accurate predictions for the vapor-phase κ_T and α_P. Most of the VT models lead to larger deviations of the vapor-phase κ_T predictions. Only the VT models of Shi *et al.*,[6] Abudour *et al.*,[3] and Chen and Li[5] result in improvement over their corresponding untranslated EOSs. The model of Shi *et al.*[6] yields the most accurate κ_T predictions for the vapor phases of both CH_4 and CO_2, with *%AADs* of 0.35% and 0.32%, respectively. As for the vapor-phase α_P predictions, the Ungerer and Batut model[10] yields the lowest *%AAD* of 0.86% for CO_2, while the constant VT-SRK EOS updated by Pina-Martinez *et al.*[4] performs relatively better for CH_4 with a *%AAD* of 0.70%.

Most VT models fail to improve the vapor-phase κ_T and α_P predictions. A vapor phase has a relatively much larger volume than a liquid phase, which renders the volume corrections provided by VT-EOS models insignificant.[11] Figure 8 compares the calculated κ_T for the vapor-phase CH_4 against the NIST data. It also shows the distribution of *%RDs* over pressure. The same results for CO_2 are shown in Figure 9. It is clear that the vapor-phase κ_T predictions for both CH_4 and CO_2 made by each model are in close agreement with the NIST data. The vapor-phase κ_T decreases with an increasing pressure, except at conditions around the critical point. At T_r = 1, the vapor-phase κ_T becomes larger as P_r approaches 1. The *%RDs* yielded by different VT models are relatively low, but they tend to grow as pressure increases.

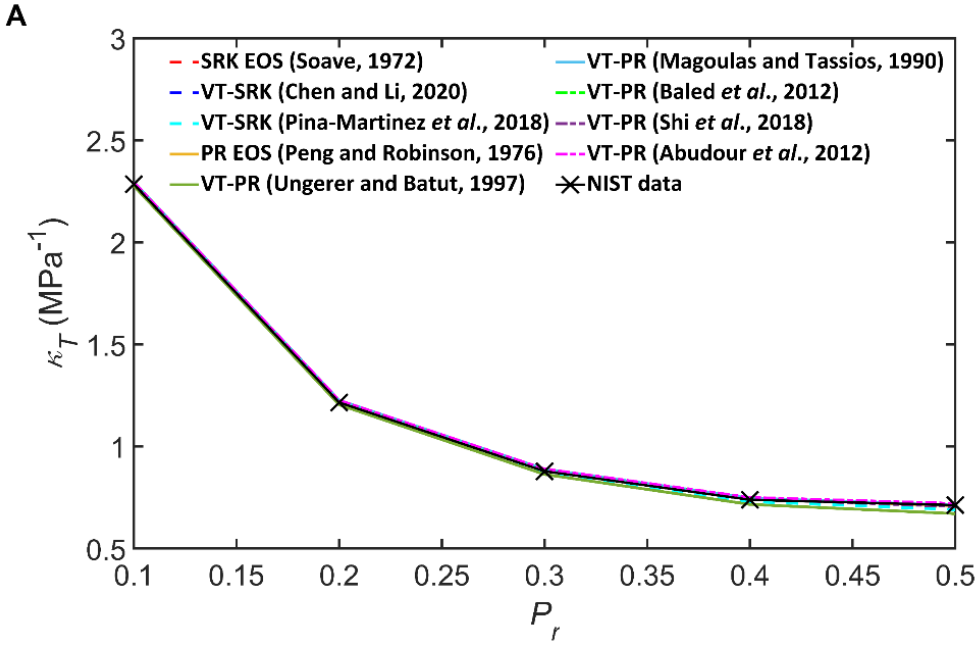

B

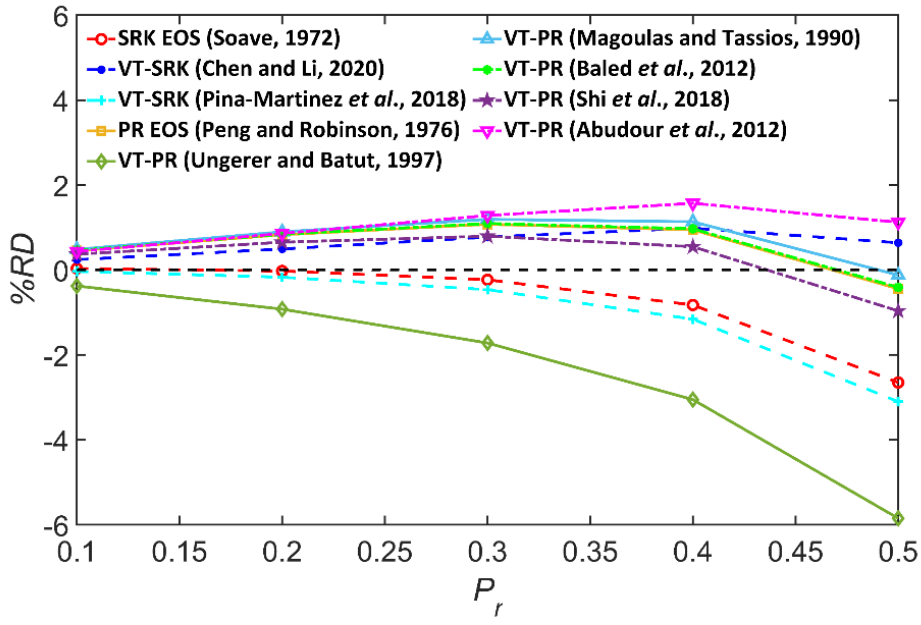
SRK EOS (Soave, 1972)
VT-SRK (Chen and Li, 2020)
VT-SRK (Pina-Martinez et al., 2018)
PR EOS (Peng and Robinson, 1976)
VT-PR (Ungerer and Batut, 1997)
VT-PR (Magoulas and Tassios, 1990)
VT-PR (Baled et al., 2012)
VT-PR (Shi et al., 2018)
VT-PR (Abudour et al., 2012)
%RD
P_r

C

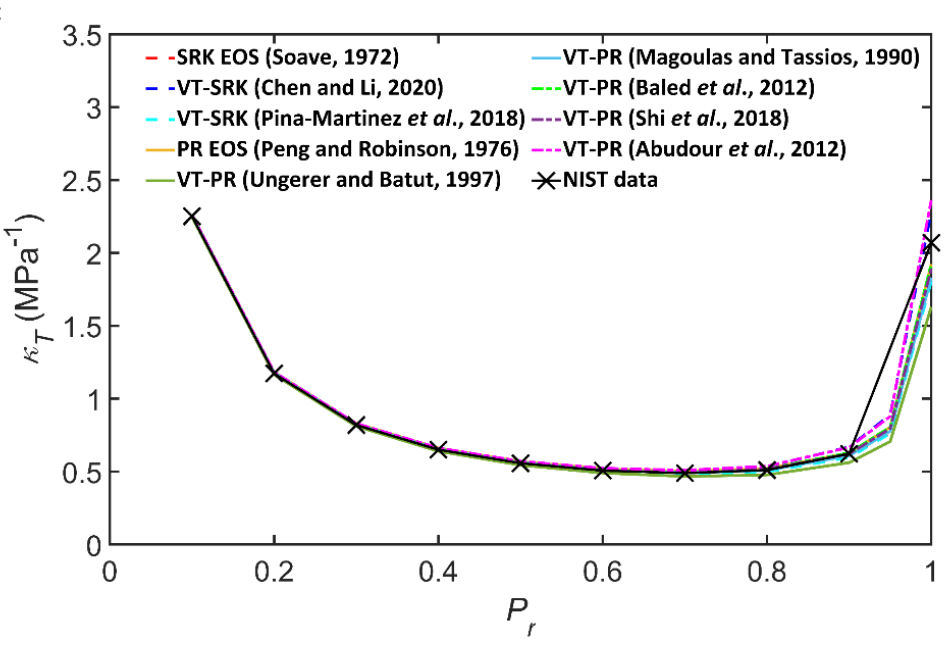
SRK EOS (Soave, 1972)
VT-SRK (Chen and Li, 2020)
VT-SRK (Pina-Martinez et al., 2018)
PR EOS (Peng and Robinson, 1976)
VT-PR (Ungerer and Batut, 1997)
VT-PR (Magoulas and Tassios, 1990)
VT-PR (Baled et al., 2012)
VT-PR (Shi et al., 2018)
VT-PR (Abudour et al., 2012)
NIST data
κ_T (MPa^{-1})
P_r

D

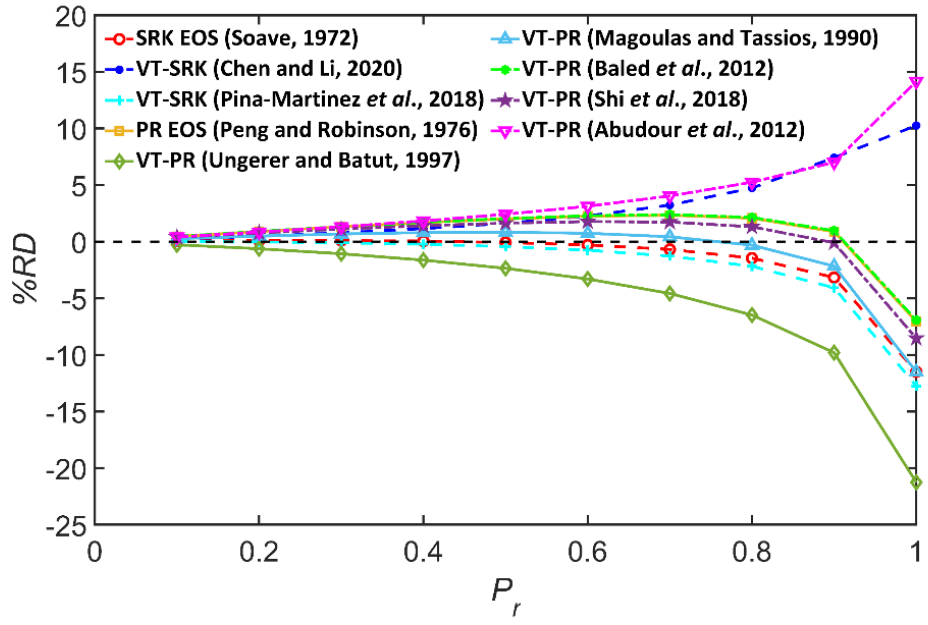
SRK EOS (Soave, 1972)
VT-SRK (Chen and Li, 2020)
VT-SRK (Pina-Martinez et al., 2018)
PR EOS (Peng and Robinson, 1976)
VT-PR (Ungerer and Batut, 1997)
VT-PR (Magoulas and Tassios, 1990)
VT-PR (Baled et al., 2012)
VT-PR (Shi et al., 2018)
VT-PR (Abudour et al., 2012)
%RD
P_r

E

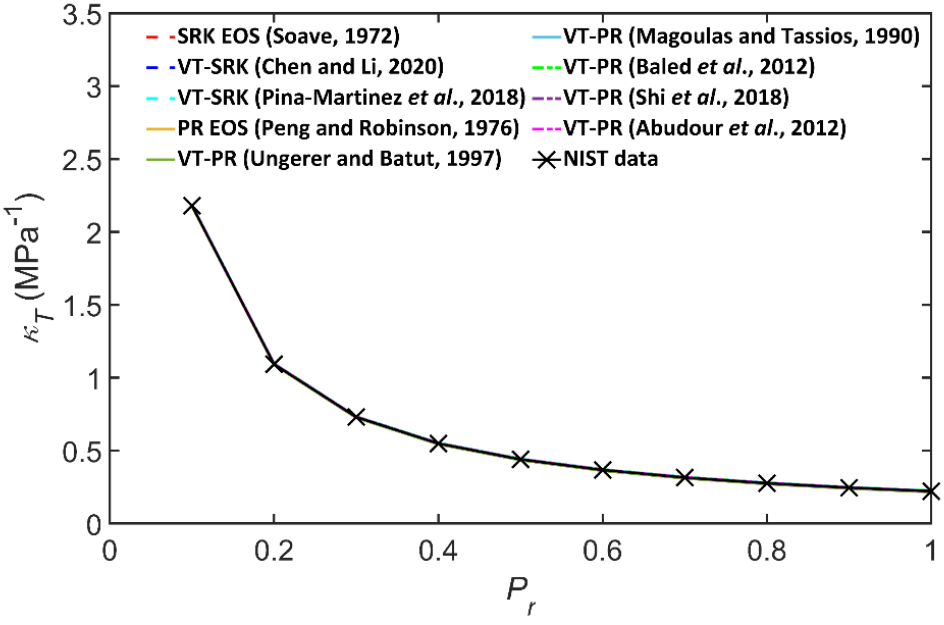
SRK EOS (Soave, 1972)
VT-SRK (Chen and Li, 2020)
VT-SRK (Pina-Martinez et al., 2018)
PR EOS (Peng and Robinson, 1976)
VT-PR (Ungerer and Batut, 1997)
VT-PR (Magoulas and Tassios, 1990)
VT-PR (Baled et al., 2012)
VT-PR (Shi et al., 2018)
VT-PR (Abudour et al., 2012)
NIST data
κ_T (MPa^{-1})
P_r

F

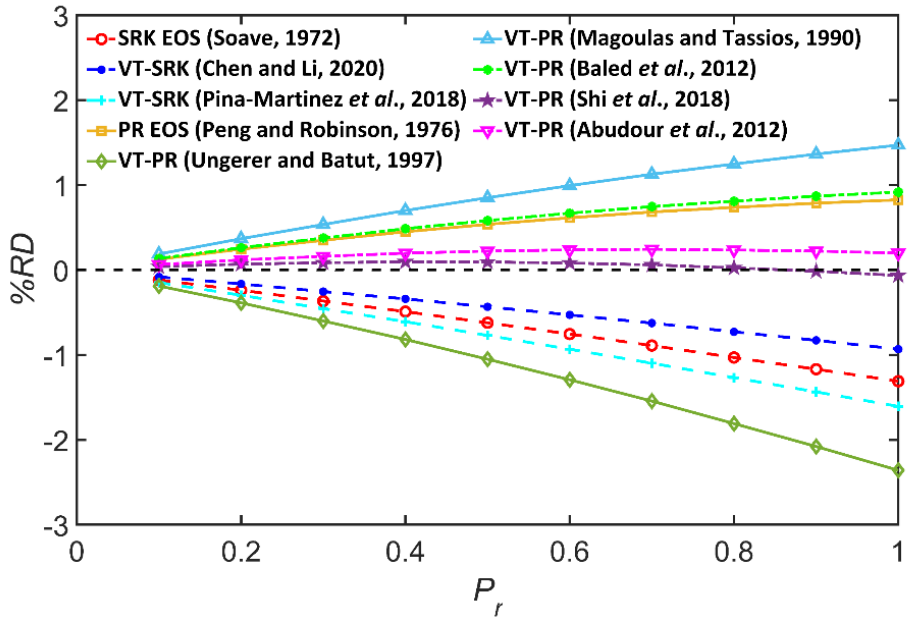
SRK EOS (Soave, 1972)
VT-SRK (Chen and Li, 2020)
VT-SRK (Pina-Martinez et al., 2018)
PR EOS (Peng and Robinson, 1976)
VT-PR (Ungerer and Batut, 1997)
VT-PR (Magoulas and Tassios, 1990)
VT-PR (Baled et al., 2012)
VT-PR (Shi et al., 2018)
VT-PR (Abudour et al., 2012)
%RD
P_r

G

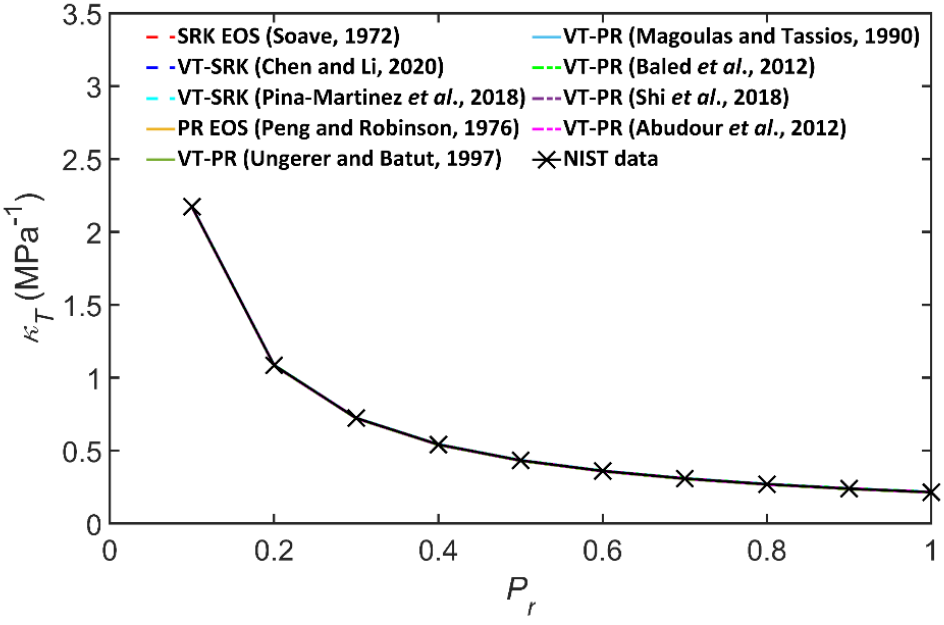
SRK EOS (Soave, 1972)
VT-SRK (Chen and Li, 2020)
VT-SRK (Pina-Martinez et al., 2018)
PR EOS (Peng and Robinson, 1976)
VT-PR (Ungerer and Batut, 1997)
VT-PR (Magoulas and Tassios, 1990)
VT-PR (Baled et al., 2012)
VT-PR (Shi et al., 2018)
VT-PR (Abudour et al., 2012)
NIST data
κ_T (MPa^{-1})
P_r

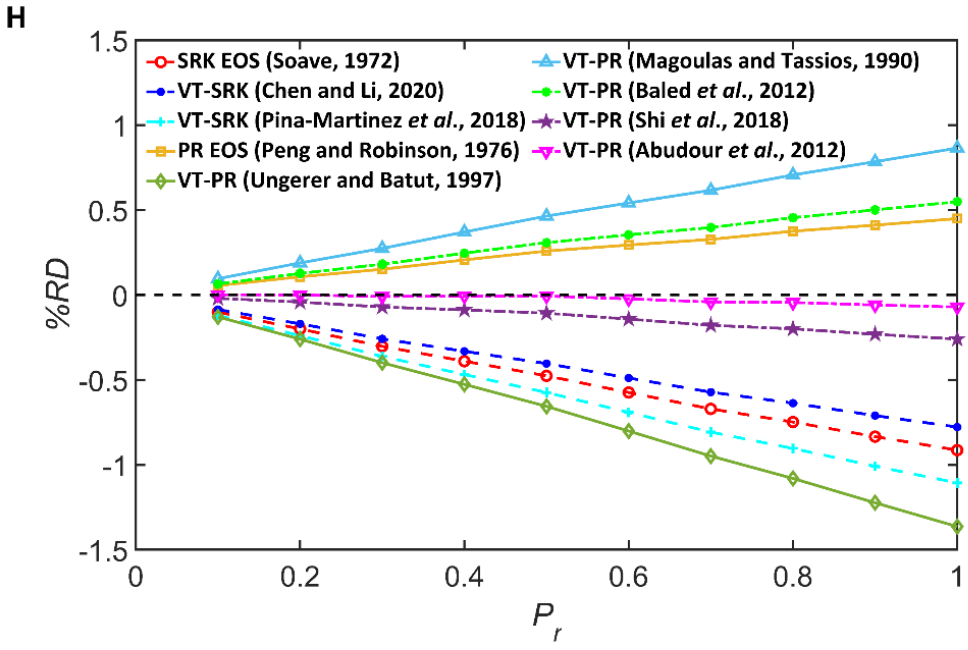

Figure 8 Comparison of the calculated κ_T for the vapor-phase CH_4 against the NIST data (A, C, E, and G) and *%RDs* yielded by the models studied in this work (B, D, F, and H) at pressures from $P_r = 0.1$ to $P_r = 1$ and different temperatures: $T_r = 0.9$ (A and B), $T_r = 1$ (C and D), $T_r = 2$ (E and F), $T_r = 3$ (G and H).

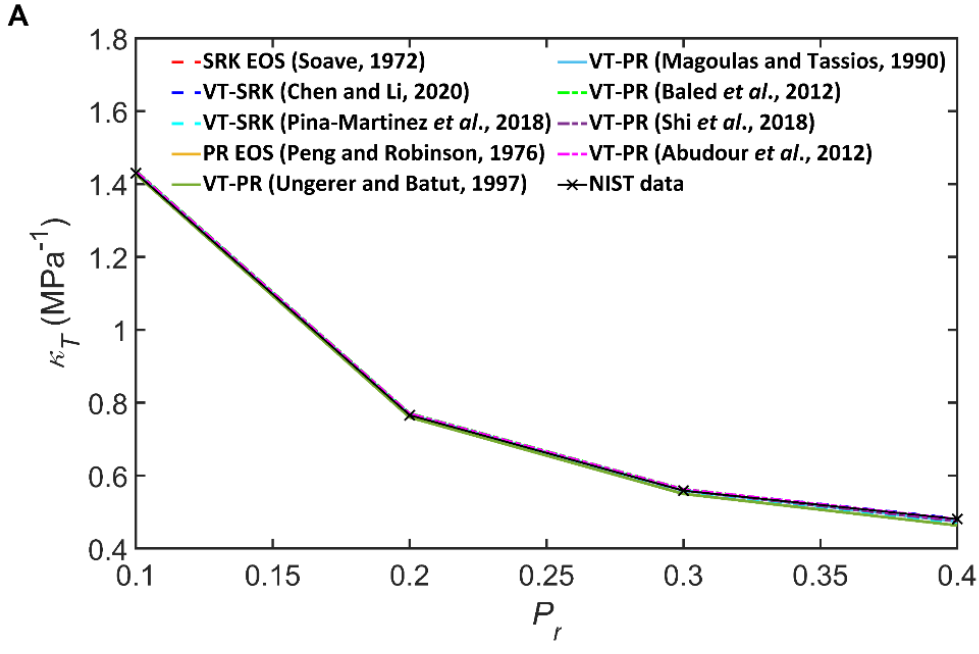

B

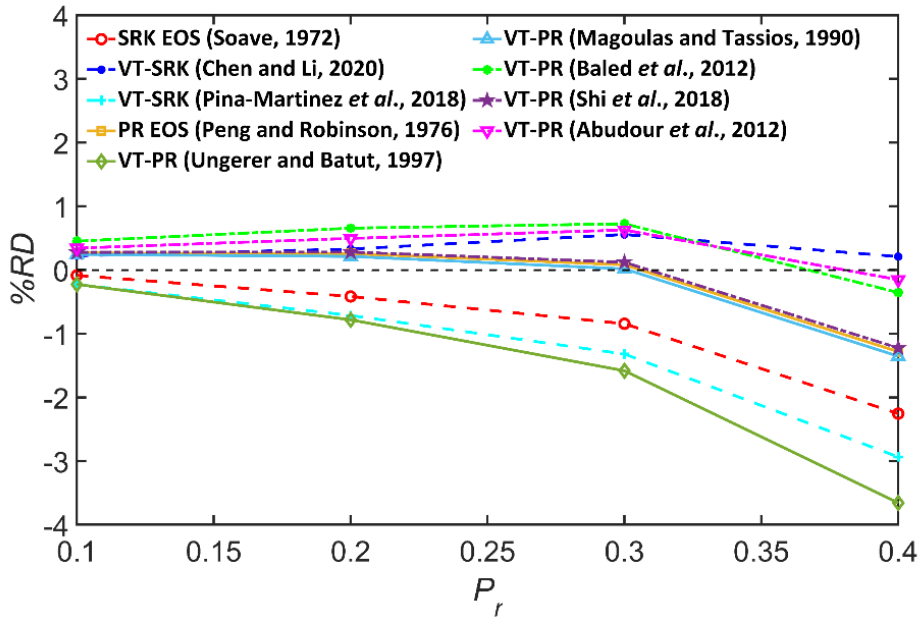
SRK EOS (Soave, 1972)
VT-SRK (Chen and Li, 2020)
VT-SRK (Pina-Martinez et al., 2018)
PR EOS (Peng and Robinson, 1976)
VT-PR (Ungerer and Batut, 1997)
VT-PR (Magoulas and Tassios, 1990)
VT-PR (Baled et al., 2012)
VT-PR (Shi et al., 2018)
VT-PR (Abudour et al., 2012)
%RD
P_r

C

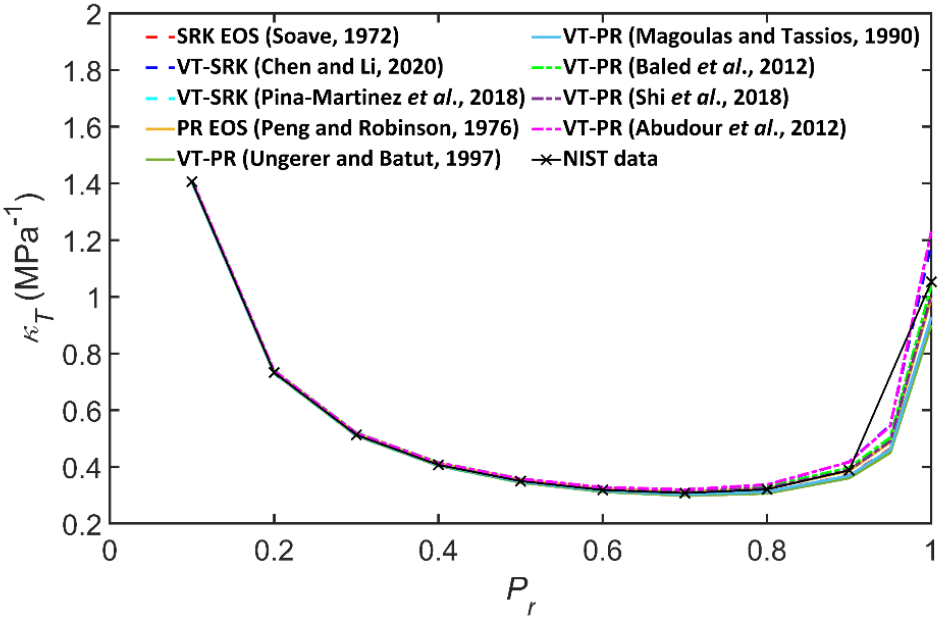
SRK EOS (Soave, 1972)
VT-SRK (Chen and Li, 2020)
VT-SRK (Pina-Martinez et al., 2018)
PR EOS (Peng and Robinson, 1976)
VT-PR (Ungerer and Batut, 1997)
VT-PR (Magoulas and Tassios, 1990)
VT-PR (Baled et al., 2012)
VT-PR (Shi et al., 2018)
VT-PR (Abudour et al., 2012)
NIST data
κ_T (MPa^{-1})
P_r

D

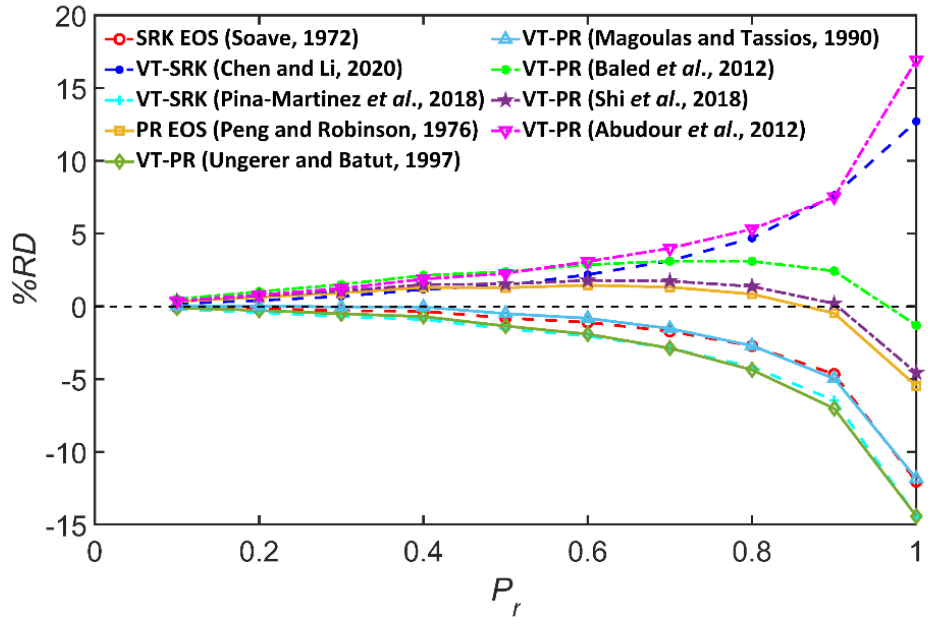
SRK EOS (Soave, 1972)
VT-SRK (Chen and Li, 2020)
VT-SRK (Pina-Martinez et al., 2018)
PR EOS (Peng and Robinson, 1976)
VT-PR (Ungerer and Batut, 1997)
VT-PR (Magoulas and Tassios, 1990)
VT-PR (Baled et al., 2012)
VT-PR (Shi et al., 2018)
VT-PR (Abudour et al., 2012)
%RD
P_r

E

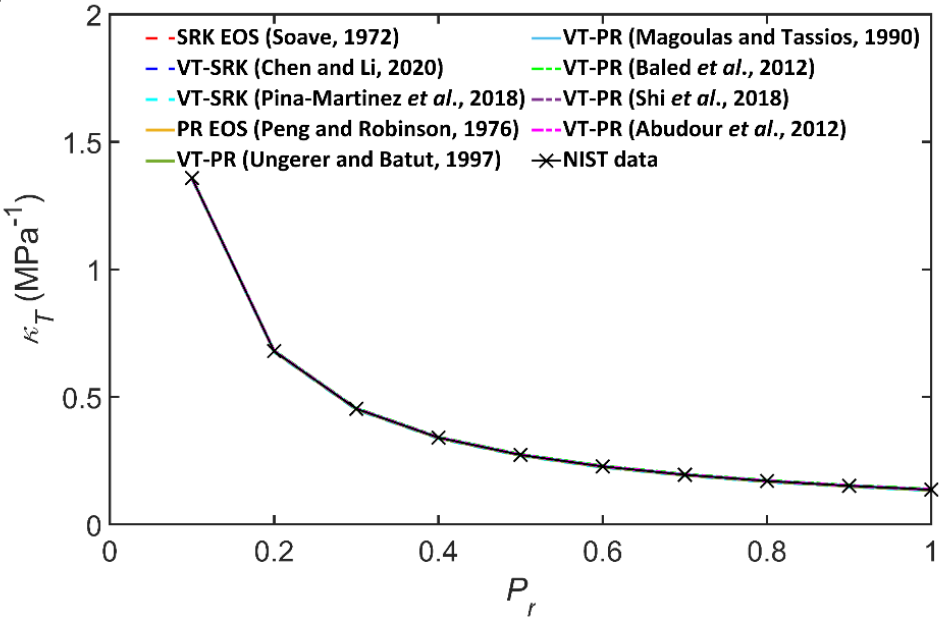
SRK EOS (Soave, 1972)
VT-SRK (Chen and Li, 2020)
VT-SRK (Pina-Martinez et al., 2018)
PR EOS (Peng and Robinson, 1976)
VT-PR (Ungerer and Batut, 1997)
VT-PR (Magoulas and Tassios, 1990)
VT-PR (Baled et al., 2012)
VT-PR (Shi et al., 2018)
VT-PR (Abudour et al., 2012)
NIST data
κ_T (MPa^{-1})
P_r

F

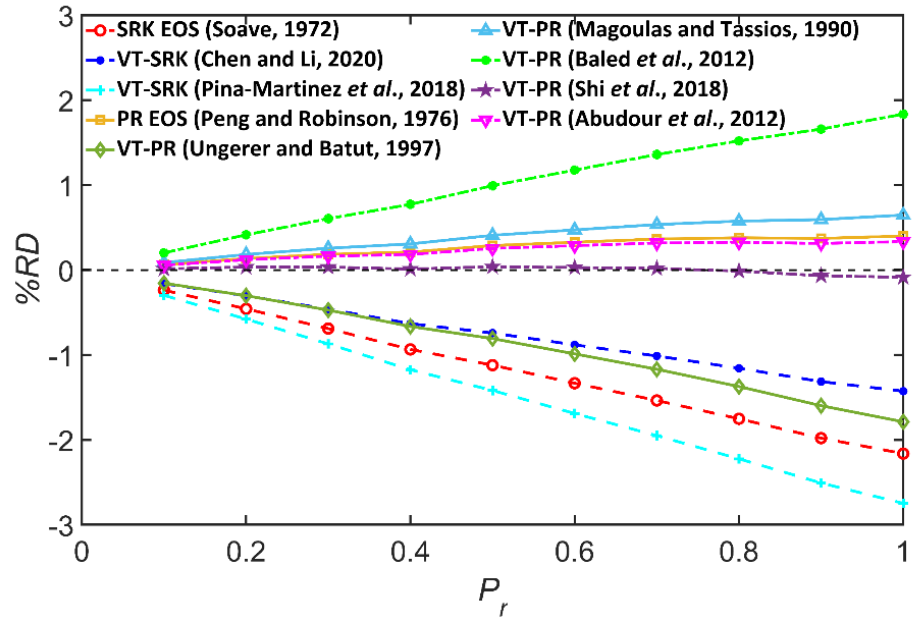
SRK EOS (Soave, 1972)
VT-SRK (Chen and Li, 2020)
VT-SRK (Pina-Martinez et al., 2018)
PR EOS (Peng and Robinson, 1976)
VT-PR (Ungerer and Batut, 1997)
VT-PR (Magoulas and Tassios, 1990)
VT-PR (Baled et al., 2012)
VT-PR (Shi et al., 2018)
VT-PR (Abudour et al., 2012)
%RD
P_r

G

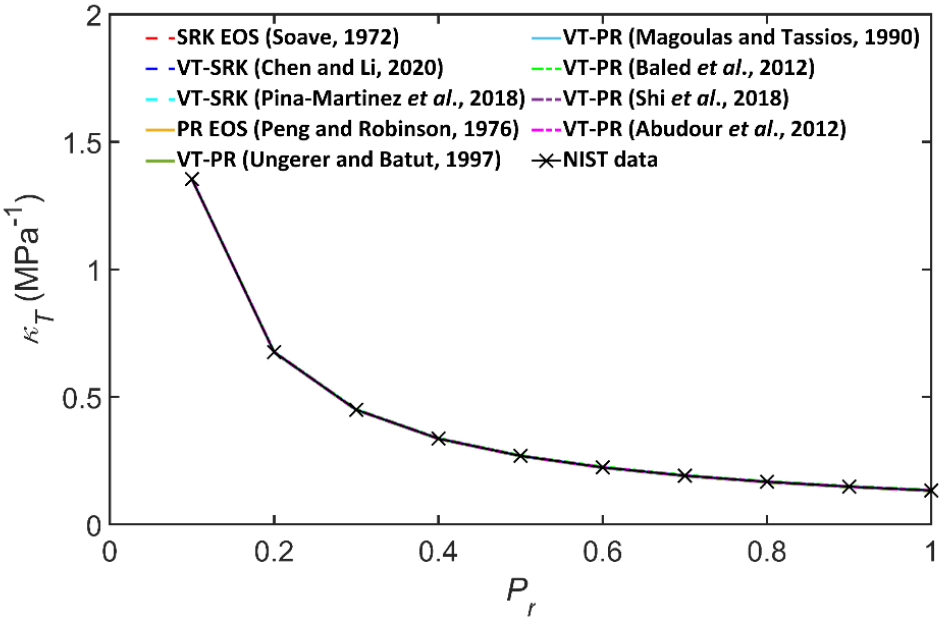
SRK EOS (Soave, 1972)
VT-SRK (Chen and Li, 2020)
VT-SRK (Pina-Martinez et al., 2018)
PR EOS (Peng and Robinson, 1976)
VT-PR (Ungerer and Batut, 1997)
VT-PR (Magoulas and Tassios, 1990)
VT-PR (Baled et al., 2012)
VT-PR (Shi et al., 2018)
VT-PR (Abudour et al., 2012)
NIST data
κ_T (MPa^{-1})
P_r

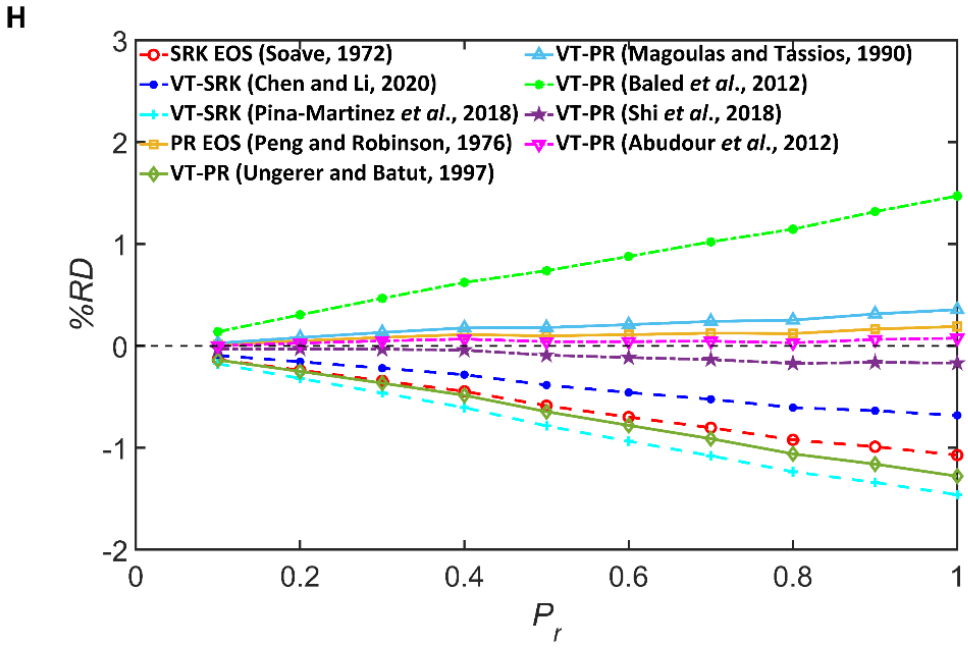

Figure 9 Comparison of the calculated κ_T for the vapor-phase CO_2 against the NIST data (A, C, E, and G) and *%RDs* yielded by the models studied in this work (B, D, F, and H) at pressures from $P_r = 0.1$ to $P_r = 1$ and different temperatures: $T_r = 0.9$ (A and B), $T_r = 1$ (C and D), $T_r = 2$ (E and F), $T_r = 3$ (G and H).

Figures 10 and 11 illustrate the performance of each model in predicting the vapor-phase α_P at different pressures for CH_4 and CO_2, respectively. It can be seen that the predictions are also consistent with the NIST data.[7] However, there is a dramatic drop in the vapor-phase α_P calculated by the Magoulas and Tassios model[12] for both CH_4 and CO_2 around the critical temperature. Based on the *%RDs* distribution yielded by each model for the vapor-phase CH_4 and CO_2, the predictions of vapor-phase α_P become more accurate as temperature increases along an isobar and are relatively more accurate at temperatures above the critical temperature.

A

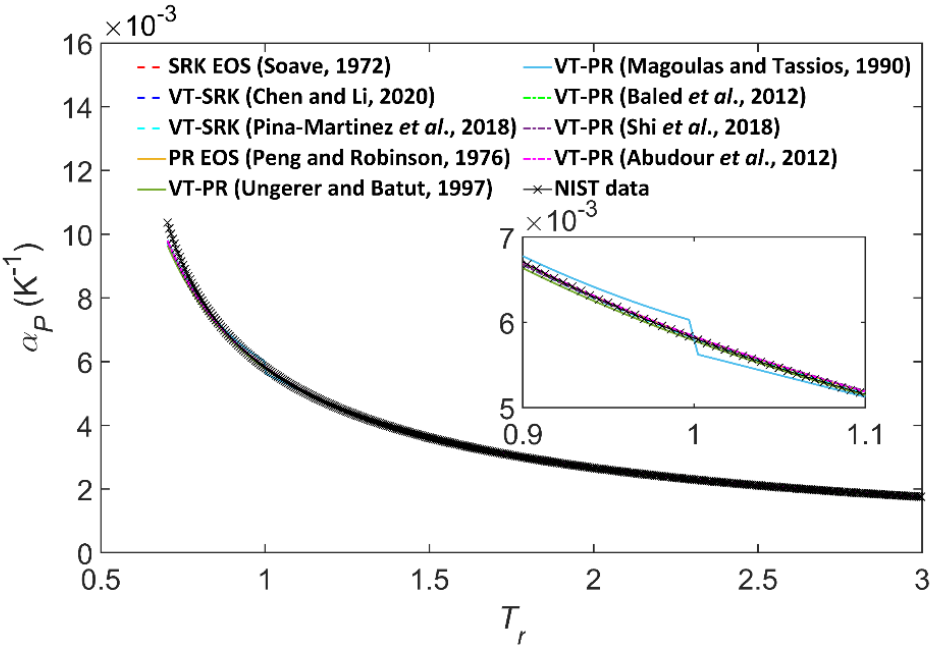
×10^-3
SRK EOS (Soave, 1972)
VT-SRK (Chen and Li, 2020)
VT-SRK (Pina-Martinez et al., 2018)
PR EOS (Peng and Robinson, 1976)
VT-PR (Ungerer and Batut, 1997)
VT-PR (Magoulas and Tassios, 1990)
VT-PR (Baled et al., 2012)
VT-PR (Shi et al., 2018)
VT-PR (Abudour et al., 2012)
NIST data
×10^-3
α_P (K^{-1})
T_r

B

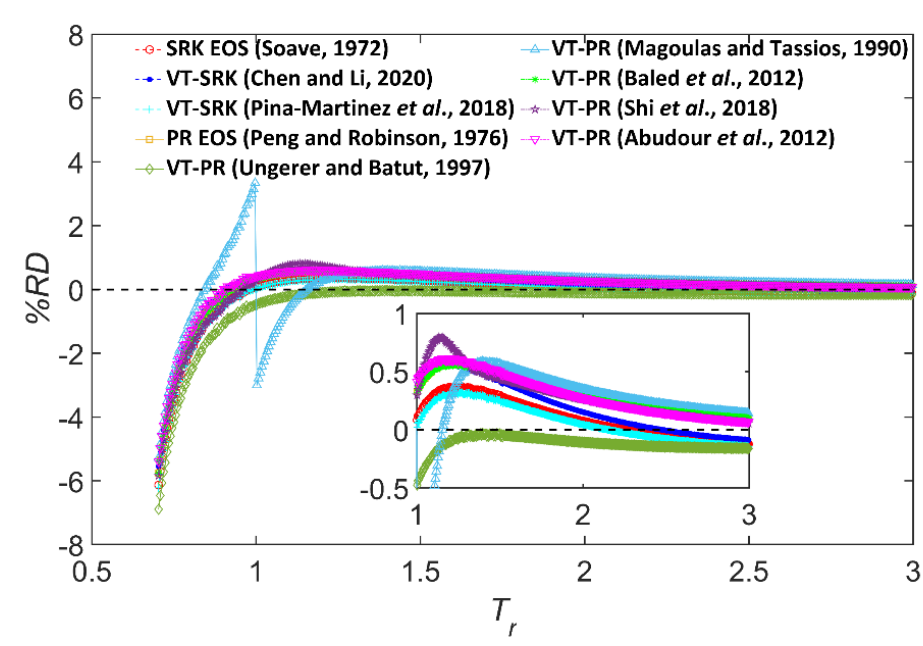
SRK EOS (Soave, 1972)
VT-SRK (Chen and Li, 2020)
VT-SRK (Pina-Martinez et al., 2018)
PR EOS (Peng and Robinson, 1976)
VT-PR (Ungerer and Batut, 1997)
VT-PR (Magoulas and Tassios, 1990)
VT-PR (Baled et al., 2012)
VT-PR (Shi et al., 2018)
VT-PR (Abudour et al., 2012)
%RD
T_r

C

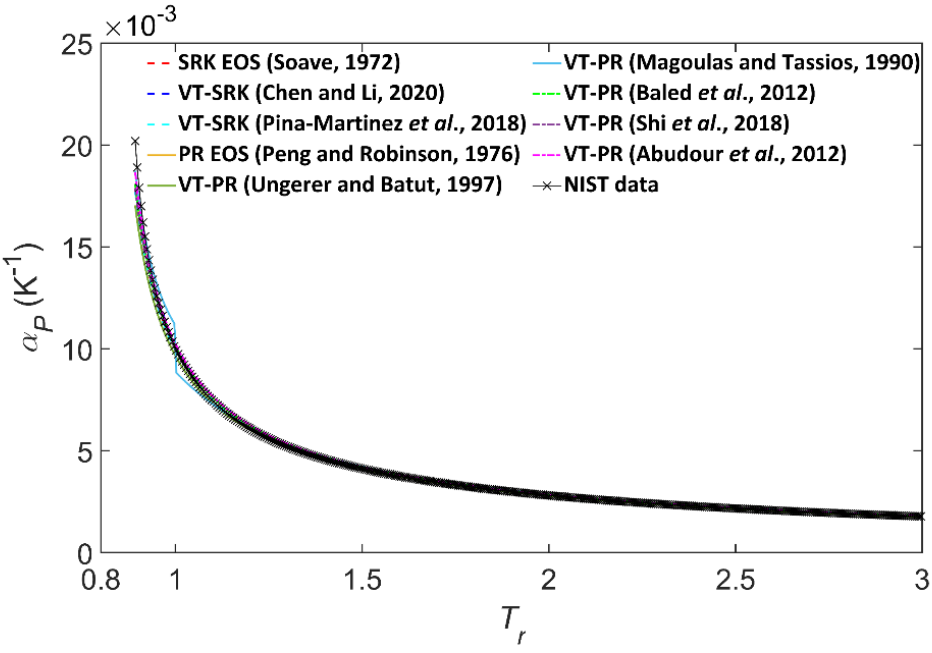
×10^-3
25
20
15
10
5
0
0.8
1
1.5
2
2.5
3
α_P (K^{-1})
T_r
SRK EOS (Soave, 1972)
VT-SRK (Chen and Li, 2020)
VT-SRK (Pina-Martinez et al., 2018)
PR EOS (Peng and Robinson, 1976)
VT-PR (Ungerer and Batut, 1997)
VT-PR (Magoulas and Tassios, 1990)
VT-PR (Baled et al., 2012)
VT-PR (Shi et al., 2018)
VT-PR (Abudour et al., 2012)
NIST data

D

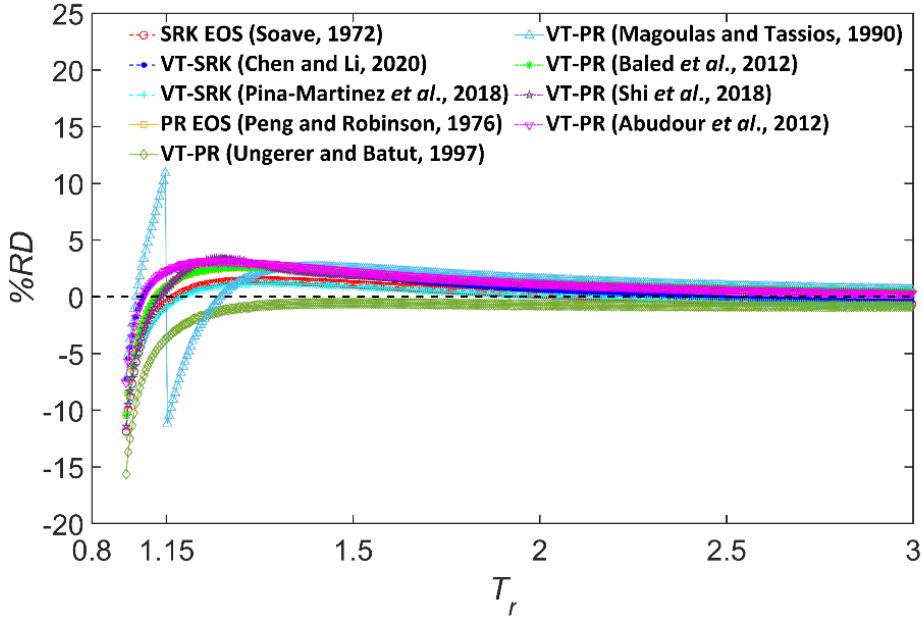
25
20
15
10
5
0
-5
-10
-15
-20
0.8
1.15
1.5
2
2.5
3
%RD
T_r
SRK EOS (Soave, 1972)
VT-SRK (Chen and Li, 2020)
VT-SRK (Pina-Martinez et al., 2018)
PR EOS (Peng and Robinson, 1976)
VT-PR (Ungerer and Batut, 1997)
VT-PR (Magoulas and Tassios, 1990)
VT-PR (Baled et al., 2012)
VT-PR (Shi et al., 2018)
VT-PR (Abudour et al., 2012)

E

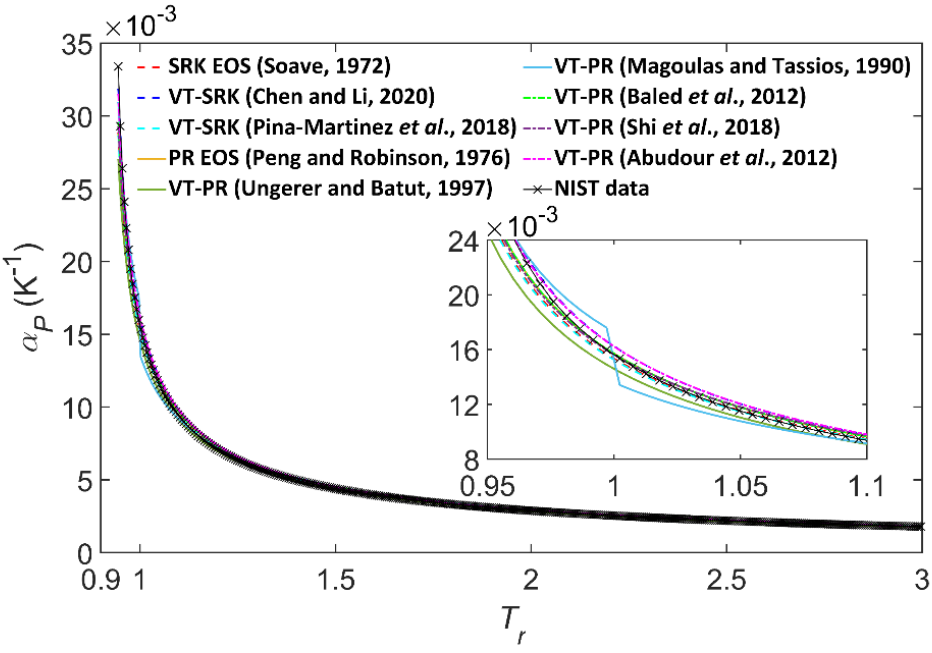
×10^-3
SRK EOS (Soave, 1972)
VT-SRK (Chen and Li, 2020)
VT-SRK (Pina-Martinez et al., 2018)
PR EOS (Peng and Robinson, 1976)
VT-PR (Ungerer and Batut, 1997)
VT-PR (Magoulas and Tassios, 1990)
VT-PR (Baled et al., 2012)
VT-PR (Shi et al., 2018)
VT-PR (Abudour et al., 2012)
NIST data
×10^-3
α_P (K^{-1})
T_r

F

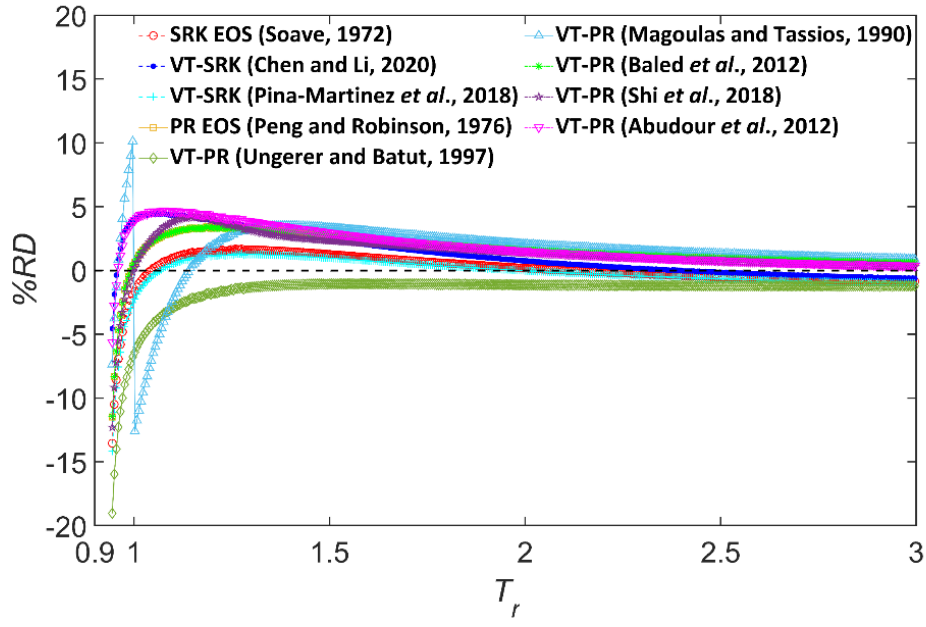
SRK EOS (Soave, 1972)
VT-SRK (Chen and Li, 2020)
VT-SRK (Pina-Martinez et al., 2018)
PR EOS (Peng and Robinson, 1976)
VT-PR (Ungerer and Batut, 1997)
VT-PR (Magoulas and Tassios, 1990)
VT-PR (Baled et al., 2012)
VT-PR (Shi et al., 2018)
VT-PR (Abudour et al., 2012)
%RD
T_r

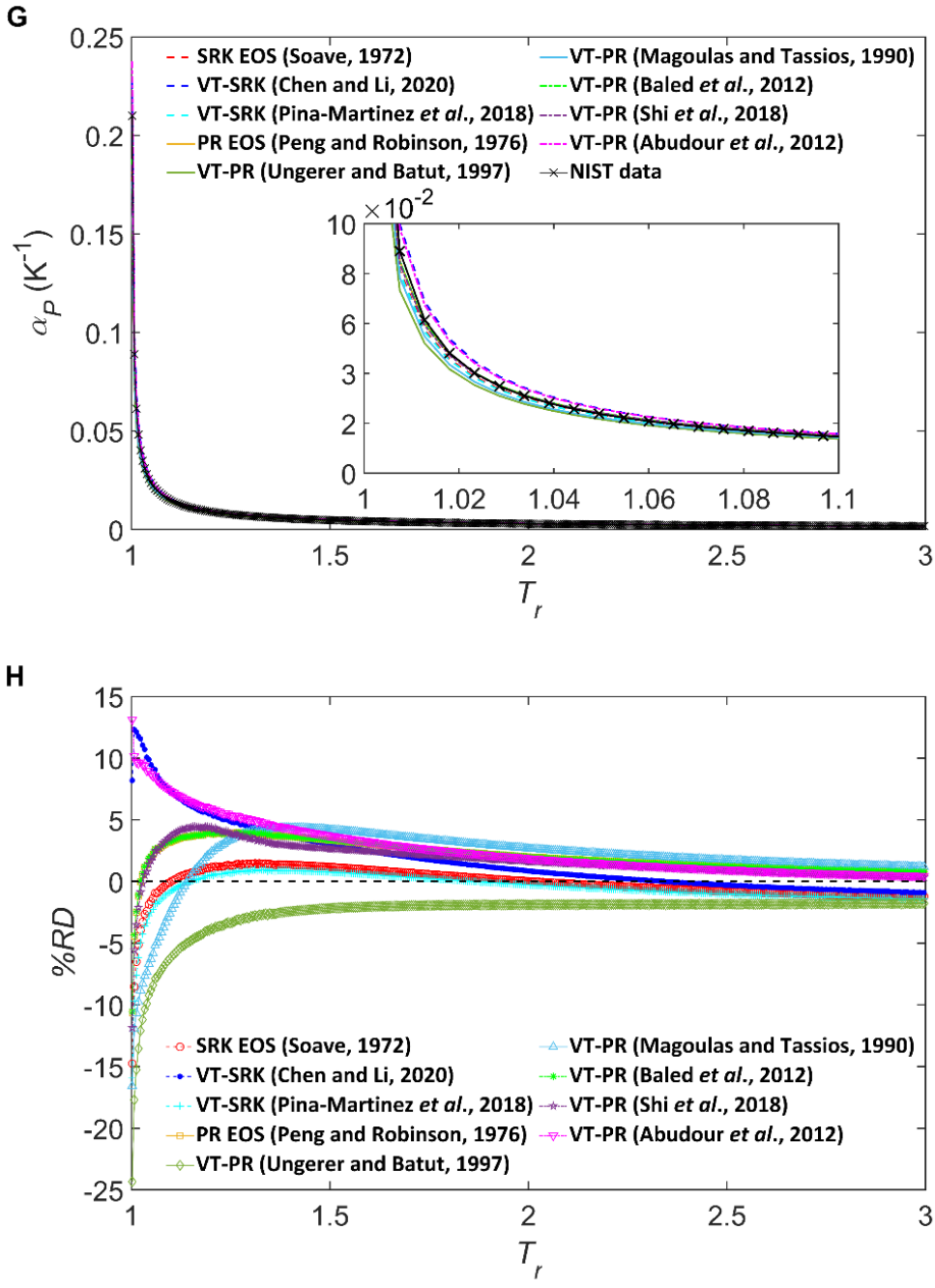

Figure 10 Comparison of the calculated α_P for the vapor-phase CH_4 against the NIST data (A, C, E, and G) and *%RDs* yielded by the models studied in this work (B, D, F, and H) at temperatures from the saturated vapor temperature to $T_r = 3$ and different pressures: $P_r = 0.1$ (A and B), $P_r = 0.4$ (C and D), $P_r = 0.7$ (E and F), and $P_r = 1$ (G and H).

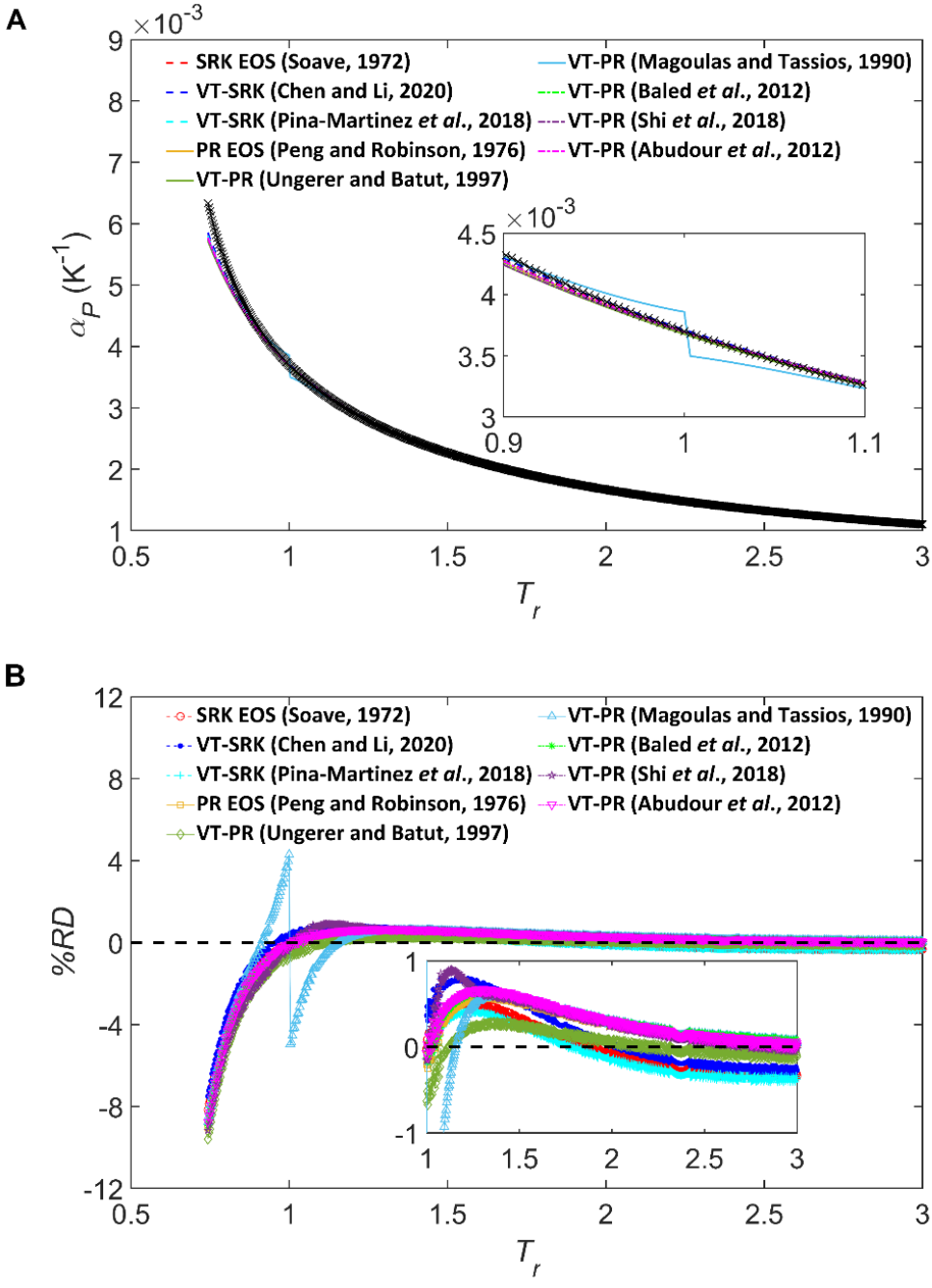
A
×10^-3
SRK EOS (Soave, 1972)
VT-SRK (Chen and Li, 2020)
VT-SRK (Pina-Martinez et al., 2018)
PR EOS (Peng and Robinson, 1976)
VT-PR (Ungerer and Batut, 1997)
VT-PR (Magoulas and Tassios, 1990)
VT-PR (Baled et al., 2012)
VT-PR (Shi et al., 2018)
VT-PR (Abudour et al., 2012)
α_P (K^{-1})
T_r
B
%RD
T_r

C

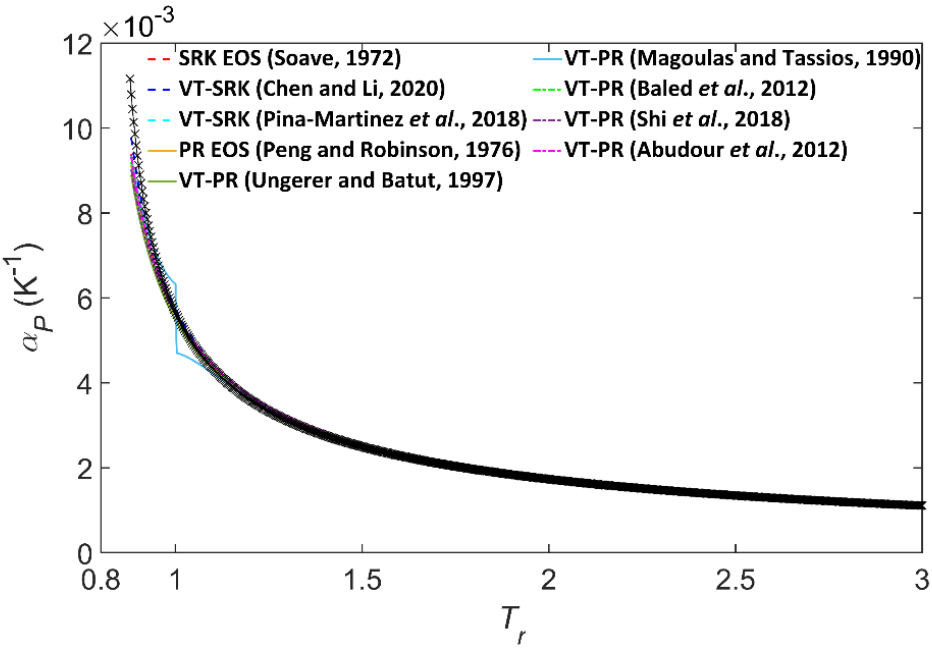
×10^-3
12
10
8
6
4
2
0
0.8
1
1.5
2
2.5
3
α_P (K^{-1})
T_r
SRK EOS (Soave, 1972)
VT-SRK (Chen and Li, 2020)
VT-SRK (Pina-Martinez et al., 2018)
PR EOS (Peng and Robinson, 1976)
VT-PR (Ungerer and Batut, 1997)
VT-PR (Magoulas and Tassios, 1990)
VT-PR (Baled et al., 2012)
VT-PR (Shi et al., 2018)
VT-PR (Abudour et al., 2012)

D

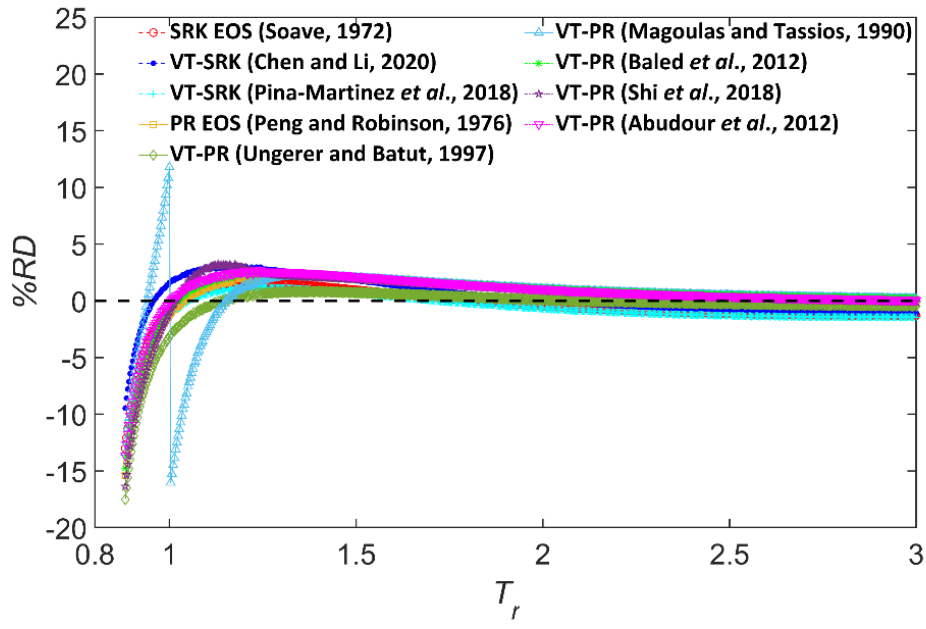
25
20
15
10
5
0
-5
-10
-15
-20
0.8
1
1.5
2
2.5
3
%RD
T_r
SRK EOS (Soave, 1972)
VT-SRK (Chen and Li, 2020)
VT-SRK (Pina-Martinez et al., 2018)
PR EOS (Peng and Robinson, 1976)
VT-PR (Ungerer and Batut, 1997)
VT-PR (Magoulas and Tassios, 1990)
VT-PR (Baled et al., 2012)
VT-PR (Shi et al., 2018)
VT-PR (Abudour et al., 2012)

E

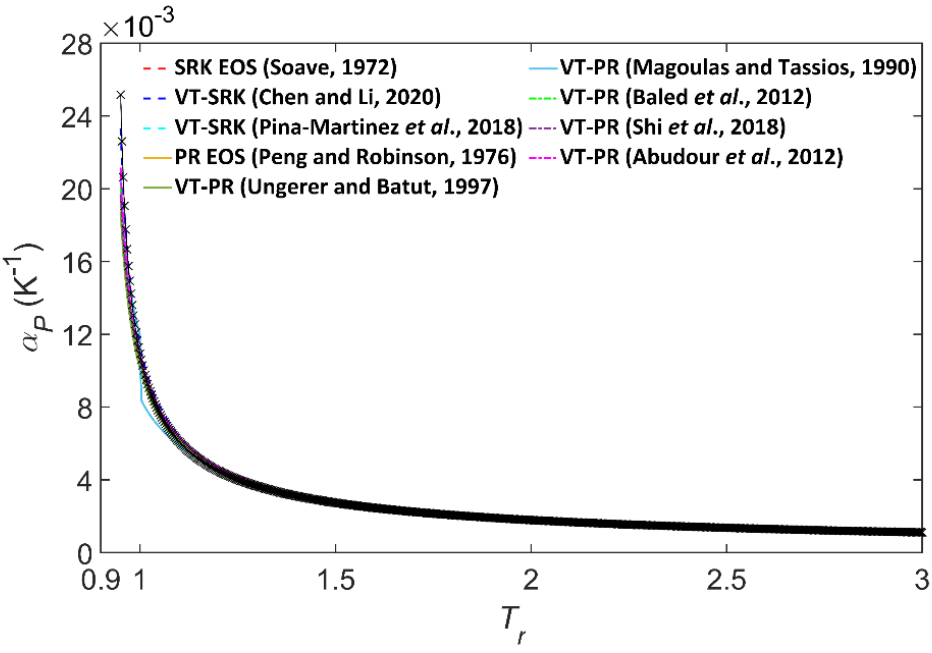
×10^-3
28
24
20
16
12
8
4
0
0.9
1
1.5
2
2.5
3
α_P (K^{-1})
T_r
SRK EOS (Soave, 1972)
VT-SRK (Chen and Li, 2020)
VT-SRK (Pina-Martinez et al., 2018)
PR EOS (Peng and Robinson, 1976)
VT-PR (Ungerer and Batut, 1997)
VT-PR (Magoulas and Tassios, 1990)
VT-PR (Baled et al., 2012)
VT-PR (Shi et al., 2018)
VT-PR (Abudour et al., 2012)

F

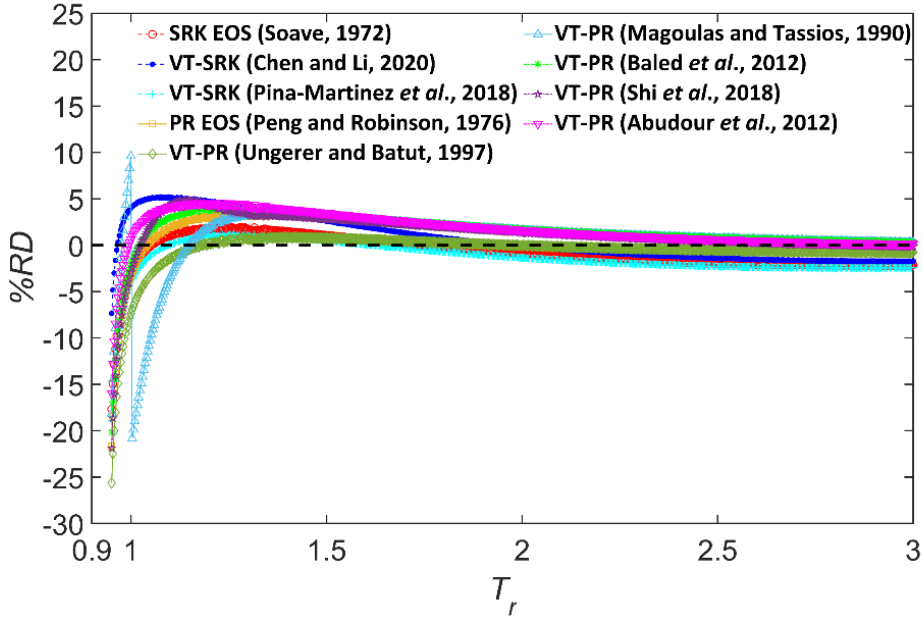
25
20
15
10
5
0
-5
-10
-15
-20
-25
-30
0.9
1
1.5
2
2.5
3
%RD
T_r
SRK EOS (Soave, 1972)
VT-SRK (Chen and Li, 2020)
VT-SRK (Pina-Martinez et al., 2018)
PR EOS (Peng and Robinson, 1976)
VT-PR (Ungerer and Batut, 1997)
VT-PR (Magoulas and Tassios, 1990)
VT-PR (Baled et al., 2012)
VT-PR (Shi et al., 2018)
VT-PR (Abudour et al., 2012)

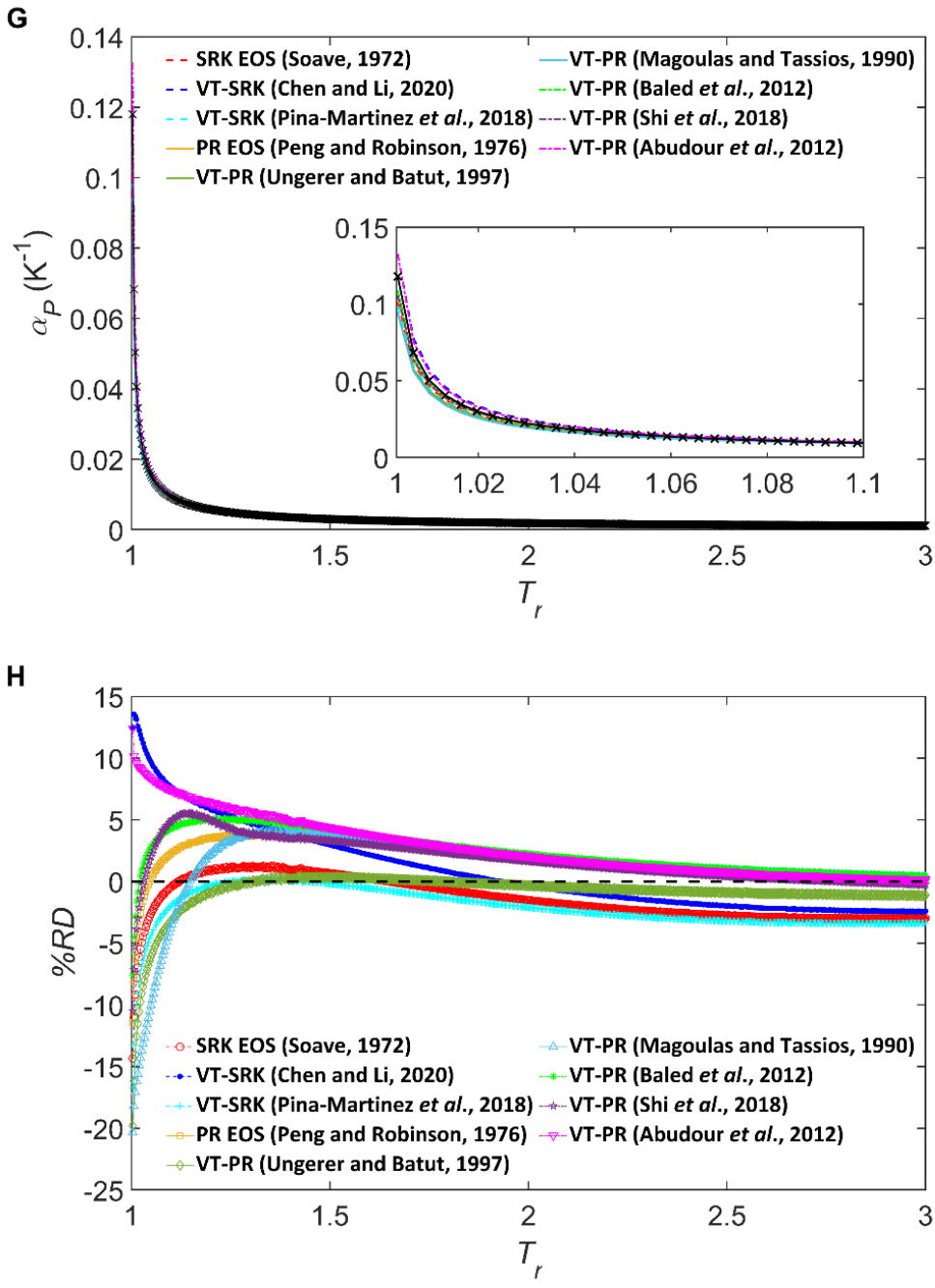

Figure 11 Comparison of the calculated α_P for the vapor-phase CO_2 against the NIST data (A, C, E, and G) and *%RDs* yielded by the models studied in this work (B, D, F, and H) at temperatures from the saturated vapor temperature to $T_r = 3$ and different pressures: $P_r = 0.1$ (A and B), $P_r = 0.4$ (C and D), $P_r = 0.7$ (E and F), and $P_r = 1$ (G and H).

3.2.3. Predicted Results for the Supercritical-phase κ_T and α_P

The predictions of the supercritical-phase κ_T and α_P by different VT models are still relatively accurate. This can be partially attributed to the relatively good performance of the untranslated PR EOS and SRK EOS in the supercritical-phase region. According to the *%AADs* of κ_T predictions for the supercritical CO_2 and CH_4, the VT models of Abudour *et al*.[3] and Chen and Li[5] can double the accuracy yielded by their corresponding untranslated EOSs. The VT-PR EOS by Abudour *et al*.[3] yields the lowest *%AADs* of 1.11% and 1.41% of κ_T predictions for the supercritical phases of CO_2 and CH_4, respectively. The Chen and Li VT-SRK EOS[5] yields the second-lowest *%AAD* of 2.26% for the supercritical-phase κ_T of CH_4. The Magoulas and Tassios VT-PR EOS[12] provides relatively accurate results for the supercritical phase of CO_2 with a *%AAD* of 2.04% but a larger *%AAD* of 3.52% for CH_4. The other VT models yield higher *%AADs* than their corresponding untranslated EOSs for the supercritical phases of CO_2 and CH_4. Figure 12 compares the predicted κ_T for the supercritical CH_4 against the NIST data,[7] as well as the corresponding *%RDs* yielded by each EOS model. Figure 13 shows the same information for the supercritical CO_2. Compared to the NIST data,[7] all models can correctly capture the variation trend of κ_T versus pressure change. κ_T in the supercritical-phase region tends to decreases with an increasing pressure at a given temperature. The calculated *%RDs* are relatively low but tend to become enlarged as pressure increases at a fixed temperature.

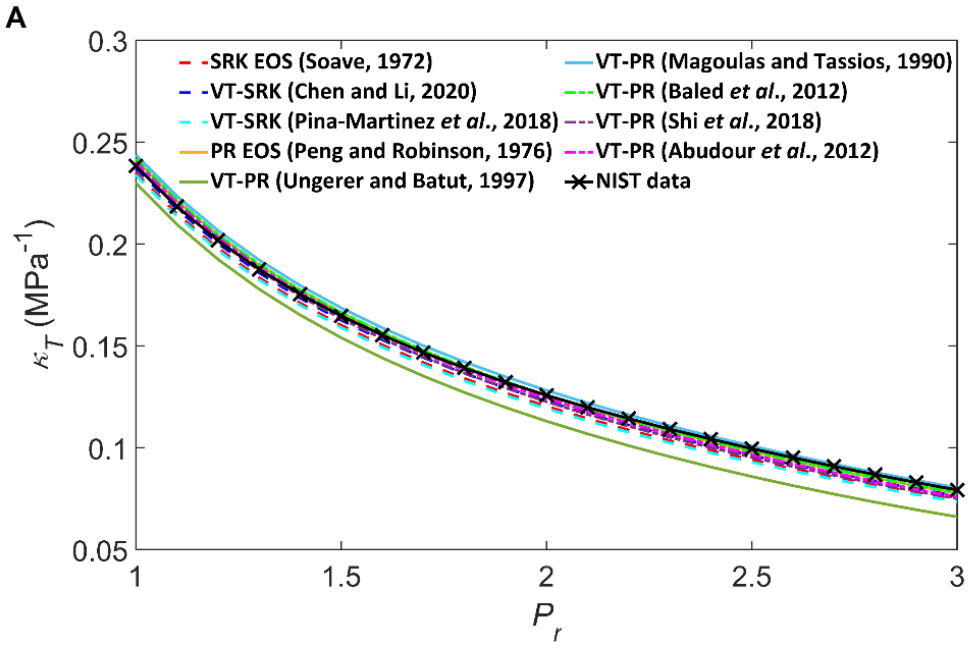
A
SRK EOS (Soave, 1972)
VT-SRK (Chen and Li, 2020)
VT-SRK (Pina-Martinez et al., 2018)
PR EOS (Peng and Robinson, 1976)
VT-PR (Ungerer and Batut, 1997)
VT-PR (Magoulas and Tassios, 1990)
VT-PR (Baled et al., 2012)
VT-PR (Shi et al., 2018)
VT-PR (Abudour et al., 2012)
NIST data
κ_T (MPa^{-1})
P_r

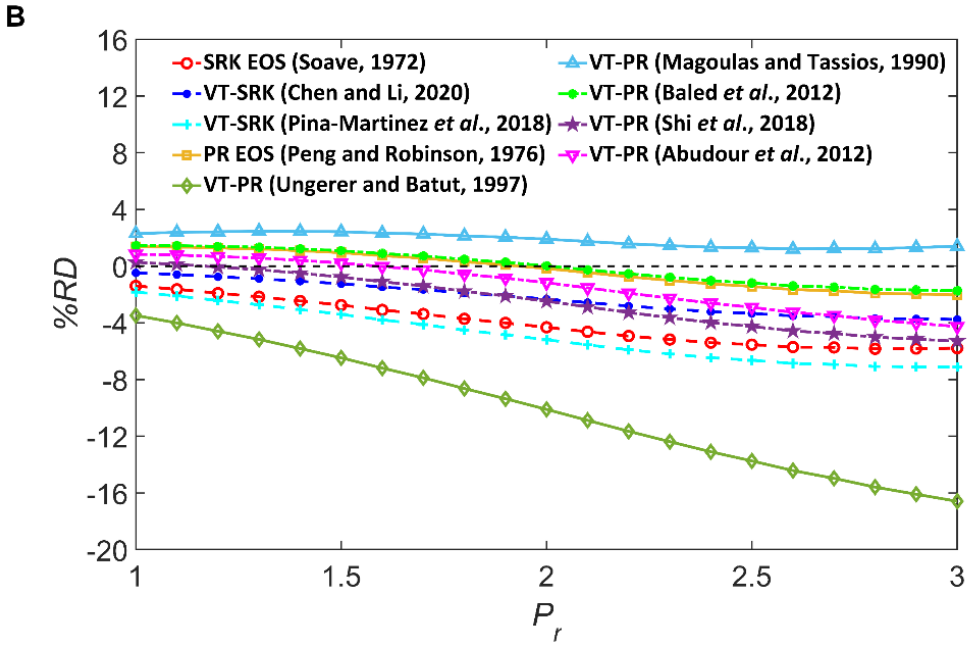
B
SRK EOS (Soave, 1972)
VT-SRK (Chen and Li, 2020)
VT-SRK (Pina-Martinez et al., 2018)
PR EOS (Peng and Robinson, 1976)
VT-PR (Ungerer and Batut, 1997)
VT-PR (Magoulas and Tassios, 1990)
VT-PR (Baled et al., 2012)
VT-PR (Shi et al., 2018)
VT-PR (Abudour et al., 2012)
%RD
P_r

C

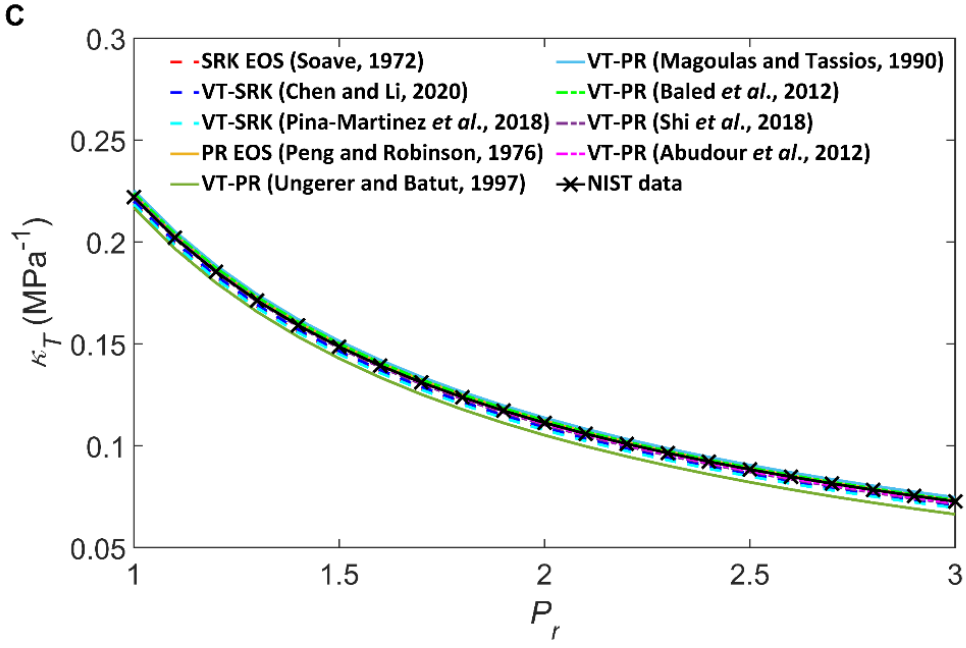
SRK EOS (Soave, 1972)
VT-SRK (Chen and Li, 2020)
VT-SRK (Pina-Martinez et al., 2018)
PR EOS (Peng and Robinson, 1976)
VT-PR (Ungerer and Batut, 1997)
VT-PR (Magoulas and Tassios, 1990)
VT-PR (Baled et al., 2012)
VT-PR (Shi et al., 2018)
VT-PR (Abudour et al., 2012)
NIST data
κ_T (MPa^{-1})
P_r

D

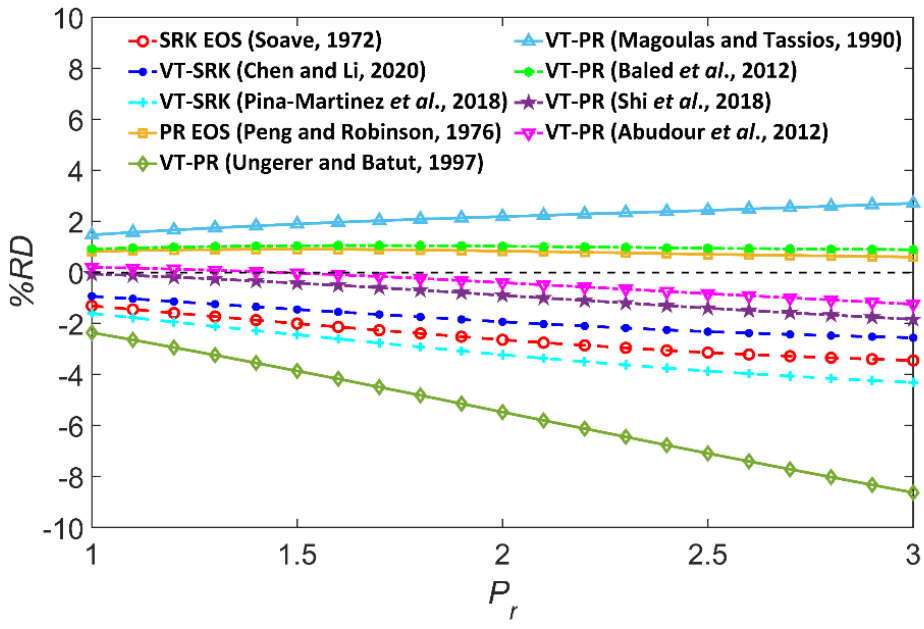
SRK EOS (Soave, 1972)
VT-SRK (Chen and Li, 2020)
VT-SRK (Pina-Martinez et al., 2018)
PR EOS (Peng and Robinson, 1976)
VT-PR (Ungerer and Batut, 1997)
VT-PR (Magoulas and Tassios, 1990)
VT-PR (Baled et al., 2012)
VT-PR (Shi et al., 2018)
VT-PR (Abudour et al., 2012)
%RD
P_r

E

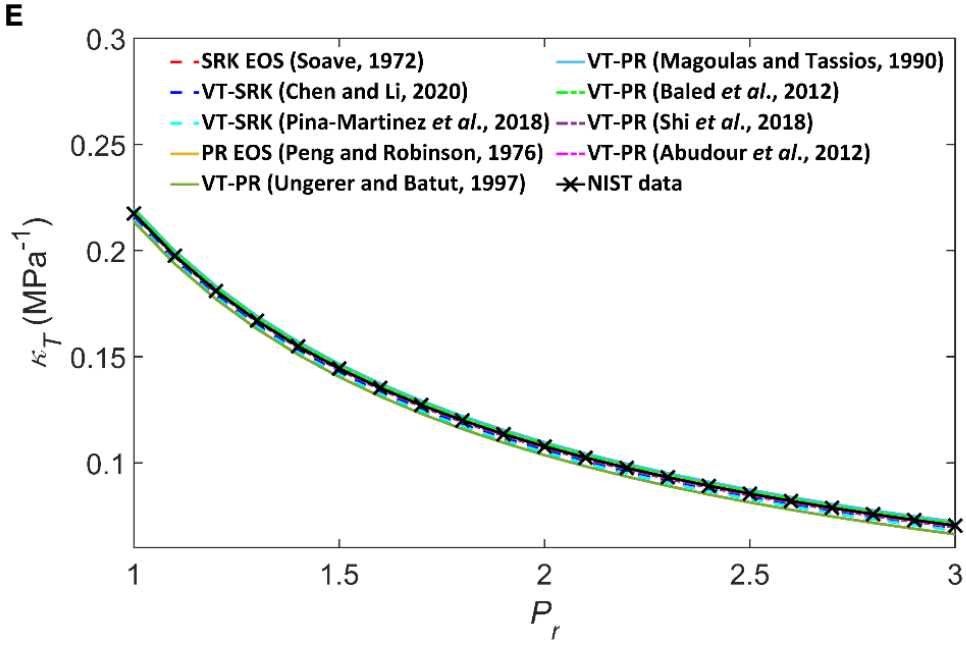
SRK EOS (Soave, 1972)
VT-SRK (Chen and Li, 2020)
VT-SRK (Pina-Martinez et al., 2018)
PR EOS (Peng and Robinson, 1976)
VT-PR (Ungerer and Batut, 1997)
VT-PR (Magoulas and Tassios, 1990)
VT-PR (Baled et al., 2012)
VT-PR (Shi et al., 2018)
VT-PR (Abudour et al., 2012)
NIST data
κ_T (MPa^{-1})
P_r

F

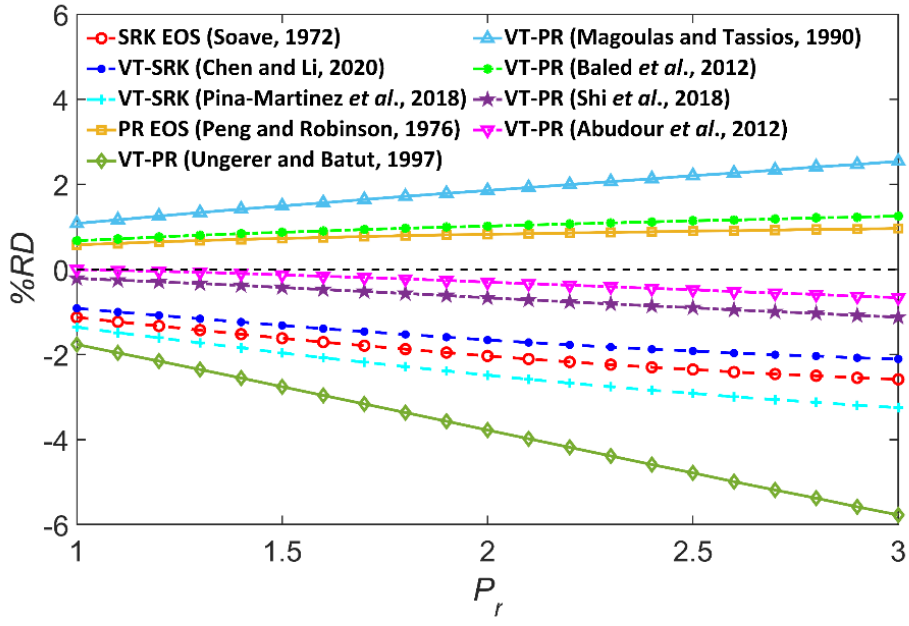
SRK EOS (Soave, 1972)
VT-SRK (Chen and Li, 2020)
VT-SRK (Pina-Martinez et al., 2018)
PR EOS (Peng and Robinson, 1976)
VT-PR (Ungerer and Batut, 1997)
VT-PR (Magoulas and Tassios, 1990)
VT-PR (Baled et al., 2012)
VT-PR (Shi et al., 2018)
VT-PR (Abudour et al., 2012)
%RD
P_r

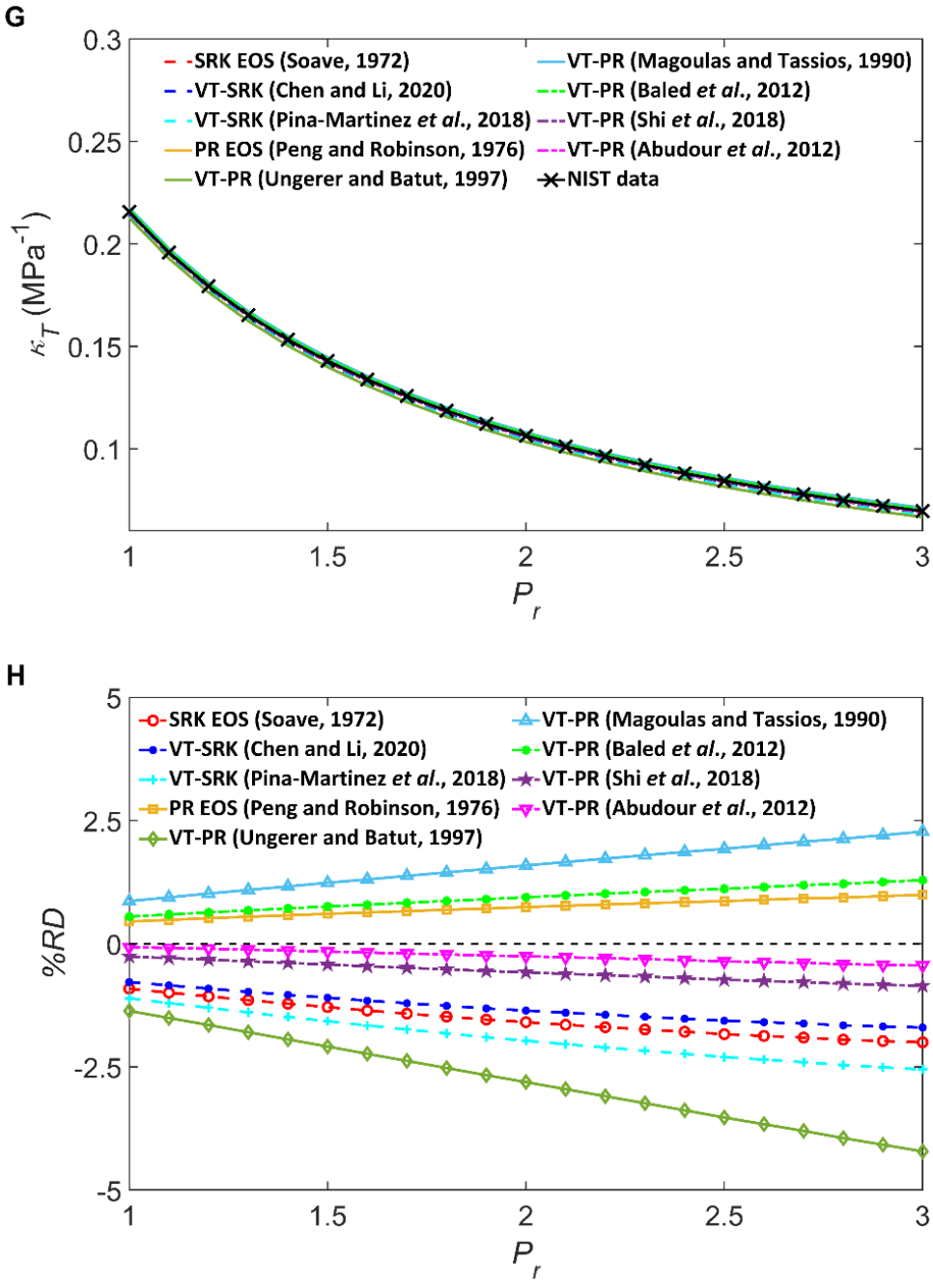

Figure 12 Comparison of the calculated κ_T for the supercritical-phase CH_4 against the NIST data (A, C, E, and G) and *%RDs* yielded by the models studied in this work (B, D, F, and H) at pressures from $P_r = 1$ to $P_r = 3$ and different temperatures: $T_r = 1.5$ (A and B), $T_r = 2$ (C and D), $T_r = 2.5$ (E and F), and $T_r = 3$ (G and H).

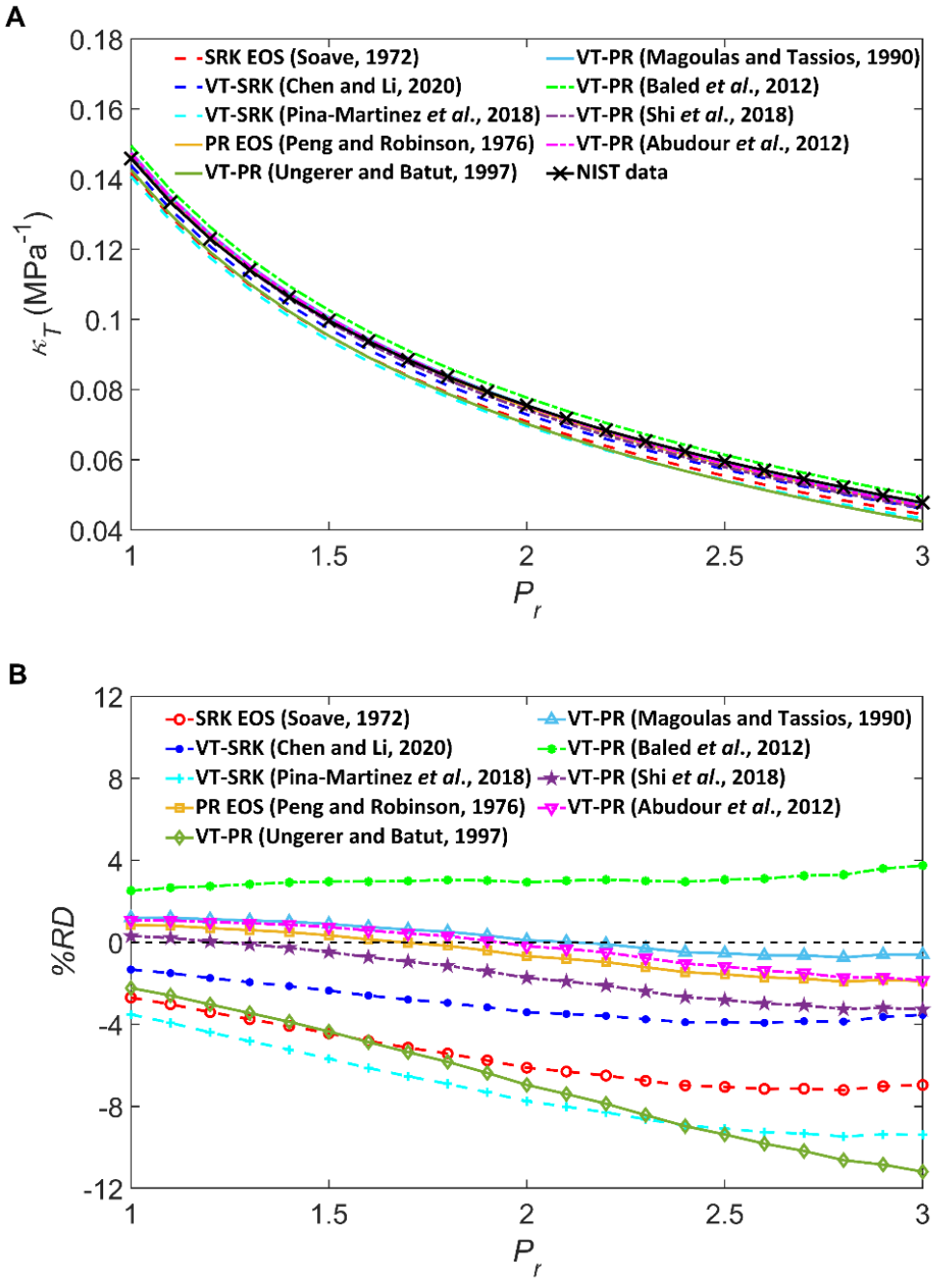
A
SRK EOS (Soave, 1972)
VT-SRK (Chen and Li, 2020)
VT-SRK (Pina-Martinez et al., 2018)
PR EOS (Peng and Robinson, 1976)
VT-PR (Ungerer and Batut, 1997)
VT-PR (Magoulas and Tassios, 1990)
VT-PR (Baled et al., 2012)
VT-PR (Shi et al., 2018)
VT-PR (Abudour et al., 2012)
NIST data
κ_T (MPa^{-1})
P_r
B
%RD
P_r

C

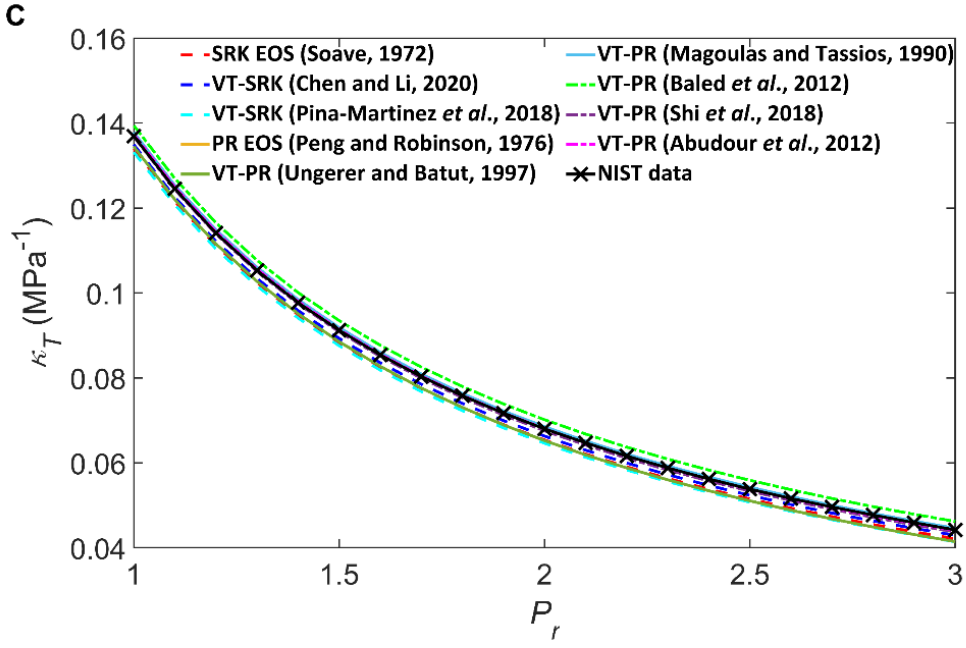
SRK EOS (Soave, 1972)
VT-SRK (Chen and Li, 2020)
VT-SRK (Pina-Martinez et al., 2018)
PR EOS (Peng and Robinson, 1976)
VT-PR (Ungerer and Batut, 1997)
VT-PR (Magoulas and Tassios, 1990)
VT-PR (Baled et al., 2012)
VT-PR (Shi et al., 2018)
VT-PR (Abudour et al., 2012)
NIST data
κ_T (MPa^{-1})
P_r

D

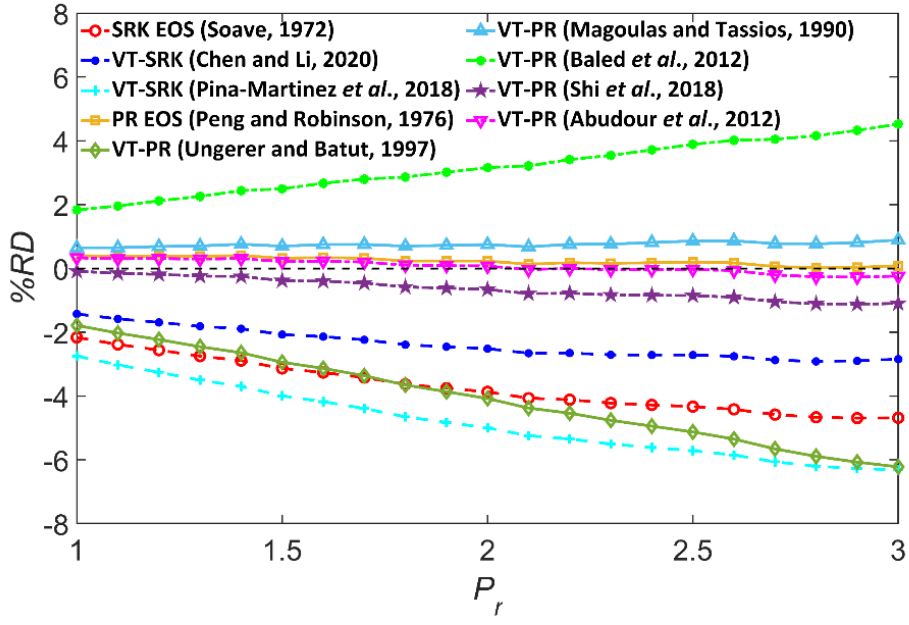
SRK EOS (Soave, 1972)
VT-SRK (Chen and Li, 2020)
VT-SRK (Pina-Martinez et al., 2018)
PR EOS (Peng and Robinson, 1976)
VT-PR (Ungerer and Batut, 1997)
VT-PR (Magoulas and Tassios, 1990)
VT-PR (Baled et al., 2012)
VT-PR (Shi et al., 2018)
VT-PR (Abudour et al., 2012)
%RD
P_r

E

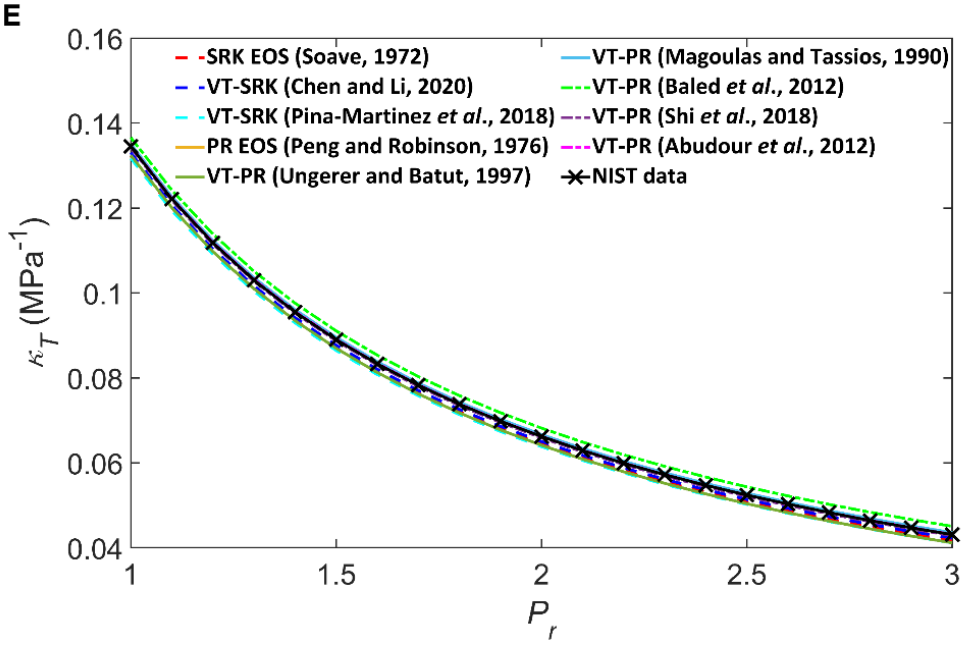
SRK EOS (Soave, 1972)
VT-SRK (Chen and Li, 2020)
VT-SRK (Pina-Martinez et al., 2018)
PR EOS (Peng and Robinson, 1976)
VT-PR (Ungerer and Batut, 1997)
VT-PR (Magoulas and Tassios, 1990)
VT-PR (Baled et al., 2012)
VT-PR (Shi et al., 2018)
VT-PR (Abudour et al., 2012)
NIST data
0.16
0.14
0.12
0.1
0.08
0.06
0.04
1
1.5
2
2.5
3
κ_T (MPa^{-1})
P_r

F

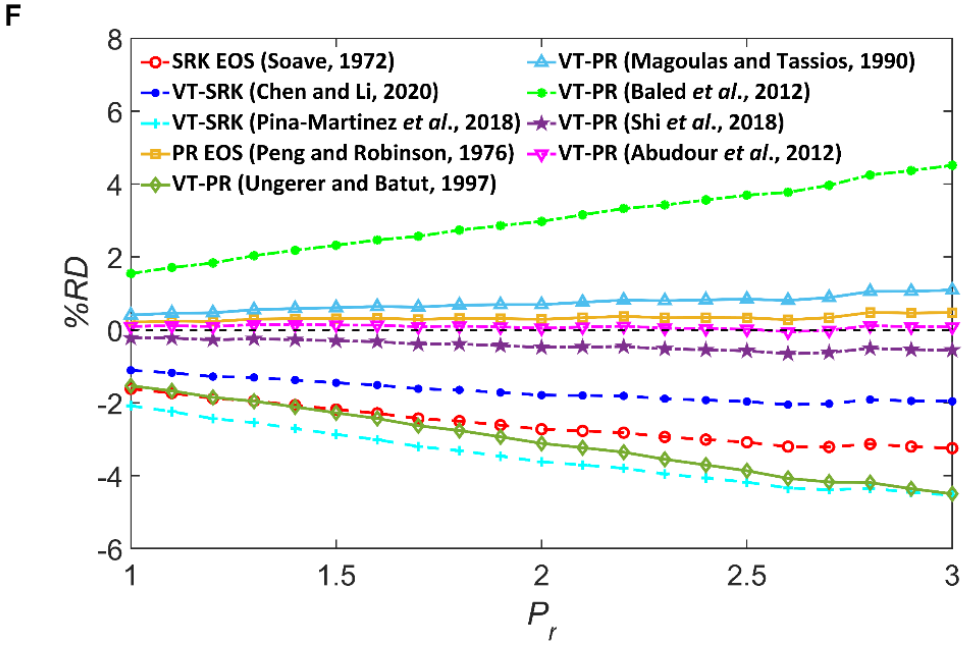
SRK EOS (Soave, 1972)
VT-SRK (Chen and Li, 2020)
VT-SRK (Pina-Martinez et al., 2018)
PR EOS (Peng and Robinson, 1976)
VT-PR (Ungerer and Batut, 1997)
VT-PR (Magoulas and Tassios, 1990)
VT-PR (Baled et al., 2012)
VT-PR (Shi et al., 2018)
VT-PR (Abudour et al., 2012)
8
6
4
2
0
-2
-4
-6
1
1.5
2
2.5
3
%RD
P_r

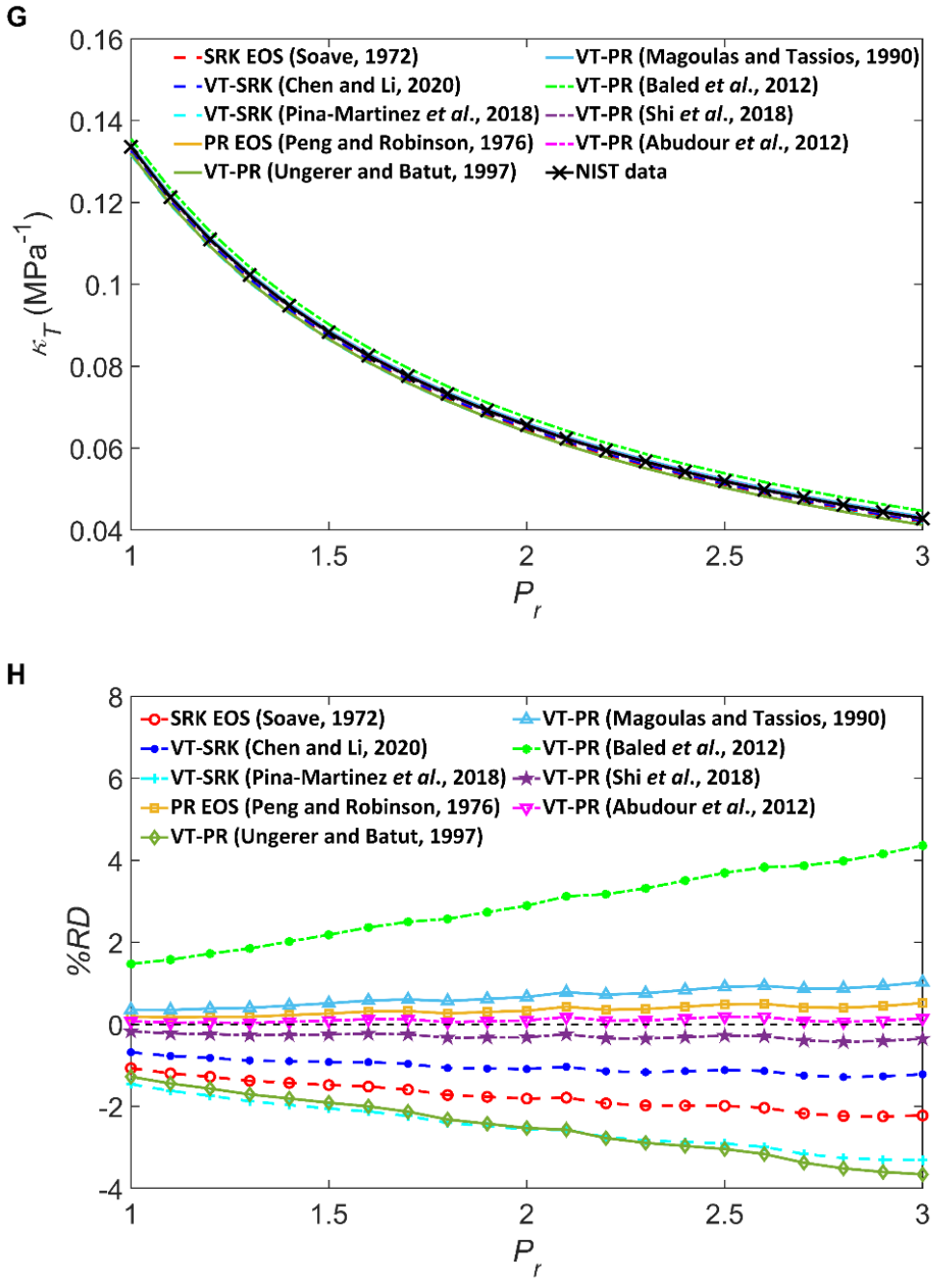

Figure 13 Comparison of the calculated κ_T for the supercritical-phase CO_2 against the NIST data (A, C, E, and G) and *%RDs* yielded by the models studied in this work (B, D, F, and H) at pressures from $P_r = 1$ to $P_r = 3$ and different temperatures: $T_r = 1.5$ (A and B), $T_r = 2$ (C and D), $T_r = 2.5$ (E and F), $T_r = 3$ (G and H).

The predictions of α_P for the supercritical phase by each EOS model are compared to the NIST data,[7] and the corresponding *%RDs* are also calculated. The results for CH_4 and CO_2 are shown in Figures 14 and 15, respectively. As shown in Figures 14 and 15, the predicted

values of α_P tend to peak at temperatures above the critical temperature. Such variation trend of α_P could be attributed to the existence of the Widom line.[13] The Widom line can be considered as an extension of the vapor pressure line.[13] The upper left side of the Widom line can be considered as a liquid-like supercritical phase, while the lower right side of the Widom line can be considered as a vapor-like supercritical phase.[13] Along an isobaric line in the liquid-like region, α_P increases with an increasing temperature. Along an isobaric line in the vapor-like region, α_P decreases with an increasing temperature. Therefore, α_P can reach a maximum at the pseudo-saturation line in the supercritical phase. All models can predict the occurrence of the peaks but tend to yield relatively larger deviations of α_P predictions around the peaks. It is worthwhile noting that the α_P predicted by the Magoulas and Tassios model[12] for the supercritical phases of both CH_4 and CO_2 can be less than zero. These negative α_P values appear around the critical temperature at P_r above 2.5. This can be attributed to the occurrence of the isotherm crossover phenomenon. Shi *et al*.[14] also reported that the Magoulas and Tassios model[12] has an isotherm crossover issue.

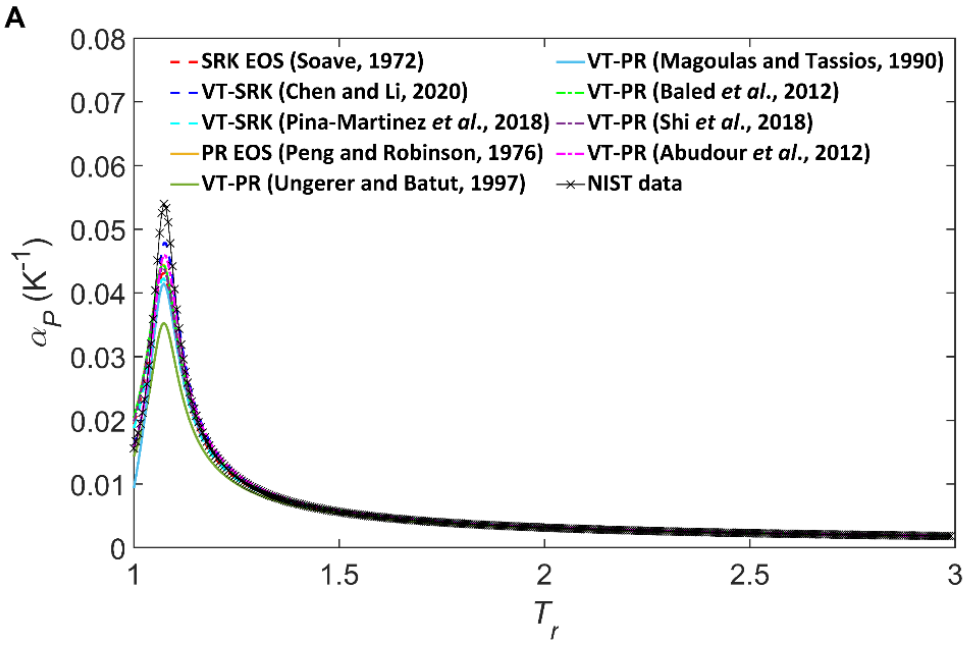
A
SRK EOS (Soave, 1972)
VT-SRK (Chen and Li, 2020)
VT-SRK (Pina-Martinez et al., 2018)
PR EOS (Peng and Robinson, 1976)
VT-PR (Ungerer and Batut, 1997)
VT-PR (Magoulas and Tassios, 1990)
VT-PR (Baled et al., 2012)
VT-PR (Shi et al., 2018)
VT-PR (Abudour et al., 2012)
NIST data
α_P (K^{-1})
T_r

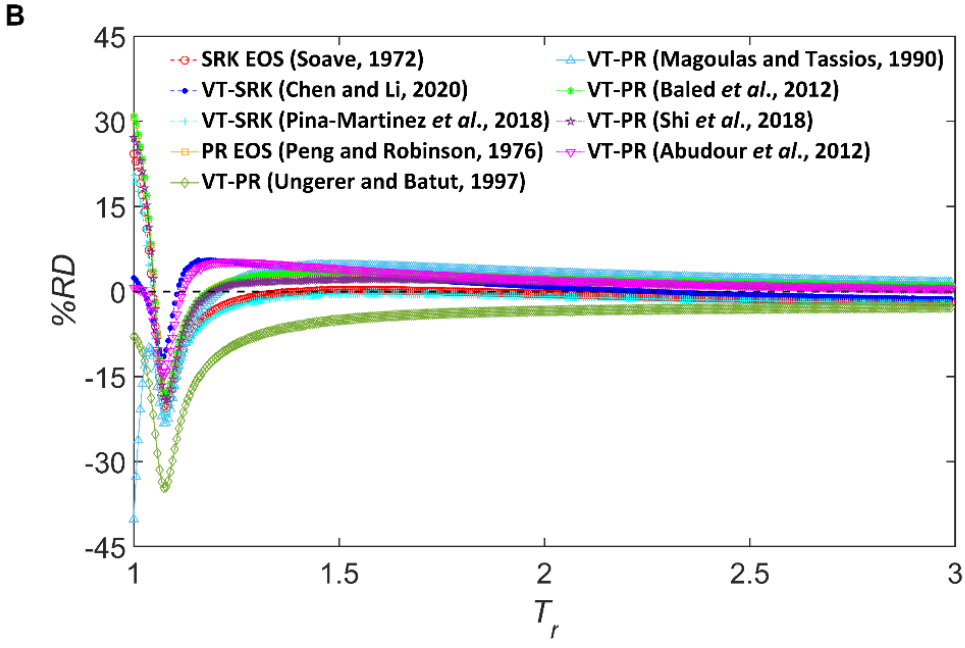
B
SRK EOS (Soave, 1972)
VT-SRK (Chen and Li, 2020)
VT-SRK (Pina-Martinez et al., 2018)
PR EOS (Peng and Robinson, 1976)
VT-PR (Ungerer and Batut, 1997)
VT-PR (Magoulas and Tassios, 1990)
VT-PR (Baled et al., 2012)
VT-PR (Shi et al., 2018)
VT-PR (Abudour et al., 2012)
%RD
T_r

C

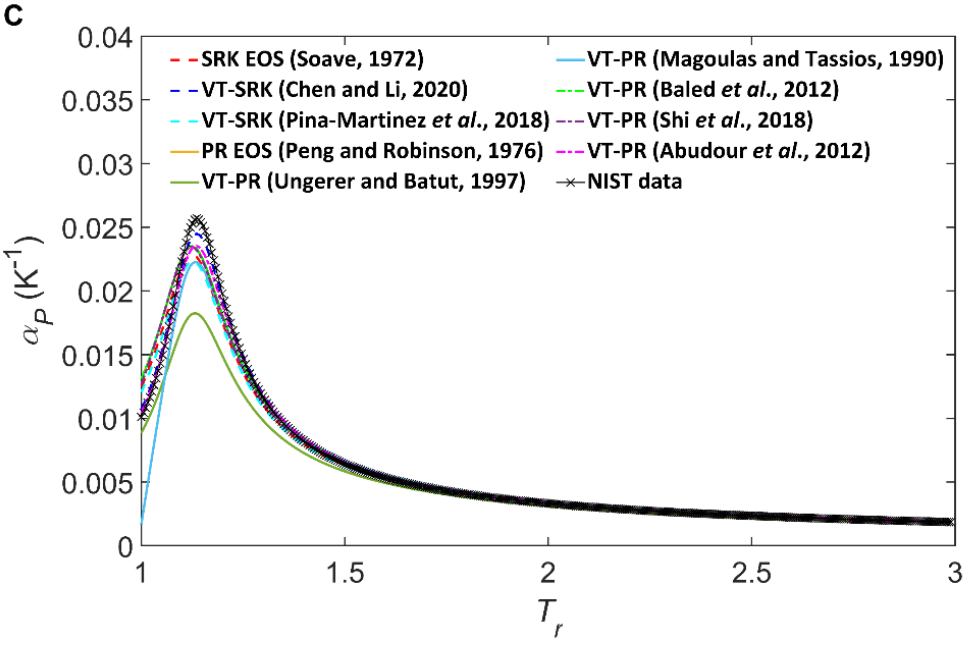
SRK EOS (Soave, 1972)
VT-SRK (Chen and Li, 2020)
VT-SRK (Pina-Martinez et al., 2018)
PR EOS (Peng and Robinson, 1976)
VT-PR (Ungerer and Batut, 1997)
VT-PR (Magoulas and Tassios, 1990)
VT-PR (Baled et al., 2012)
VT-PR (Shi et al., 2018)
VT-PR (Abudour et al., 2012)
NIST data
α_P (K^{-1})
T_r

D

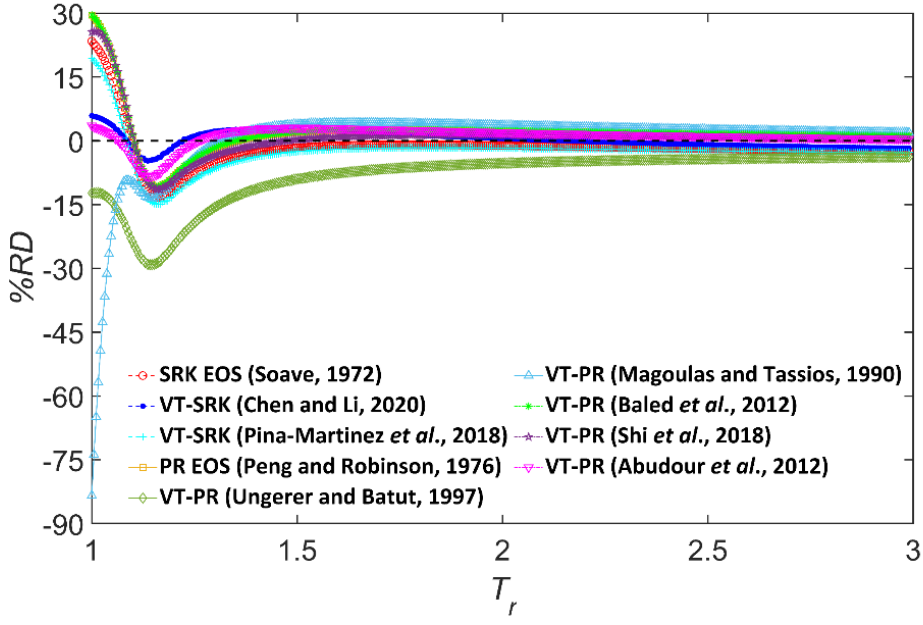
%RD
SRK EOS (Soave, 1972)
VT-SRK (Chen and Li, 2020)
VT-SRK (Pina-Martinez et al., 2018)
PR EOS (Peng and Robinson, 1976)
VT-PR (Ungerer and Batut, 1997)
VT-PR (Magoulas and Tassios, 1990)
VT-PR (Baled et al., 2012)
VT-PR (Shi et al., 2018)
VT-PR (Abudour et al., 2012)
T_r

E

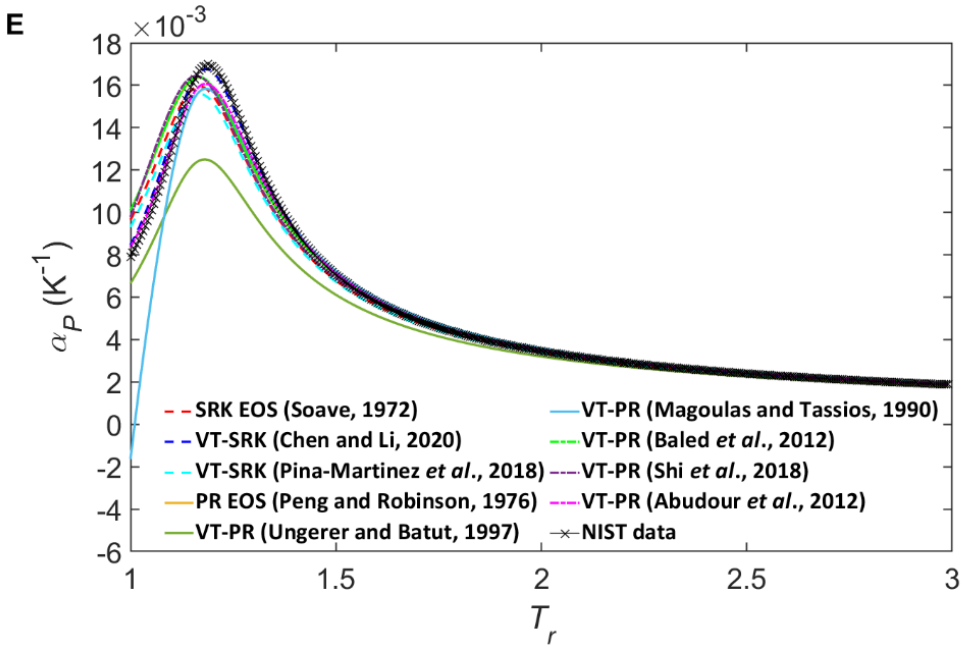
×10^-3
18
16
14
12
10
8
6
4
2
0
-2
-4
-6
α_P (K^{-1})
1
1.5
2
2.5
3
T_r
SRK EOS (Soave, 1972)
VT-SRK (Chen and Li, 2020)
VT-SRK (Pina-Martinez *et al.*, 2018)
PR EOS (Peng and Robinson, 1976)
VT-PR (Ungerer and Batut, 1997)
VT-PR (Magoulas and Tassios, 1990)
VT-PR (Baled *et al.*, 2012)
VT-PR (Shi *et al.*, 2018)
VT-PR (Abudour *et al.*, 2012)
NIST data

F

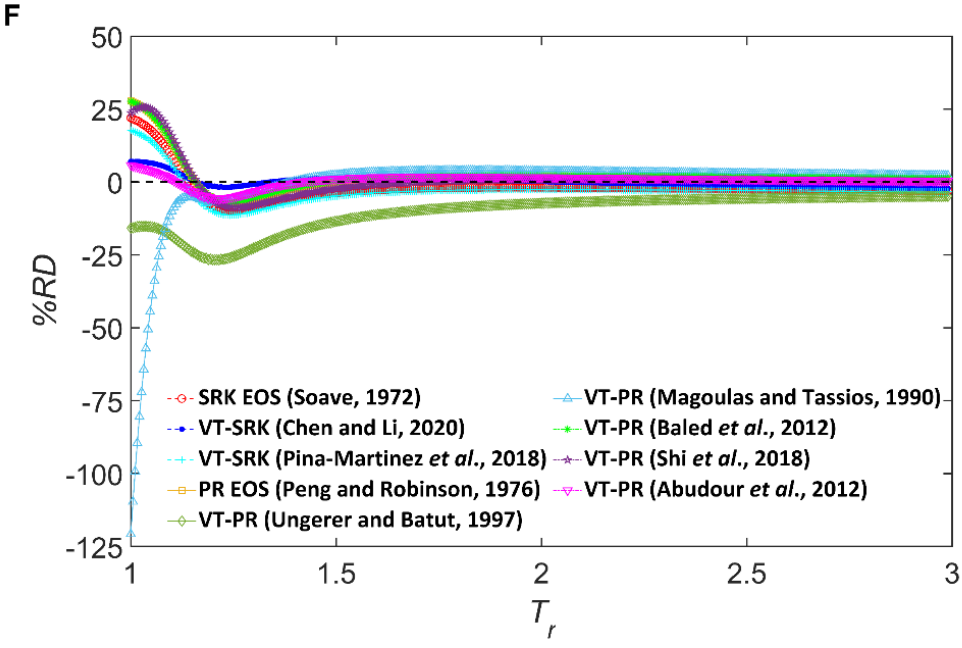
50
25
0
-25
-50
-75
-100
-125
%RD
1
1.5
2
2.5
3
T_r
SRK EOS (Soave, 1972)
VT-SRK (Chen and Li, 2020)
VT-SRK (Pina-Martinez *et al.*, 2018)
PR EOS (Peng and Robinson, 1976)
VT-PR (Ungerer and Batut, 1997)
VT-PR (Magoulas and Tassios, 1990)
VT-PR (Baled *et al.*, 2012)
VT-PR (Shi *et al.*, 2018)
VT-PR (Abudour *et al.*, 2012)

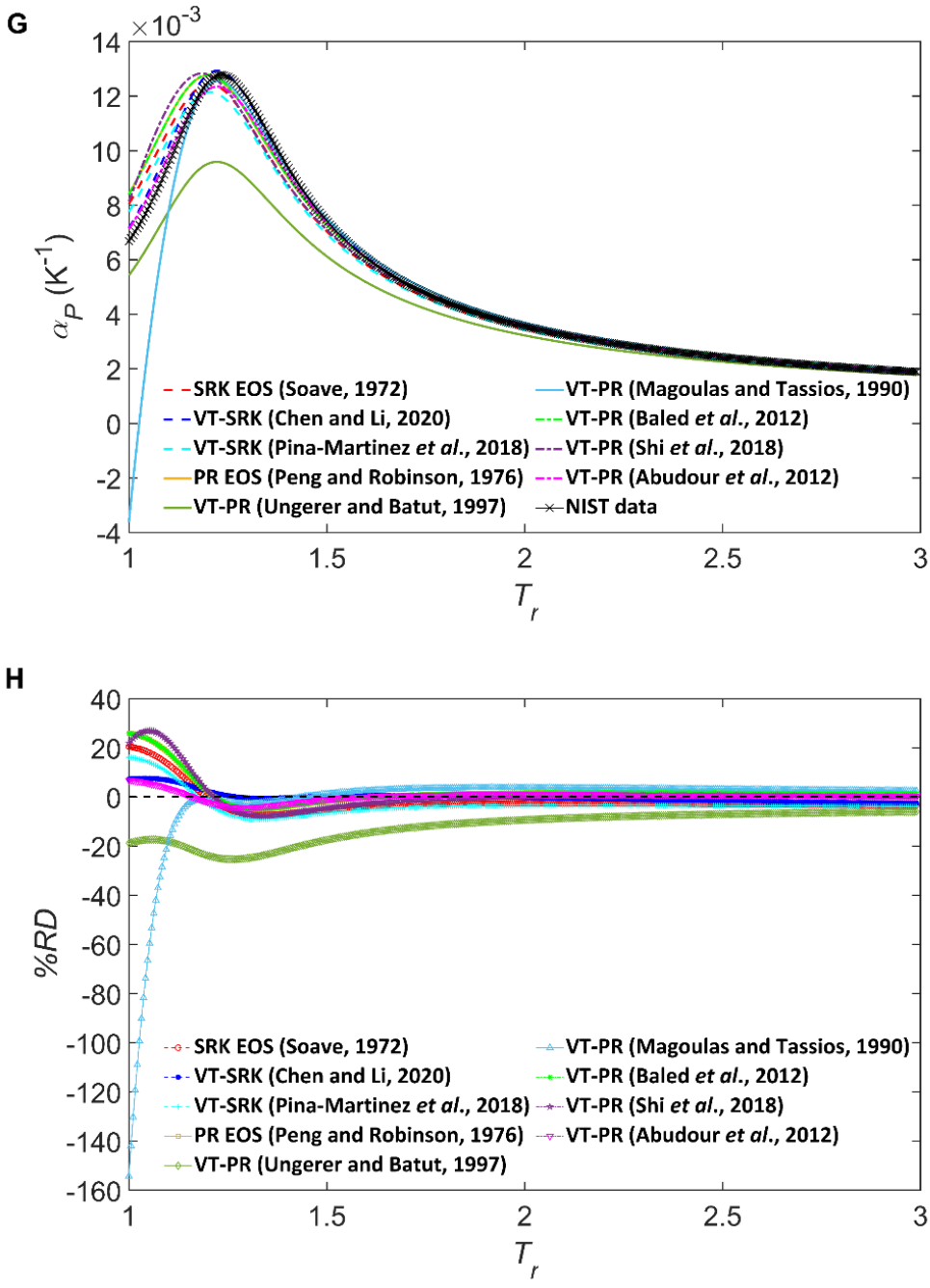

Figure 14 Comparison of the calculated α_P for the supercritical-phase CH_4 against the NIST data (A, C, E, and G) and *%RDs* yielded by the models studied in this work (B, D, F, and H) at temperatures from the $T_r = 1$ to $T_r = 3$ and different pressures: $P_r = 1.5$ (A and B), $P_r = 2$ (C and D), $P_r = 2.5$ (E and F), and $P_r = 3$ (G and H).

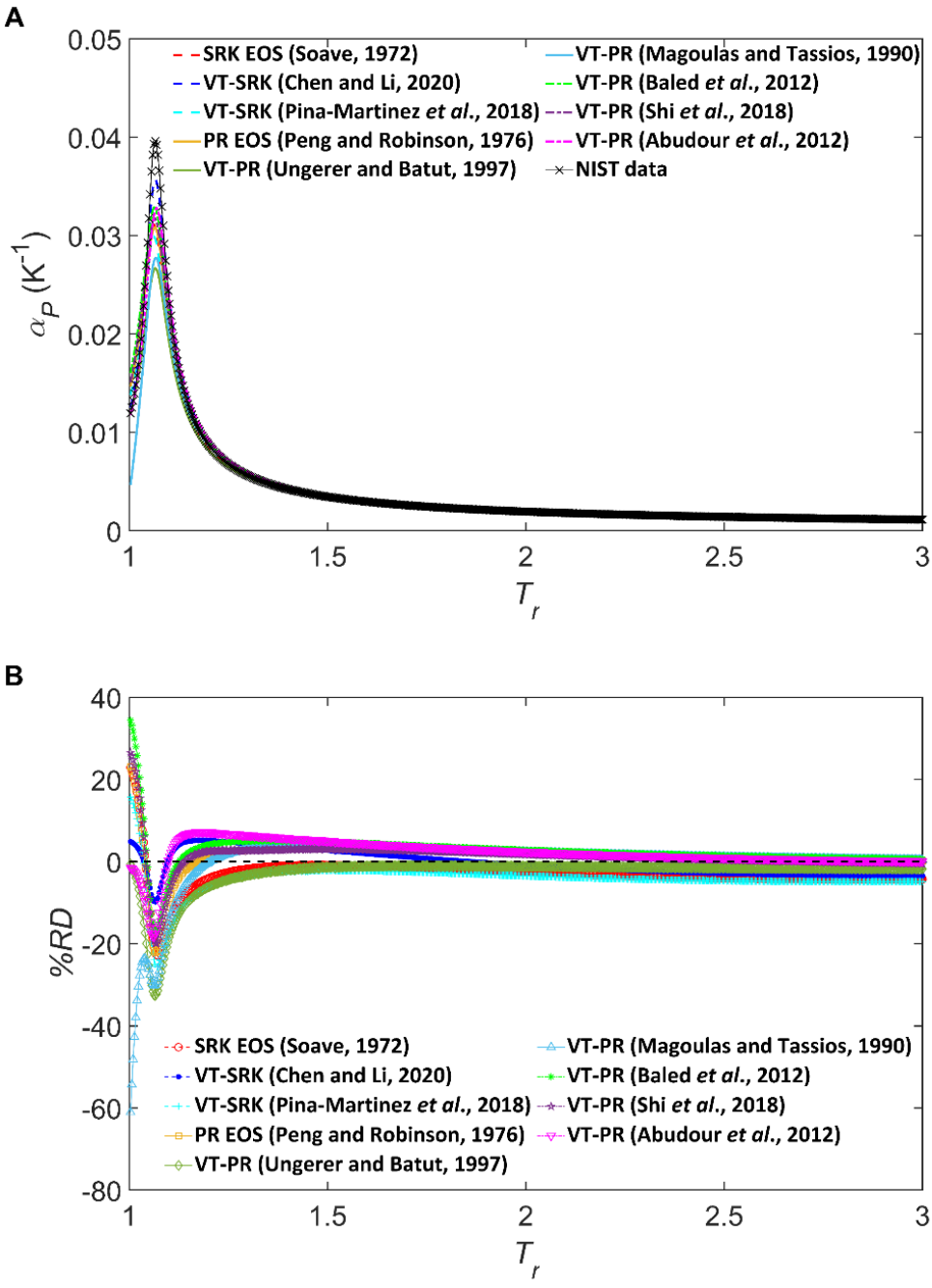
A
0.05
0.04
0.03
0.02
0.01
0
α_P (K^{-1})
1
1.5
2
2.5
3
T_r
SRK EOS (Soave, 1972)
VT-SRK (Chen and Li, 2020)
VT-SRK (Pina-Martinez et al., 2018)
PR EOS (Peng and Robinson, 1976)
VT-PR (Ungerer and Batut, 1997)
VT-PR (Magoulas and Tassios, 1990)
VT-PR (Baled et al., 2012)
VT-PR (Shi et al., 2018)
VT-PR (Abudour et al., 2012)
NIST data
B
40
20
0
-20
-40
-60
-80
%RD
1
1.5
2
2.5
3
T_r
SRK EOS (Soave, 1972)
VT-SRK (Chen and Li, 2020)
VT-SRK (Pina-Martinez et al., 2018)
PR EOS (Peng and Robinson, 1976)
VT-PR (Ungerer and Batut, 1997)
VT-PR (Magoulas and Tassios, 1990)
VT-PR (Baled et al., 2012)
VT-PR (Shi et al., 2018)
VT-PR (Abudour et al., 2012)

C

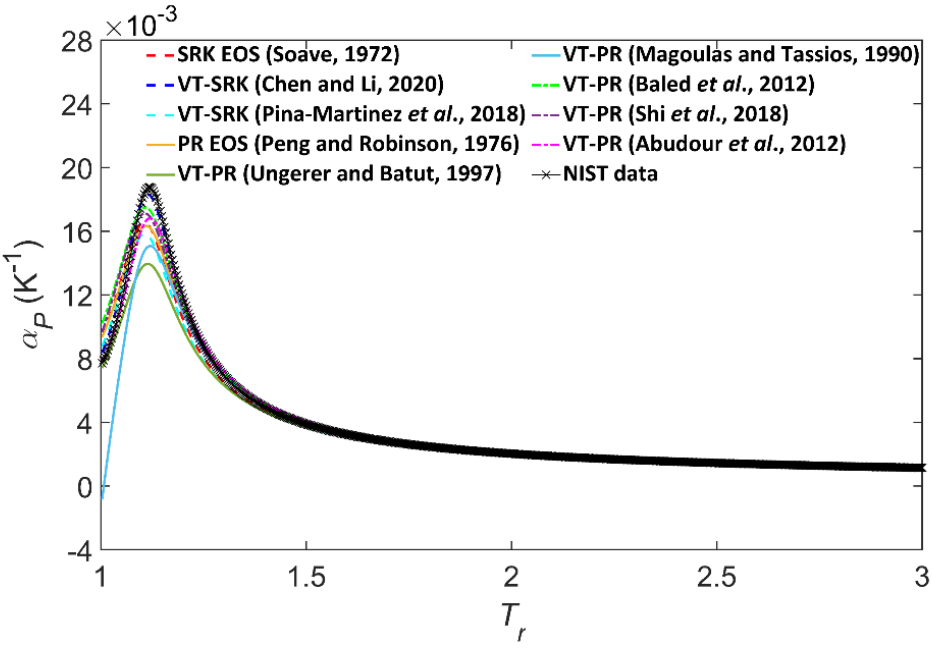
×10^-3
28
24
20
16
12
8
4
0
-4
1
1.5
2
2.5
3
T_r
α_P (K^{-1})
SRK EOS (Soave, 1972)
VT-SRK (Chen and Li, 2020)
VT-SRK (Pina-Martinez et al., 2018)
PR EOS (Peng and Robinson, 1976)
VT-PR (Ungerer and Batut, 1997)
VT-PR (Magoulas and Tassios, 1990)
VT-PR (Baled et al., 2012)
VT-PR (Shi et al., 2018)
VT-PR (Abudour et al., 2012)
NIST data

D

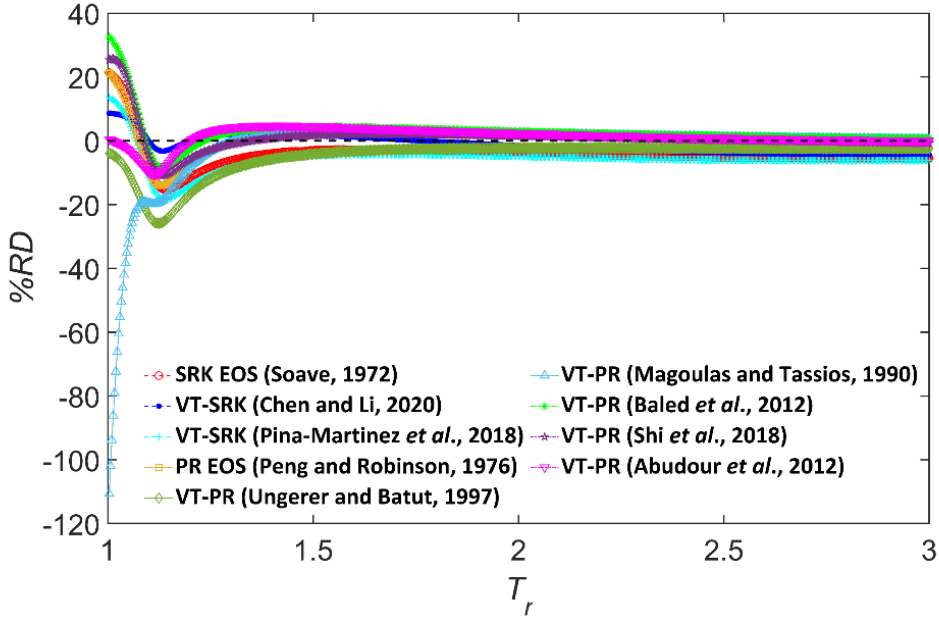
40
20
0
-20
-40
-60
-80
-100
-120
1
1.5
2
2.5
3
T_r
%RD
SRK EOS (Soave, 1972)
VT-SRK (Chen and Li, 2020)
VT-SRK (Pina-Martinez et al., 2018)
PR EOS (Peng and Robinson, 1976)
VT-PR (Ungerer and Batut, 1997)
VT-PR (Magoulas and Tassios, 1990)
VT-PR (Baled et al., 2012)
VT-PR (Shi et al., 2018)
VT-PR (Abudour et al., 2012)

E

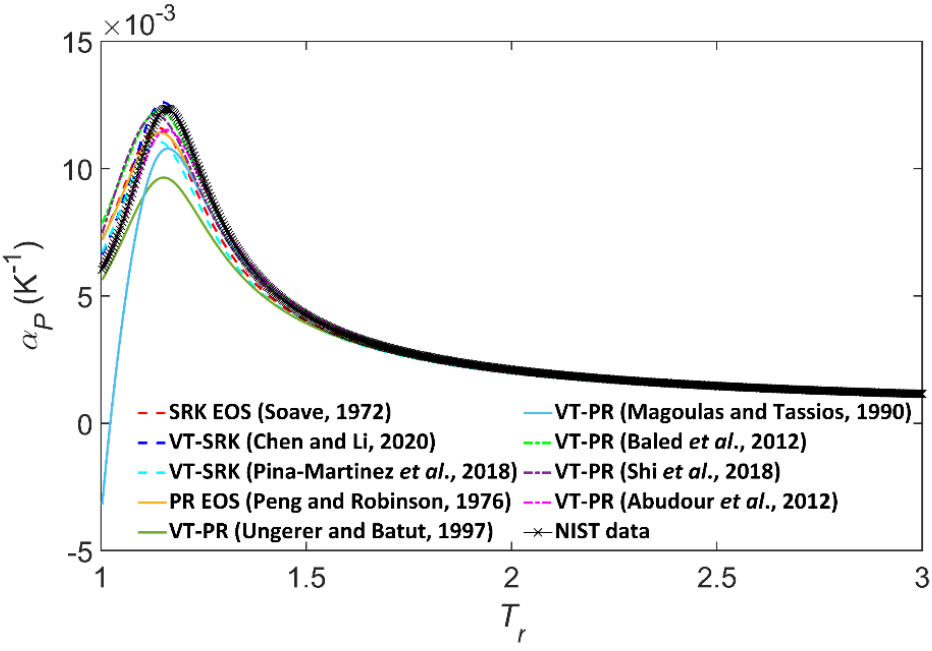
×10^-3
15
10
5
0
-5
1
1.5
2
2.5
3
α_P (K^{-1})
T_r
SRK EOS (Soave, 1972)
VT-SRK (Chen and Li, 2020)
VT-SRK (Pina-Martinez et al., 2018)
PR EOS (Peng and Robinson, 1976)
VT-PR (Ungerer and Batut, 1997)
VT-PR (Magoulas and Tassios, 1990)
VT-PR (Baled et al., 2012)
VT-PR (Shi et al., 2018)
VT-PR (Abudour et al., 2012)
NIST data

F

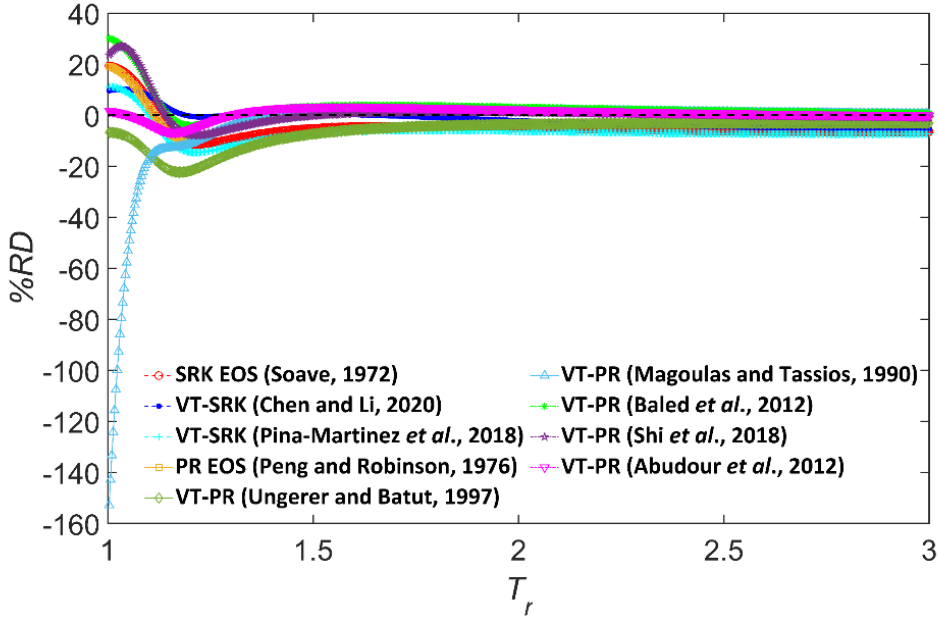
40
20
0
-20
-40
-60
-80
-100
-120
-140
-160
1
1.5
2
2.5
3
%RD
T_r
SRK EOS (Soave, 1972)
VT-SRK (Chen and Li, 2020)
VT-SRK (Pina-Martinez et al., 2018)
PR EOS (Peng and Robinson, 1976)
VT-PR (Ungerer and Batut, 1997)
VT-PR (Magoulas and Tassios, 1990)
VT-PR (Baled et al., 2012)
VT-PR (Shi et al., 2018)
VT-PR (Abudour et al., 2012)

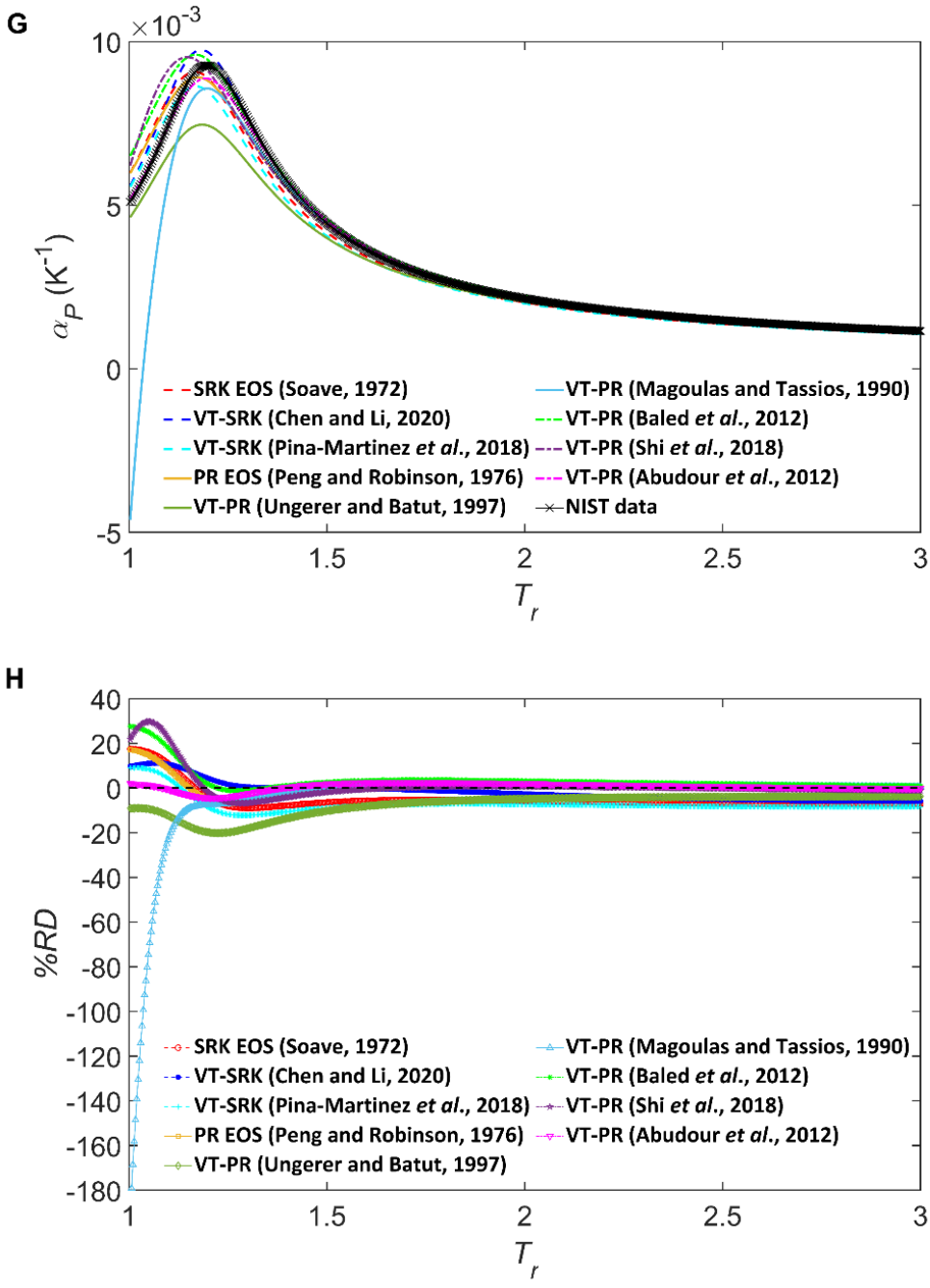

Figure 15 Comparison of the calculated α_P for the supercritical-phase CO_2 against the NIST data (A, C, E, and G) and *%RDs* yielded by the models studied in this work (B, D, F, and H) at temperatures from the $T_r = 1$ to $T_r = 3$ and different pressures: $P_r = 1.5$ (A and B), $P_r = 2$ (C and D), $P_r = 2.5$ (E and F), and $P_r = 3$ (G and H).

The overall *%AADs* yielded by different EOS models for the liquid, vapor, and supercritical phases are summarized in Figure 16. The *%AADs* yielded by all EOS models in predicting κ_T and α_P for the vapor phase are much lower than those for the liquid

phase. However, when being compared to the untranslated EOSs, most VT models have inferior performance in predicting the vapor-phase κ_T and α_P. Regarding the κ_T and α_P predictions for the liquid and supercritical phases, it is clear that the Abudour *et al*. model[3] is the most accurate VT-PR EOS model and the Chen and Li model[5] is the most accurate VT-SRK EOS model. This is because both models can provide more accurate molar-volume predictions by using the distance-function-based volume translations. On the contrary, in the temperature-dependent and the constant VT models, only the same volume translation value is used for the same PV isotherm without considering the pressure change, so these two types of VT models provide relatively poorer predictions of molar volume.

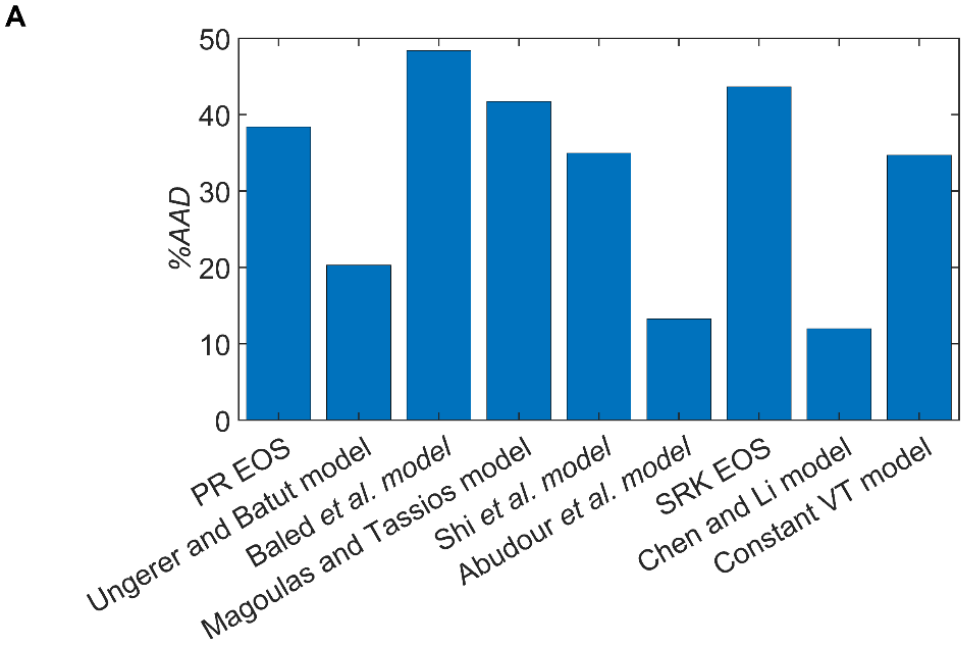

B

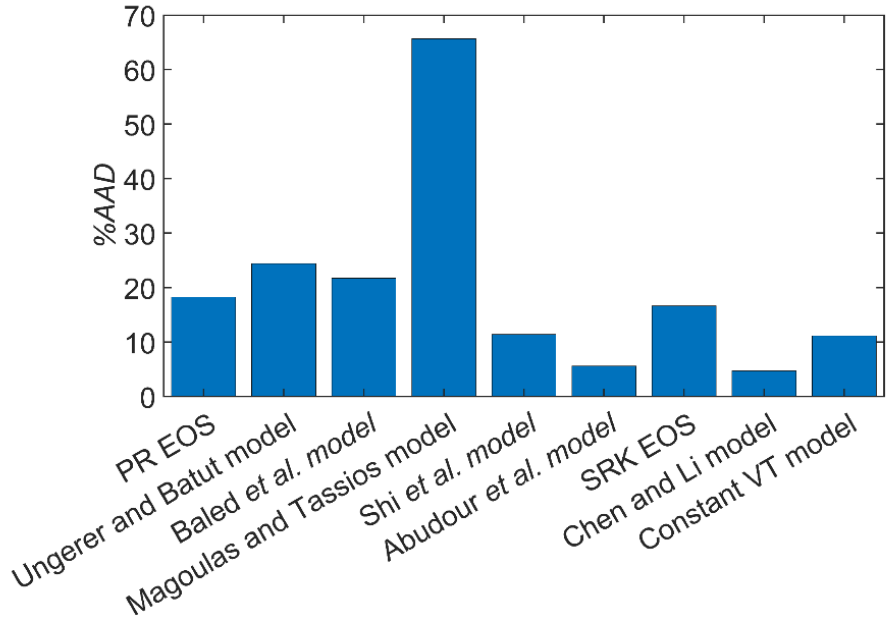
70
60
50
40
30
20
10
0
%AAD
PR EOS
Ungerer and Batut model
Baled et al. model
Magoulas and Tassios model
Shi et al. model
Abudour et al. model
SRK EOS
Chen and Li model
Constant VT model

C

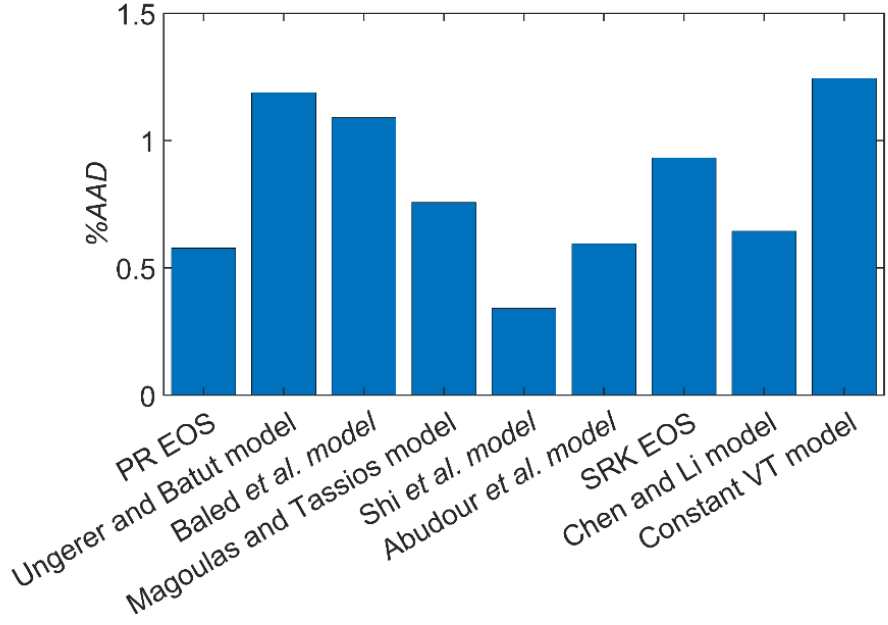
1.5
1
0.5
0
%AAD
PR EOS
Ungerer and Batut model
Baled et al. model
Magoulas and Tassios model
Shi et al. model
Abudour et al. model
SRK EOS
Chen and Li model
Constant VT model

D

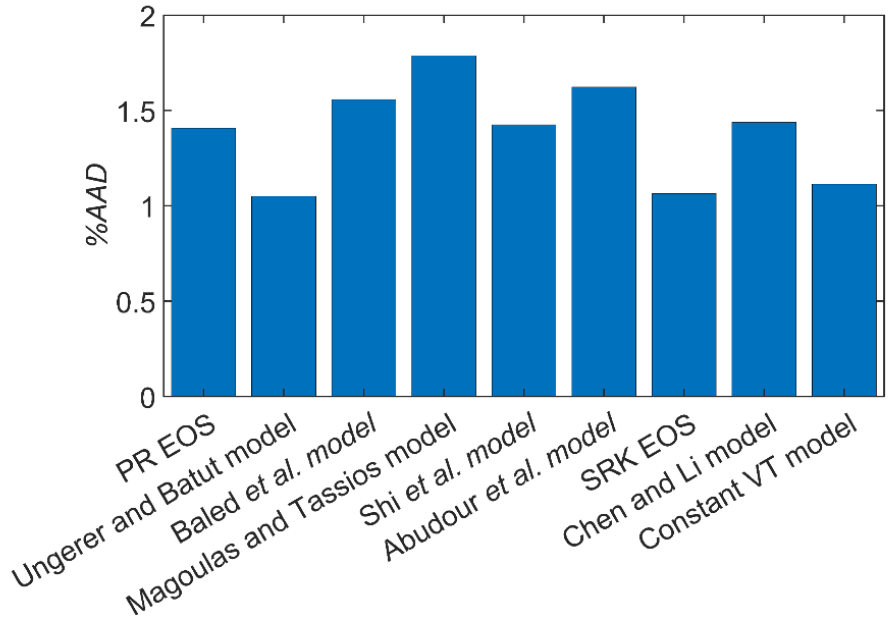
%AAD
2
1.5
1
0.5
0
PR EOS
Ungerer and Batut model
Baled et al. model
Magoulas and Tassios model
Shi et al. model
Abudour et al. model
SRK EOS
Chen and Li model
Constant VT model

E

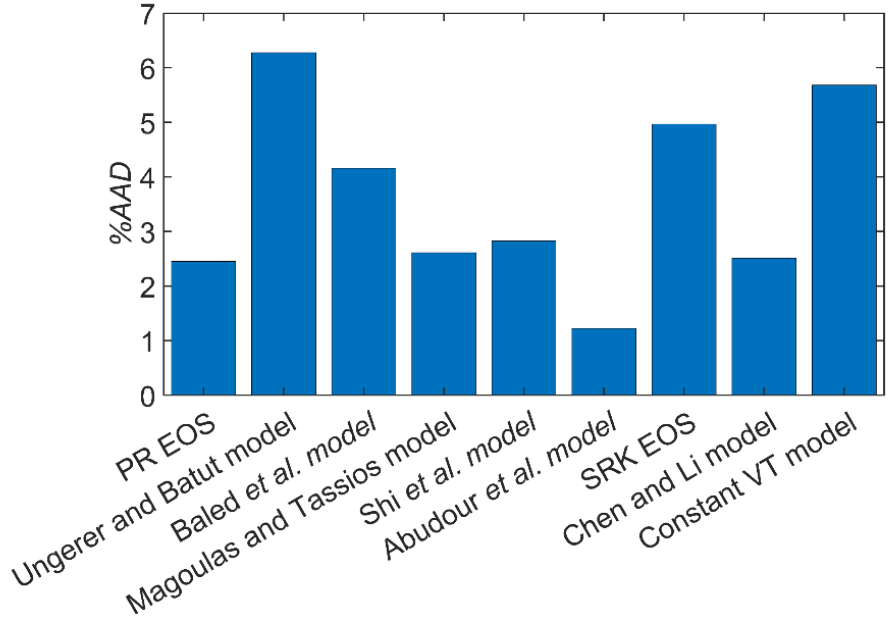
%AAD
7
6
5
4
3
2
1
0
PR EOS
Ungerer and Batut model
Baled et al. model
Magoulas and Tassios model
Shi et al. model
Abudour et al. model
SRK EOS
Chen and Li model
Constant VT model

F

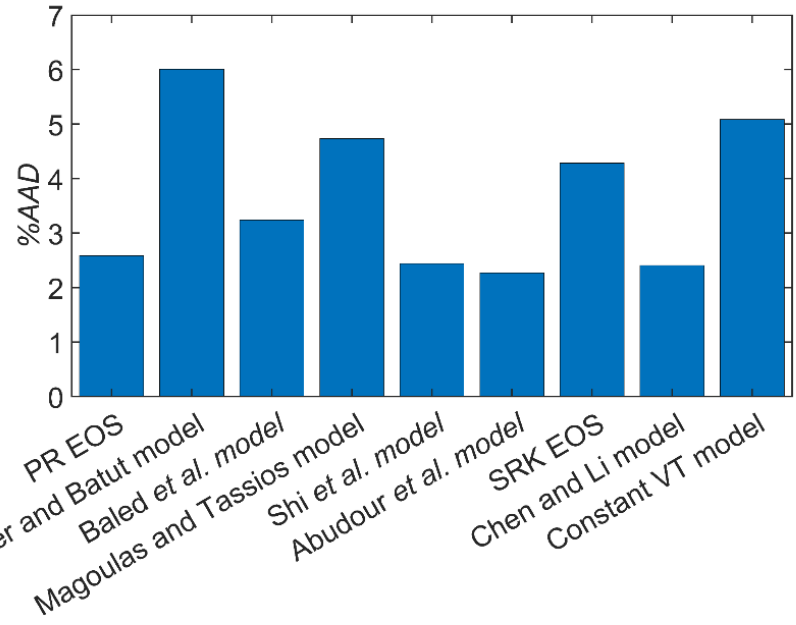

Figure 16 The overall *%AADs* of the predicted κ_T (A, C, and E) and α_P (B, D, and F) yielded by the models studied in this work for the liquid-phase region (A and B), the vaper-phase region (C and D), and the supercritical-phase region (E and F).

Considering the prediction accuracy of κ_T and α_P within the entire examined temperature and pressure ranges for the liquid, vapor, and supercritical phases, overall, the VT-PR EOS proposed by Abudour *et al.*[3] provides the most accurate κ_T predictions, while the VT-SRK EOS proposed by Chen and Li[5] provides the most accurate α_P predictions. In summary, it can be concluded that a VT-EOS that can provide more accurate PVT predictions can also yield more accurate predictions of κ_T and α_P.

References

[1] Benner, S. A.; Ricardo, A.; Carrigan, M. A. Is there a common chemical model for life in the universe? *Curr. Opin. Chem. Biol.* **2004**, *8* (6), 672–689.

[2] Braeuer, A. In situ spectroscopic techniques at high pressure. *Supercritical Fluid Science and Technology*, Vol. 7; Elsevier, 2015.

[3] Abudour, A. M.; Mohammad, S. A.; Robinson, R. L.; Gasem, K. A. M. Volume-translated Peng–Robinson equation of state for saturated and single-phase liquid densities. *Fluid Phase Equilib*. **2012**, *335*, 74–87.

[4] Pina-Martinez, A.; Le Guennec, Y.; Privat, R.; Jaubert, J. N.; Mathias, P. M. Analysis of the combinations of property data that are suitable for a safe estimation of consistent Twu α-function parameters: Updated parameter values for the translated-consistent tc-PR and tc-RK cubic equations of state. *J. Chem. Eng. Data* **2018,** *63* (10), 3980–3988.

[5] Chen, X.; Li, H. An improved volume-translated SRK EOS dedicated to more accurate determination of saturated and single-phase liquid densities. *Fluid Phase Equilib.* **2020**, *521*, No. 112724.

[6] Shi, J.; Li, H.; Pang, W. An improved volume translation strategy for PR EOS without crossover issue. *Fluid Phase Equilib*. **2018**, *470*, 164–175.

[7] Kroenlein, K.; Muzny, C. D.; Kazakov, A. F.; Diky, V.; Chirico, R. D.; Magee, J. W.; Abdulagatov, I.; Frenkel, M. NIST standard reference 203, TRC Web Thermo Tables (WTT) version 2-2012-1 professional, National Institute of Standards and Technology, Gaithersburg MD, 20899.

[8] Soave, G. Equilibrium constants from a modified Redlich-Kwong equation of state. *Chem. Eng. Sci.* **1972**, *27* (6), 1197–1203.

[9] Peng, D. Y.; Robinson, D. B. A new two-constant equation of state. *Ind. Eng. Chem. Fundam.* **1976**, *15* (1), 59–64.

[10] Ungerer, P.; Batut, C.; Prédiction des propriétés volumétriques des hydrocarbures par une translation de volume améliorée. *Rev. Inst. Fr. Pét.* **1997**, *52* (6), 609–623.

[11] Baled, H.; Enick, R. M.; Wu, Y.; McHugh, M. A.; Burgess, W.; Tapriyal, D.; Morreale, B. D. Prediction of hydrocarbon densities at extreme conditions using volume-translated SRK and PR equations of state fit to high temperature, high pressure PVT data. *Fluid Phase Equilib*. **2012**, *317*, 65–76.

[12] Magoulas, K.; Tassios, D. Thermophysical properties of n-alkanes from C1 to C20 and their prediction for higher ones. *Fluid Phase Equilib*. **1990**, *56*, 119–140.

[13] Banuti, D. T. Crossing the Widom-line – Supercritical pseudo-boiling. *J. Supercrit. Fluids* **2015**, *98*, 12–16.

[14] Shi, J.; Li, H. Criterion for determining crossover phenomenon in volume-translated equation of states. *Fluid Phase Equilib*. **2016**, *430*, 1–12.

CHAPTER 4 CONCLUSIONS AND RECOMMENDATIONS

4.1. Conclusions

Seven VT-EOS models (including the constant VT-SRK EOS updated by Pina-Martinez *et al*.,[1] two linear temperature-dependent VT-PR EOS models including the Ungerer and Batut model[2] and the Baled *et al*. model,[3] two exponential temperature-dependent VT-PR EOS models including the Magoulas and Tassios model[4] and the Shi *et al*. model,[5] and two temperature-pressure-dependent models including the VT-PR EOS model proposed by Abudour *et al*.[6] and the VT-SRK EOS proposed by Chen and Li[7]), together with the untranslated PR EOS[8] and SRK EOS[9], are implemented in this study in an attempt to obtain more accurate predictions of κ_T and α_P. Since the molar volume is treated as a function of both temperature and pressure in the distance-function-based VT models, analytical expressions of κ_T and α_P cannot be obtained by using the VT-EOS models that adopt the distance function. To predict κ_T and α_P by these distance-function-based VT-EOS models developed by Abudour *et al*.[6] and Chen and Li[7], a numerical method is proposed to approximate the partial derivatives of the molar volume with respect to temperature and pressure, respectively. The predictions of κ_T and α_P are made in the liquid-phase region, the vapor-phase region, and the supercritical-phase region for pure CH_4 and CO_2 within the temperature range from their corresponding T_{triple} to $T_r = 3$ and the pressures from $P_r = 0.1$ to $P_r = 3$. The predictions of κ_T and α_P by each model are compared with the pseudo-experimental data of NIST[10]. The prediction accuracy of each model is evaluated by comparing the *%AADs* and the *%RDs*. The predicted results show that the distance-function-based VT models exhibit relatively better performance in

predicting κ_T and α_P than the temperature-dependent and the constant VT models. Overall, the distance-function-based VT-PR EOS model proposed by Abudour *et al*.[6] is the most accurate VT model for predicting κ_T with an overall *%AAD* of 5.11%, while the distance-function-based VT-SRK EOS model proposed by Chen and Li[7] is the most accurate VT model for predicting α_P with an overall *%AAD* of 2.77%. In addition, it can be concluded that the more accurate the PVT relation is, the more accurate the predictions of κ_T and α_P can be.

4.2. Recommendations

The best overall prediction accuracy of κ_T and α_P are provided by the temperature-pressure-dependent VT models proposed by Abudour *et al*.[6] and Chen and Li,[7] respectively. In future studies, more experimental data of κ_T and α_P at high-temperature and high-pressure conditions should be made available so that they can be used to check if the superior performance of these two models in predicting κ_T and α_P can be preserved at high-temperature and high-pressure conditions.

In this thesis, the prediction accuracy of VT-EOS models is only evaluated for two example pure substances. However, the processes encountered in the petroleum and chemical industry often involve more complex fluids. Therefore, future studies should examine the predictions of κ_T and α_P for more pure substances and mixtures by the VT models of Abudour *et al*.[6] and Chen and Li[7]. In addition, appropriate mixing rules need to be implemented to apply VT-EOSs to predict κ_T and α_P for mixtures.

References

[1] Pina-Martinez, A.; Le Guennec, Y.; Privat, R.; Jaubert, J. N.; Mathias, P. M. Analysis of the combinations of property data that are suitable for a safe estimation of consistent Twu α-function parameters: Updated parameter values for the translated-consistent tc-PR and tc-RK cubic equations of state. *J. Chem. Eng. Data* **2018,** *63* (10), 3980–3988.

[2] Ungerer, P.; Batut, C.; Prédiction des propriétés volumétriques des hydrocarbures par une translation de volume améliorée. *Rev. Inst. Fr. Pét.* **1997**, *52* (6), 609–623.

[3] Baled, H.; Enick, R. M.; Wu, Y.; McHugh, M. A.; Burgess, W.; Tapriyal, D.; Morreale, B. D. Prediction of hydrocarbon densities at extreme conditions using volume-translated SRK and PR equations of state fit to high temperature, high pressure PVT data. *Fluid Phase Equilib*. **2012**, *317*, 65–76.

[4] Magoulas, K.; Tassios, D. Thermophysical properties of n-alkanes from C1 to C20 and their prediction for higher ones. *Fluid Phase Equilib*. **1990**, *56*, 119–140.

[5] Shi, J.; Li, H.; Pang, W. An improved volume translation strategy for PR EOS without crossover issue. *Fluid Phase Equilib*. **2018**, *470*, 164–175.

[6] Abudour, A. M.; Mohammad, S. A.; Robinson, R. L.; Gasem, K. A. M. Volume-translated Peng–Robinson equation of state for saturated and single-phase liquid densities. *Fluid Phase Equilib*. **2012**, *335*, 74–87.

[7] Chen, X.; Li, H. An improved volume-translated SRK EOS dedicated to more accurate determination of saturated and single-phase liquid densities. *Fluid Phase Equilib.* **2020**, *521*, No. 112724.

[8] Peng, D. Y.; Robinson, D. B. A new two-constant equation of state. *Ind. Eng. Chem. Fundam.* **1976**, *15* (1), 59–64.

[9] Soave, G. Equilibrium constants from a modified Redlich-Kwong equation of state. *Chem. Eng. Sci.* **1972**, *27* (6), 1197–1203.

[10] Kroenlein, K.; Muzny, C. D.; Kazakov, A. F.; Diky, V.; Chirico, R. D.; Magee, J. W.; Abdulagatov, I.; Frenkel, M. NIST standard reference 203, TRC Web Thermo Tables (WTT) version 2-2012-1 professional, National Institute of Standards and Technology, Gaithersburg MD, 20899.

BIBLIOGRAPHY

Abudour, A. M.; Mohammad, S. A.; Robinson, R. L.; Gasem, K. A. M. Volume-translated Peng–Robinson equation of state for saturated and single-phase liquid densities. *Fluid Phase Equilib*. **2012**, *335*, 74–87.

Adepoju, O. O. Coefficient of isothermal oil compressibility for reservoir fluids by cubic equation-of-state. M.Sc. thesis, Texas Tech University, 2006.

Ahmed, T.; Meehan, D. N. *Advanced reservoir management and engineering*; Gulf Professional Publishing, 2011.

Avasthi, S. M.; Kennedy, H. T. The prediction of volumes, compressibilities and thermal expansion coefficients of hydrocarbon mixtures. *SPE J.* **1968**, *8* (02), 95–106.

Baled, H.; Enick, R. M.; Wu, Y.; McHugh, M. A.; Burgess, W.; Tapriyal, D.; Morreale, B. D. Prediction of hydrocarbon densities at extreme conditions using volume-translated SRK and PR equations of state fit to high temperature, high pressure PVT data. *Fluid Phase Equilib*. **2012**, *317*, 65–76.

Banuti, D. T. Crossing the Widom-line – Supercritical pseudo-boiling. *J. Supercrit. Fluids* **2015**, *98*, 12–16.

Baonza, V. G.; Alonso, M. C.; Delgado, J. N. Application of simple expressions for the high-pressure volumetric behaviour of liquid mesitylene. *J. Chem. Soc., Faraday Trans.* **1994**, *90* (4), 553–557.

Beggs, H. D. *Production optimization using NODAL analysis*; 1991.

Benner, S. A.; Ricardo, A.; Carrigan, M. A. Is there a common chemical model for life in the universe? *Curr. Opin. Chem. Biol.* **2004**, *8* (6), 672–689.

Braeuer, A. In situ spectroscopic techniques at high pressure. *Supercritical Fluid Science and Technology*, Vol. 7; Elsevier, 2015.

Burgess, W. A.; Bamgbade, B. A.; Gamwo, I. K. Experimental and predictive PC-SAFT modeling results for density and isothermal compressibility for two crude oil samples at elevated temperatures and pressures. *Fuel* **2018,** *218*, 385–395.

Cerdeiriña, C. A.; Tovar, C. A.; González-Salgado, D.; Carballo, E.; Romaní, L. Isobaric thermal expansivity and thermophysical characterization of liquids and liquid mixtures. *Phys. Chem. Chem. Phys.* **2001**, *3* (23), 5230–5236.

Chen, X.; Li, H. An improved volume-translated SRK EOS dedicated to more accurate determination of saturated and single-phase liquid densities. *Fluid Phase Equilib.* **2020**, *521*, No. 112724.

Cho, J.; Park, G.; Kwon, S.; Lee, K. S.; Lee, H. S.; Min, B. Compositional modeling to analyze the effect of CH_4 on coupled carbon storage and enhanced oil recovery process. *Appl. Sci.* **2020**, *10* (12), 4272.

Choi, W.; Lee, Y.; Seo, Y. Experimental verification of CH_4-CO_2 replacement in various gas hydrate structures for CH_4 production and CO_2 sequestration; *The Twenty-eighth International Ocean and Polar Engineering Conference*, Sapporo, Japan, June 2018; ISOPE-I-18-735.

Chorążewski, M.; Postnikov, E. B. Thermal properties of compressed liquids: Experimental determination via an indirect acoustic technique and modeling using the volume fluctuations approach. *Int. J. Therm. Sci.* **2015**, *90*, 62–69.

Chou, G. F.; Prausnitz, J. M. A phenomenological correction to an equation of state for the critical region. *AIChE J.* **1989**, *35* (9), 1487–1496.

Christie, B. On the correlation between isothermal compressibility and isobaric expansivity. *Pipeline Simulation Interest Group Annual Meeting*; Baltimore, Maryland, May 2014; PSIG 1426.

Daridon, J. L.; Bazile, J. P. Computation of liquid isothermal compressibility from density measurements: An application to toluene. *J. Chem. Eng. Data* **2018**, *63* (6), 2162–2178.

Frey, K.; Modell, M.; Tester, J. Density-and-temperature-dependent volume translation for the SRK EOS: 1. Pure fluids. *Fluid Phase Equilib*. **2009**, *279* (1), 56–63.

Frey, K.; Modell, M.; Tester, J. Density-and-temperature-dependent volume translation for the SRK EOS: 2. Mixtures. *Fluid Phase Equilib*. **2013**, *343*, 13–23.

Gasem, K. A. M.; Gao, W.; Pan, Z.; Robinson Jr., R. L. A modified temperature dependence for the Peng-Robinson equation of state. *Fluid Phase Equilib*. **2001**, *181* (1–2), 113–125.

Gaskell, D.R. *Introduction to the thermodynamics of materials*; CRC Press, 2012.

Izgec, O.; Demiral, B.; Bertin, H. J.; Akin, S. CO_2 injection in carbonates; *SPE Western Regional Meeting*, Irvine, California, March 2005; SPE-93773-MS.

Jaubert, J. N.; Privat, R.; Le Guennec, Y.; Coniglio, L. Note on the properties altered by application of a Péneloux-type volume translation to an equation of state. *Fluid Phase Equilib*. **2016**, *419*, 88–95.

Kalikhman, V.; Kost, D.; Polishuk, I. About the physical validity of attaching the repulsive terms of analytical EOS models by temperature dependencies. *Fluid Phase Equilib*. **2010**, *293* (2), 164–167.

Kroenlein, K.; Muzny, C. D.; Kazakov, A. F.; Diky, V.; Chirico, R. D.; Magee, J. W.; Abdulagatov, I.; Frenkel, M. NIST standard reference 203, TRC Web Thermo Tables (WTT) version 2-2012-1 professional, National Institute of Standards and Technology, Gaithersburg MD, 20899.

Le Guennec, Y.; Lasala, S.; Privat, R.; Jaubert, J. N. A consistency test for α-functions of cubic equations of state. *Fluid Phase Equilib*. **2016**, *427*, 513–538.

Lin, C. W.; Trusler, J. P. M. The speed of sound and derived thermodynamic properties of pure water at temperatures between (253 and 473) K and at pressures up to 400 MPa. *J. Chem. Phys.* **2012**, *136* (9), No. 094511.

Lin, H.; Duan, Y. Y. Empirical correction to the Peng-Robinson equation of state for the saturated region. *Fluid Phase Equilib.* **2005**, *233* (2), 194–203.

Lin, H.; Duan, Y. Y.; Zhang, T.; Huang, Z. M. Volumetric property improvement for the Soave-Redlich-Kwong equation of state. *Ind. Eng. Chem. Res.* **2006**, *45* (5), 1829–1839.

Macias, L. C.; Ramey Jr., H. J. Multiphase, multicomponent compressibility in petroleum reservoir engineering; *SPE Annual Technical Conference and Exhibition*; New Orleans, Louisiana, October 1986; SPE-15538-MS.

Magoulas, K.; Tassios, D. Thermophysical properties of n-alkanes from C1 to C20 and their prediction for higher ones. *Fluid Phase Equilib*. **1990**, *56*, 119–140.

Martin, J. J. Cubic equations of state-which? *Ind. Eng. Chem. Fundam.* **1979**, *18* (2), 81–97.

Mathias, P. M.; Naheiri, T.; Oh, E. M. A density correction for the Peng-Robinson equation of state. *Fluid Phase Equilib*. **1989**, *47*, 77–87.

Monnery, W. D.; Svrcek, W. Y.; Satyro, M. A. Gaussian-like volume shifts for the Peng-Robinson equation of state. *Ind. Eng. Chem. Res*. **1998,** *37* (5), 1663–1672.

Navia, P.; Troncoso, J.; Romaní, L. New calibration methodology for calorimetric determination of isobaric thermal expansivity of liquids as a function of temperature and pressure. *J. Chem. Phys.* **2011**, *134* (9), No. 094502.

Nazarzadeh, M.; Moshfeghian, M. New volume translated PR equation of state for pure compounds and gas condensate systems. *Fluid Phase Equilib*. **2013**, *337*, 214–223.

Péneloux, A.; Rauzy, E.; Fréze, R. A consistent correction for Redlich-Kwong-Soave volumes. *Fluid Phase Equilib*. **1982**, *8* (1), 7–23.

Peng, D. Y.; Robinson, D. B. A new two-constant equation of state. *Ind. Eng. Chem. Fundam.* **1976**, *15* (1), 59–64.

Peters, E. J. *Advanced Petrophysics: Volume 1: Geology, Porosity, Absolute Permeability, Heterogeneity and Geostatistics*; Live Oak Book Co, 2012.

Pina-Martinez, A.; Le Guennec, Y.; Privat, R.; Jaubert, J. N.; Mathias, P. M. Analysis of the combinations of property data that are suitable for a safe estimation of consistent Twu α-function parameters: Updated parameter values for the translated-consistent tc-PR and tc-RK cubic equations of state. *J. Chem. Eng. Data* **2018,** *63* (10), 3980–3988.

Privat, R.; Jaubert, J. N. Thermodynamic models for the prediction of petroleum-fluid phase behaviour. *Crude Oil Emulsions-Composition Stability and Characterization*; InTechOpen, 2012.

Regueira, T.; Glykioti, M. L.; Kottaki, N.; Stenby, E. H.; Yan, W. Density, compressibility and phase equilibrium of high pressure-high temperature reservoir fluids up to 473 K and 140 MPa. *J. Supercrit. Fluids* **2020**, *159*, No. 104781.

Shi, J.; Li, H. Criterion for determining crossover phenomenon in volume-translated equation of states. *Fluid Phase Equilib*. **2016**, *430*, 1–12.

Shi, J.; Li, H.; Pang, W. An improved volume translation strategy for PR EOS without crossover issue. *Fluid Phase Equilib*. **2018**, *470*, 164–175.

Soave, G. Equilibrium constants from a modified Redlich-Kwong equation of state. *Chem. Eng. Sci.* **1972**, *27* (6), 1197–1203.

Trujillo, M. F.; Torres, D. J.; O'Rourke, P. J. High-pressure multicomponent liquid sprays: Departure from ideal behaviour. *Int. J. Engine Res.* **2004**, *5* (3), 229–246.

Trusler, J. P. M.; Lemmon, E.W. Determination of the thermodynamic properties of water from the speed of sound. *J. Chem. Thermodyn.* **2017**, *109*, 61–70.

Twu, C. H.; Bluck, D.; Cunningham, J. R.; Coon, J. E. A cubic equation of state with a new alpha function and a new mixing rule. *Fluid Phase Equilib*. **1991**, *69*, 33–50.

Ungerer, P.; Batut, C.; Prédiction des propriétés volumétriques des hydrocarbures par une translation de volume améliorée. *Rev. Inst. Fr. Pét.* **1997**, *52* (6), 609–623.

Valderrama, J. O. The state of the cubic equations of state. *Ind. Eng. Chem. Res.* **2003**, *43* (8), 1603–1618.

Valderrama, J. O.; Alfaro, M. Liquid volumes from generalized cubic equations of state: Take it with care. *Oil Gas Sci. Technol.* **2000**, *55* (5), 523–531.

Watson, P.; Cascella, M.; May, D.; Salerno, S.; Tassios, D. Prediction of vapor pressures and saturated molar volumes with a simple cubic equation of state: Part II: The Van der Waals - 711 EOS. *Fluid Phase Equilib*. **1986**, *27*, 35–52.

Young, A. F.; Pessoa, F. L. P.; Ahón, V. R. R. Comparison of volume translation and co-volume functions applied in the Peng-Robinson EoS for volumetric corrections. *Fluid Phase Equilib*. **2017**, *435*, 73–87.

Zanganeh, P.; Dashti, H.; Ayatollahi, S. Comparing the effects of CH_4, CO_2, and N_2 injection on asphaltene precipitation and deposition at reservoir condition: A visual and modeling study. *Fuel* **2018**, *217*, 633–641.

Zhu, T.; McGrail, P.; Kulkarni, A.; White, M. D.; Phale, H. A. Development of a thermodynamic model and reservoir simulator for the CH_4, CO_2, and CH_4-CO_2 gas hydrate system; *SPE Western Regional Meeting*, Irvine, California, March 2005; SPE-93976-MS.